Interplay of ferromagnetism and superconductivity : (in hybrid structures)

Caroline Richard

UNIVERSITÉ DE GRENOBLE

THÈSE

Pour obtenir le grade de

DOCTEUR DE L'UNIVERSITÉ DE GRENOBLE

Spécialité : **Physique**

Arrêté ministériel :

Présentée par

Caroline RICHARD

Thèse dirigée par **Manuel HOUZET**
et codirigée par **Julia MEYER**

préparée au sein **du SPSMS/INAC, CEA/UJF Grenoble-1**
et de **l'Ecole doctorale de physique**

Interplay of ferromagnetism and superconductivity (in hybrid structures)

Thèse soutenue publiquement le **6 novembre 2013**,
devant le jury composé de :

M. Denis FEINBERG
Chercheur-Institut Neel, Président
M. Alexandre BUZDIN
Professeur-Universite de Bordeaux 1, Rapporteur
M. Piet BROUWER
Professeur-Freie Universtat Berlin, Rapporteur
M. Hugues POTHIER
Chercheur-CEA Saclay, Examinateur
M. Manuel HOUZET
Chercheur-CEA Grenoble, Directeur de thèse
Mme Julia MEYER
Professeur-Universite Joseph Fourier, Co-Directeur de thèse

Remerciements

En premier lieu, un merci chaleureux à Manuel et Julia pour leur sympathie et la qualité de leur encadrement. Je pense avoir beaucoup appris à leurs cotés et sans eux, thèse il n'y aurait pas. J'espère ne pas perdre le contact que ce soit au cours d'une discussion de physique ou d'une sortie en montagne, j'apprecie beaucoup leur sens de l'humour, leur puissance en physique mais aussi leur sens de l'humilité. Je tiens aussi à remercier Sacha Buzdin, Piet Brouwer, Hugues Pothier et Denis Feinberg pour avoir bien voulu lire ma thèse, la commenter et participer à mon jury.

Au quotidien dans les couloirs du C5, j'ai partagé beaucoup (voir toutes) mes pauses avec Driss, qui je l'espère, va pouvoir continuer en recherche. Merci aussi à Benoît pour les discussions du matin et de l'après midi, à nos tentatives de réponses sur la physique. Beaucoup de questions n'ont (d'ailleurs) pas trouvées de réponses et/ou appellent à d'autres questions et la thèse ne peut surement pas être un long fleuve tranquille. Il faut avoir en réserve une bonne dose de motivation et de passion pour ne pas lacher les bras. A ce sujet, je tiens tout particulierement à remercier l'équipe de l'école d'été du GDR de Cargèse, tant les organisateurs que les orateurs. Je pense sincèrement qu'ils ont su raviver passion et détermination nécessaires au démarrage de ma troisième année de thèse. Mais que serait la théorie sans les expérimentateurs, spéciale dédicace à toute l'équipe du C1, en particulier à Charlène, Benoit et Boris. Enfin un petit retour dans les couloirs du C5, où j'ai souvent rencontré Marielle, Jean-Pascal, Xavier, Tanya et Vladimir.

Heureusement, les années de thèse ne sont pas seulement dédiées à la thèse, il y a aussi la famille, les amis. Entre les sorties de ski ou d'escalade (selon la saison) et les soirées (en toutes saisons) merci à Maël, Armin et Dawan, Svet et FX, Seb, Simon, Rachel, Franz, et Jean-Luc et Isa. Avec Maël, maintenant mon mari, un nouveau départ nous attend dans le Montana, j'espère que le séjour sera riche tant pour la physique que pour les rencontres et le dépaysement.

Enfin, un grand merci à mes parents, Martine et François, pour m'avoir introduit au monde de la recherche et de la physique et m'avoir permi de poursuivre mes études à ma guise sans me soucier de la finance.

Contents

Symbols

FMR	**F**erro**M**agnetic **R**esonance
AP	**A**nti**P**arallel
P	**P**arallel
CPR	**C**urrent **P**hase **R**elation
ZEP	**Z**ero **E**nergy **P**eak
JJ	**J**osephson **J**unction
DoS	**D**ensity **o**f **S**tates

Introduction

The story of superconductivity started in 1911, when Kammerling Onnes observed that the electrical resistance of some metals, such as mercury, tin and lead, disappears at low temperature featuring a perfect conductivity. Impressively, once launched, currents in superconducting rings persist with no measurable decay after more than one year[1]. Then, in 1933, Meissner discovered the second hallmark of superconductivity, namely perfect diamagnetism. Namely, the magnetic field is expelled from a superconductor. The simplest, but remarkable, example is the levitation of a magnet above a superconductor. While at large scale, the industrial applications are, e.g. to levitate trains above the rails (Maglev project) or to build high transmission lines to transport energy. At small scale, superconductivity is promising for tomorrow low-consuming smart electronic devices.

More than forty years after its discovery, in 1957, Bardeen, Cooper and Schrieffer proposed a microscopic theory which revolutionized the understanding of superconductivity. In the presence of an arbitrary weak attraction mediated by the phonons, the Fermi sea gets unstable and electrons condense in pairs with opposite spin and momenta. Due to both spin and momentum symmetries of a pair, the interaction of superconductivity and magnetism rapidly drew attention. In particular, how does the presence of a magnetic field influence superconductivity[2]?

The magnetic field acts on the momentum, this is the orbital effect and on the spin, this is the paramagnetic effect. The orbital effect stems from the Lorentz force, and tends to break a Cooper by spatially separating the electrons that constitute it. Then, in metals where ferromagnetism originates from localized electrons, the paramagnetic effect is due to the exchange interaction between the spins of itinerant and localized electrons. It tends to align them and prevents the singlet pairing. As both effects damage the coherence of a pair, ferromagnetism and conventional superconductivity

[1] The experimental evidence predicts even 10^5 years of life.

[2] Actually, Ginzburg, before the microscopic BCS theory, in 1956, was the first to formulate the problem of coexistence of superconductivity and magnetism.

appear as incompatible phases of nature. They may coexist if either the magnetic order or the superconducting pairing is changed.

In 1959, Anderson and Suhl state that superconductivity may affect the magnetic order. In particular, the magnetic susceptibility of singlets being zero, the energy gain associated with the ferromagnetic order should decrease. Instead they predict the appearance of a non-uniform magnetic order, called crypto-ferromagnetism [1].

This theory was partially confirmed in 1977 with the discovery of the rare earths (RE)Rh_4B_4 [2] and (RE)Mo_6S_8 [3], where anti-ferromagnetism and superconductivity coexist. The idea is that, over the spatial extension of a pair the exchange interaction averages to zero, and thus the magnetic order can coexist peacefully with the superconducting condensate.

By contrast, in 1964, Larkin and Ovchinnikov [4] and Fulde and Ferrel [5], demonstrated that, due to the paramagnetic effect, a non-uniform superconductivity may appear in a pure ferromagnet (FFLO phase). The idea is that in the absence of a Zeeman field, a Cooper pair consists of two electrons of opposite momenta, $+p_F$ and $-p_F$, and opposite spin, $\uparrow$ and $\downarrow$, thus, the total momentum of a pair is zero. By contrast, subject to a Zeeman field H, the momentum of the $\uparrow$ electron shifts to $p_F + \delta p$ while, for the $\downarrow$ electron, it shifts to $-p_F + \delta p$, where $\delta p = \mu_B H / v_F$ and v_F is the Fermi velocity. As a result, the pair acquires a non-zero total momentum $2\delta p$ which implies a predicted space-modulation of the superconducting order parameter with the vector $2\delta p$.

Recently, true ferromagnetic superconductors were discovered, namely UGe_2 [6] and URhGe [7]. In particular, URhGe features a ferromagnetic transition at around 9.5K with the appearance of superconductivity below $T_c = 0.3$K. The combination of singlet superconductivity and ferromagnetism being improbable, a triplet superconductivity is favored. However the triplet mechanism is yet to be understood.

Here, the main difficulty is that only few ferromagnetic superconductors have been discovered and, their experimental study demands low temperatures or high pressures.

Present research

In this thesis, to get better understanding about the coexistence of magnetism and superconductivity, we have studied hybrid ferromagnetic and superconducting structures. In such S/F structures, Cooper pairs from the superconductor can leak into the adjacent ferromagnet. As a result, the proximity effect artificially reproduces the coexistence of

superconductivity and ferromagnetism, and offers a unique opportunity to study their interplay.

Avoiding the challenge to directly study true ferromagnetic superconductors, S/F junctions are both experimentally and theoretically attractive and display a rich panel of phenomena. As an example, the oscillation of the induced superconducting correlations observed in homogeneous S/F structures may be compared with the predicted non-uniform superconductivity in pure ferromagnets (FFLO phase) [8]. Likewise, the study of the symmetries of superconducting correlations with respect to space, spin, and frequency [9] may give insight about the triplet superconductivity. The interest is that both the paramagnetic and orbital effects as well as interface effects in hybrid structures may change the symmetries of the induced correlations [10–12]. For example, the recent observation of a long-range proximity effect, in inhomogeneous $S/F/S$ Josephson junctions, would evidence the presence of even-parity spin-triplet odd-frequency induced superconducting correlations [13, 14].

In this thesis, to qualitatively describe hybrid metallic junctions, like in [13, 14], we will consider only dirty metals, where the motion of electrons is diffusive. In such diffusive metals, only s-waves (even-parity in space) are robust with respect to disorder. As a result, induced superconducting correlations may only be either spin-singlet even-frequency or spin-triplet odd-frequency.

In the first part, to get more insight about the triplet odd-frequency correlations, we study the Josephson current in $S/F/S$ junctions at equilibrium. In particular, we will first show that a non-collinear bilayer ferromagnet is enough to generate a long-range triplet Josephson current. Besides its long-range property, an experimental evidence of the triplet nature is the superharmonicity of the current phase relation. Then, we consider the competition between singlet and triplet pairing in a multilayer $S'/F/S/F/S'$ Josephson. Interestingly, we will predict that the singlet/triplet competition may be directly observed by performing critical current measurements.

In the second part, we will study the interplay of the magnetization dynamics with superconductivity at an F/S interface. Here, by contrast with the first part, the magnetization is inhomogeneous in time instead of space. We will predict that, due to interface effects, a spin-pumping mechanism in the ferromagnet may induce a non-negligeable singlet current in the superconductor. Thus, it addresses the dynamically generation of triplet pairs in the ferromagnet.

Descriptions of the chapters

In chapter 1, we introduce the proximity effect and the concept of Andreev reflection in both a normal metal and a ferromagnet. The proximity effect in the ferromagnet is very rich and fascinating, we will explain with simple arguments some of it and motivate the present research. Starting with the peculiar oscillatory, but short range, critical current measured in π-junctions, we then show that on contrary a inhomogeneous magnetization induces triplet correlations between electrons with the same spin, that can propagate on a long range. Additionally, the triplet correlations feature a strange odd-frequency nature in diffusive metals, we look for additional experimental evidence to confirm their reality (Chapter 3 and 4). In the second part, we connect superconductivity with spintronics. Since one of the bottlenecks of spintronics devices is the efficient generation of spin currents, the dissipationless nature of supercurrents looks promising.

In chapter 2, we build the theoretical machinery we used all along the thesis to describe hybrid ferromagnetic and superconducting structures, namely the quasiclassical formalism in the diffusive limit (Usadel equation). Then, chapter 3, 4 and 5 are devoted to the results of the thesis.

In chapter 3, we predict a long range triplet proximity effect in bilayer ferromagnetic Josephson junctions. In such junctions, the long range current is carried by pairs of triplet pairs with the same spin and the current phase relation is dominated by its second harmonic. In chapter 4, we further play with symmetries, by connecting two effective odd-frequency reservoirs through an even-frequency superconducting layer. We show that the temperature dependence of the critical current of the junction exhibits a peculiar maximum at finite temperature. This maximum reveals a competition between odd and even-frequency superconductivity.

Finally, in chapter 5, we study an out-of-equilibrium problem where the ferromagnetic resonance (FMR) is as an alternative way to generate both spin and charge currents. The FMR induces a spin current which is further transformed in a measurable charge current flowing in the leads at room temperature. In this chapter, we predict that the phenomenon survives at a low temperature when one of the lead is superconducting, namely FMR induces an Andreev current.

Introduction (Francais)

L'histoire de la supraconductivité débuta en 1911, quand Kammerlings Onnes observa la disparition de la résistance électrique dans des matériaux tels que le mercure, l'étain et le plomb. De manière impressionante, une fois lancé dans une boucle supraconductrice, le courant persiste sans faiblir pendant plus d'un an. Puis en 1933, Meissner découvrit la deuxième propriété remarquable des supraconducteurs : un parfait diamagnétisme. Un supraconducteur expulse le champ magnétique en son sein. La lévitation d'un aimant au dessus d'un supraconducteur à basse température est un exemple simple et considérable de ce diamagnétisme. Les applications de la supraconductivité touchent à la fois les grandes échelles, avec les trains en lévitation (projet Maglev) ou les lignes supraconductrices hauts débits. Cependant elle est aussi prometteuse pour l'électronique dans la fabrication de composants à faible consommation.

Plus de 40 ans après sa découverte, Bardeen, Cooper et Schrieffer proposèrent un modèle microscopique révolutionant la compréhension de la supraconductivité. En présence d'une attraction médiée par les phonons, aussi faible soit-elle, la mer de Fermi devient instable. Les électrons condensent en paires de moment et de spin opposés. La présence de telles symétries en spin et en espace a drainé l'attention des chercheurs sur l'étude de l'interaction entre supraconductivité et magnétisme. Quelle est l'influence du magnetisme sur la supraconductivité ?

Le champ magnétique agit à la fois sur le moment, c'est l'effet orbital, et sur le spin, c'est l'effet paramagnétique. L'effet orbital est attribué à la force de Lorentz qui tend à séparer les électrons d'une paire affaiblissant cette dernière. Dans les métaux, le ferromagnétisme est dû aux électrons localisés. L'effet paramagnétique nait de l'interaction d'échange entre les spins des électrons localisés et itinérants. Il favorise l'alignement des spins empêchant l'appariement singulet. Comme les effets paramagnétiques et orbitaux détruisent la cohérence, le ferromagnétisme et la supraconductivité conventionelle semblent incompatibles. Les deux phases pourraient coexister si, soit l'ordre magnétique, soit la symétrie supraconductrice est changée.

En 1959, Anderson et Suhl ont considéré une modification de l'ordre magnétique [1]. Ils partent du constat que la suceptiblité magnétique d'une paire singulet est nulle, et que donc le gain d'énergie de la transition ferromagnétique devrait diminuer. Ils prédisent, à la place, l'apparition d'un ordre ferromagnetique non uniforme, appelé crypto-ferromagnétisme.

La découverte des terres rares, telles (RE)Rh_4B_4 [2] et (RE)Mo_6S_8[3], qui présentent des phases à la fois ferromagnétiques et supraconductrices soutient partiellement cette théorie. De fait, si l'échelle de variation de l'ordre ferromagnétique et l'extension d'une paire sont du même ordre, l'énergie d'échange moyenne peut être nulle et les deux ordres peuvent coexister.

En 1964, à la fois, Larkin et Ovchiinnikov[4] , et, Fulde et Ferrel[5], montrèrent que l'effet paramagnétique tend à réaliser une phase supraconductrice non-uniforme au sein d'un ordre purement ferromagnétique (FFLO). Sans champ Zeeman, une paire de Cooper apparie deux électrons de moments $+p_F$ et $-p_F$ et de spins opposés. Le moment total de la paire est nulle. En présence d'un champ Zeeman H, le moment de l'électron $\uparrow$ devient $p_F + \delta p$ alors que l'électron $\downarrow$ devient $-p_F + \delta p$ où $\delta p = \mu_B H/v_F$ (v_F est la vitesse de Fermi). Ainsi, la paire acquiert un moment cinétique $2\delta p$, ce qui entraîne une modulation dans l'espace du paramètre d'ordre supraconducteur selon δp.

Récemment, de véritables métaux supraconducteurs et ferromagnétiques ont été découverts (URhGe[6] et UGe_2[7]). Par exemple, URhGe présente une transition ferromagnétique autour de 9.5K avec une apparition de la supraconductivité sous 0.3K. La présence d'une supraconductivité singulet au sein d'un ordre ferromagnétique est peu probable. Une supraconductivité triplet est supposée. Cependant le mécanisme sous-jacent reste à découvrir et l'étude expérimentale de ces matériaux est difficile car elle nécessite des basses températures ou de fortes pressions.

Sujet de la thèse

Cette thèse s'intéresse à la coexistence de la supraconductivité avec le ferromagnétisme dans des structures hybrides supraconductrices/ferromagnétiques. Dans ces structures, par effet de proximité, des paires de Cooper peuvent s'échapper du supraconducteur et pénétrer dans le ferromagnétique. Ainsi, l'effet de proximité induit artificiellement de l'ordre supraconducteur dans le métal ferromagnétique et permet l'étude de la coexistence ou de l'interaction des deux phases. Ces structures, moins difficiles à étudier expérimentalement ont attirées l'attention des expérimentalistes et des théoriciens. Ainsi nous pouvons mettre en parallèle la phase FFLO avec les oscillations du courant critique observées dans les jonctions Josephson S/F/S [8]. Par ailleurs, l'étude des symétries des

corrélations supraconductrices vis-à-vis du spin, de l'espace et du temps est riche dans le cadre de la supraconductivité triplet [9] . En effet, à la fois, l'effet orbital et l'effet paramagnétique peuvent modifier les symétries [10–12]. Par exemple, l'observation récente d'un effet de proximité longue portée, dans des jonctions S/F/S non-homogénes [13, 14], serait la signature de corrélations induites pairs en espace triplet de spin et impairs en fréquence.

Dans cette thèse, afin de décrire les jonctions hybrides comme celle de [13, 14], nous considérons des métaux sales, c'est-à-dire dans lesquels le transport des électrons est diffusif. Dans la limite diffusive, seules les correlations s-wave (paires) survivent. Les corrélations supraconductrices peuvent alors soit être singulets paires en fréquence ou triplets impaires en fréquence.

Dans la première partie, nous nous sommes intéressés aux correlations impaires en fréquence. En particulier, nous montrons qu'une bicouche ferromagnétique (non-collinéaire) est suffisante pour générer un courant Josephson triplet longue portée. La signature expérimentale de ce courant triplet longue portée est la superharmonicité de la relation courant phase. Puis, nous étudions la compétition entre appariement triplet et singulet dans les multi-couches $S'/F/S/F/S'$. La compétition des courants triplets et singulets peut être directement mesurée via des mesures de courants critiques. Dans la seconde partie, nous nous intéressons à l'effet d'une dynamique de l'aimantation sur la supraconductivité à des interfaces S/F. Ici, nous considèrons donc la variation temporelle plutôt que spatiale (étudiée dans la première partie) de l'aimantation. Nous prédisons que, grâce à des effets d'interfaces, un mécanisme de pompe à spin dans le métal ferromagnétique, telle une résonance ferromagnétique, peut induire des courants singulets dans le supraconducteur en contact. Nous abordons donc la génération dynamique de pairs triplets dans le métal ferromagnétique.

Résumé des chapitres

- Chapitre 1 : nous présentons l'effet de proximité avec le concept de réflection d'Andreev dans les cas d'un métal normal ou ferromagnétique.
- Chapitre 2 : nous donnons les outils théoriques utilisés au cours de cette thèse pour la description des structures hybrides supraconductrices et ferromagnétiques. En particulier, nous dérivons étape par étape les équations quasiclassiques dans la limite diffusive (Usadel). Les chapitres suivants concernent les résultats obtenus au cours de la thèse.
- Chapitre 3 : nous prédisons l'existence d'un effet de proximité longue portée dans les jonctions Josephson hybrides bi-couches non-collinéaires. Lorsque une des deux

couches est fine, les corrélations sont transportées par des paires triplets dont les spins sont parallèles par rapport à l'aimantation de la couche longue. En particulier, le courant longue portée est dominée par la deuxième harmonique.

- Chapitre 4 : nous étudions la compétition entre corrélations singulets paires en fréquence et triplets impaires en fréquence dans une jonctions multicouches. De manière effective, nous nous intéressons au courant d'équilibre entre deux reservoirs triplet impaires via un ilot supraconducteur conventionnel. La compétition entre corrélations triplets des réservoirs et singulets de l'ilot central se traduit par une dépendence en temperature du courant critique non-monotone.

- Chapitre 5 : nous étudions le courant hors-équilibre induit par une résonance ferromagnétique dans une structures F/S. Nous montrons que, même dans un régime sous le gap, et quand l'interface est sensible au spin, la résonance ferromagnétique induit un courant alternatif de spin qui est rectifié en un courant d'Andreev de charges à l'interface avec l'électrode supraconductrice.

Chapter 1

Introduction to the proximity effect in hybrid junctions

At the heart of conventional superconductivity, an attractive interaction mediated by the phonons "shakes" the Fermi sea: the electrons condense in pairs with opposite spin and opposite momenta, realizing a singlet state. As a result, the energy spectrum is gapped and a supercurrent can flow at equilibrium.

When in contact with a piece of metal, Cooper pairs can leak out of the superconductor inducing superconducting correlations in the adjacent metal. This is the proximity effect, electron-hole correlations exist in the normal metal without any underlying attraction. As a result, the density of states inherits a (mini)-gap. Additionally, a current can even flow at equilibrium featuring a Josephson effect when the metallic layer is sandwiched between two supercondutor ($S/N/S$ junctions).

The aim of this chapter is to introduce by the basics of this proximity effect without using heavy mathematical tools.

In a first part, we introduce the proximity effect in normal metals. We explain how Andreev bound states appear and generate a Josephson effect in $S/N/S$ junctions.

In a second part, we go deeper into the subject of this thesis, namely the interplay of superconductivity and ferromagnetism. We study the peculiarities of the proximity effect in ferromagnets where the presence of the exchange field strongly impacts the coherence of a leaking pair. It may be either short-range or long-range. We start with the observation of an oscillatory and exponentially decaying critical current in $S/F/S$ junction, and try to explain this oscillatory short-range effect. Then, we see how an inhomogeneous magnetization can induce pairs with parallel spins (triplets), to restore

a long-range proximity effect. This part motivates chapters 4 and 5, on the signature of the long-range triplet currents.

Finally, in a third part, we try to connect with nowadays applications, namely spintronics [15]. How are superconducting properties promising for spintronics devices and why? It motivates chapter 5 where a precessing magnetization induces an Andreev current.

1.1 Proximity effect in normal metals

1.1.1 Charge current trough N/S interface and Andreev reflection

At $eV < \Delta$, where Δ is the gap in the superconductor and V is the applied bias voltage, how can a current flow from a normal metal into a superconductor [16]?

While in the normal metal the current is carried by quasiparticles, in the superconductor, no quasiparticle exists and the current is carried by the condensate. Actually, while low-energy quasiparticles cannot pass the N/S interface, the "real" electrons can, thanks to the Andreev reflection which we explain below[17, 18].

Let's consider a quasi-electron of energy ϵ from the normal metal propagating toward the superconductor, see Fig. 1.1.

If $\epsilon > \Delta$ the electron can enter the superconductor[1].

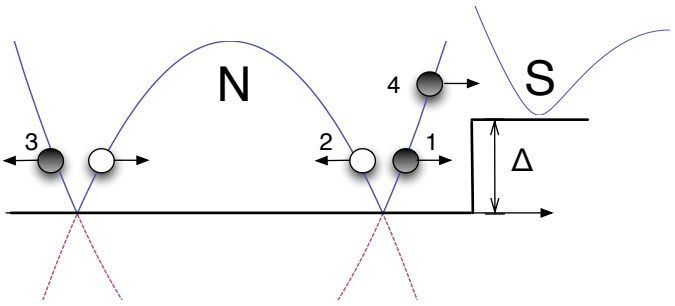

FIGURE 1.1: The Andreev reflection mechanism at an N/S interface. The curves represent the electrons and holes dispersion at the fermi surface. The electrons and holes are depicted respectively as black and white balls, the arrow indicate the direction of propagation. Electron #4 can directly enter the superconductor ($\epsilon(4) > \Delta$). However, electrons #1 cannot enter alone: it can either be reflected as electron #3, or as hole #2. For perfectly tranparent interface the reflection as electron #3 is not possible, thus electron #1 is Andreev-reflected as a hole #2 of opposite velocity , simultaneously a Cooper pair is created in S.

[1]Note that however the electron is partly reflected as a hole even above the gap. This is due to the structure of excitations (bogolons) which are an electron-hole superposition.

Otherwise if $\epsilon < \Delta$, the incoming electron of momentum $k_e = k_F + \epsilon/v_F$ cannot enter the superconductor, it can be either reflected in a quasi-electron of opposite momentum ($\sim -k_F$) or in a quasi-hole of momentum $k_h = k_e - 2\epsilon/v_F$, where v_F is the Fermi velocity and $k_F = mv_F$. Note that the impinging quasielectron has necessary the same energy as its "reflected" partner since the superconductor cannot "absorb" energy.

In the case of a transparent interface and for a slowly varying potential, no big change in momentum is possible. The normal reflection, in a quasi-electron, demands a $2k_F$ big change in the momentum and is very unlikely. The quasi-electron is thus reflected as a quasi-hole of opposite velocity, with a slighlty different momentum $k_e - k_h = 2\epsilon/v_F \ll k_F$. Simultaneously, a Cooper pair is created in the superconductor (charge $2e$). To summarize in one sentence:

The incoming electron above the Fermi sea picks up an electron below the Fermi sea before entering the superconductor leaving a hole behind.

This scenario works as well for a quasi-hole: it gets Andreev reflected as a quasi-electron by absorbing a Cooper pair[2].

Following a scattering approach and without entering the tedious calculations of the Bogoliubov-de-Gennes equation [19], the amplitude of the electron/hole reflection coefficients (and hole/electrons) reads [20–22]

$$r_{\mathrm{eh(he)}} = e^{\mp i\varphi} \begin{cases} \exp\left(-i \arccos \epsilon/\Delta\right) & , \epsilon < \Delta \\ \exp\left(-\operatorname{arccosh} \epsilon/\Delta\right) & , \epsilon > \Delta \end{cases}. \tag{1.1}$$

Then, the scattering state of an incident electron (hole) from the normal ($x < 0$) at energy $\epsilon < \Delta$ reads

$$\Psi_{\mathrm{e(h)}}(x) = \psi^0_{\mathrm{e(h)}}(x) + \psi_{\mathrm{he(eh)}}(x) = \begin{pmatrix} e^{i\epsilon.x/v_F} \\ r_{\mathrm{eh(he)}} e^{-i\epsilon.x/v_F} \end{pmatrix} e^{ik_F.x}, \text{ for } x < 0, \tag{1.2}$$

where ψ^0_e and ψ_{he} are respectively the incident and the reflected waves[3].

This the essence of the proximity effect: the Andreev reflections induces a coherent superposition of electron and hole in N, in other words superconducting correlations are induced in the normal metal.

[2] For a non-perfectly transparent interface, the normal reflection is authorized, namely the quasi-electron is reflected as a superposition of quasi-hole and quasi-electrons.

[3] For readability, we omitted the spin index but a spin-up (down) electron is reflected as a spin-down (up) hole

At $\epsilon = 0$ the reflected quasi-hole exactly retraces the way back of the incident electron. However at finite ϵ, the penetration length is finite $\xi^c_{N,\epsilon} \sim v_F/\epsilon$, beyond this distance the quasi-electron and the reflected quasi-hole get dephased (the c exponent stands for "clean").

At finite temperature, the energy spreads over T ($\delta\epsilon \sim T$), and the coherence length of superconductivity is $\xi^c_N = v_F/T$. Note that the coherence length diverges at low temperature where the cutoff is set by the inelastic processes, L_ϕ.

Up to now we considered the ballistic case corresponding to perfectly clean samples. In the limit of dirty samples, due to many impurity scatterings (elastic), the electrons diffuse in any directions. In the diffusion motion, displacement and time are related via $< x >= \sqrt{Dt}$, where D is the diffusion constant[4]. Consequently, the penetration length in a dirty metal is now $\xi^d_N = \sqrt{D/T}$, the exponent d stands for "dirty". In particular, $\xi^d_N \gg \lambda_F$, where λ_F is the Fermi wavelength. At low temperature, the penetration length $\xi_N = \xi^d_N$ still diverges. As a result, as we discussed in the next section, a supercurrent can flow in long $S/N/S$ junctions.

1.1.2 $S/N/S$ junctions and Andreev bound states

1 D ballistic case

Let us consider a normal metallic layer of length L sandwiched between 2 superconductors. In the metallic layer, the subgap quasi-particles cannot escape, they are trapped. Moreover, this superconducting potential well is for the formation of very peculiar quantized bound states which are current carrying (Josephson effect).

In a first step, we illustrate this effect by considering the simple case of a ballistic 1D junction, see Fig. 1.2.

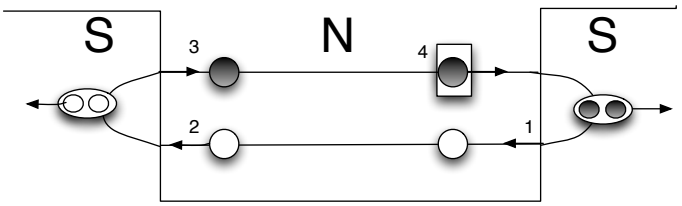

FIGURE 1.2: Andreev Bound State formation. Electrons are in black and holes in white. The rectangular box is the starting point of the process.

Let us consider a subgap quasi-electron of energy ϵ_+ from the normal layer impinging the right interface. Then:

[4] Between each impurity scattering the motion is ballistic and the electron's speed is v_F.

1. It is Andreev reflected as a quasi-hole of opposite velocity, ($\delta\phi_1 = -\arccos(\epsilon_+/\Delta) - \varphi_R$)
2. the reflected quasi-hole propagates to the left interface, ($\delta\phi_2 = -L.k_h(\epsilon_+)$)
3. it is Andreev reflected back as the quasi-electron, ($\delta\phi_3 = -\arccos(\epsilon_+/\Delta) + \varphi_L$)
4. the quasi-electron propagates back to the right interface (return to step 1). ($\delta\phi_4 = L.k_e(\epsilon_+)$)

where $k_{e/h} \sim k_F \pm \epsilon/\hbar v_F$.

Another possibility is to start with a subgap quasi-hole of energy ϵ_- and momentum $(-)k_h(\epsilon_-)$ impinging the right interface.

1. It is Andreev reflected as a quasi-electron of opposite velocity, ($\delta\phi_1 = -\arccos(\epsilon_-/\Delta) + \varphi_R$)
2. the reflected quasi-electron propagates to the left interface, ($\delta\phi_2 = +L.k_e(\epsilon_-)$)
3. it is Andreev reflected back as the quasi-hole, ($\delta\phi_3 = -\arccos(\epsilon_-/\Delta) - \varphi_L$)
4. the quasi-hole propagates back to the right interface (return to step 1). ($\delta\phi_4 = -L.k_h(\epsilon_-)$)

These processes are coherent. A bound state is formed when the phase accumulated between step 1. to 4. ($= \sum_i \delta\phi_i$) is a multiple of 2π. This gives the quantization of the bound state energy ($\epsilon_\pm$) [23], namely

$$-2\arccos(\epsilon_\pm/\Delta) \pm \varphi + L.(k_e(\epsilon_\pm) - k_h(\epsilon_\pm)) = 2n\pi, \tag{1.3}$$

where $\varphi = \varphi_L - \varphi_R$ is the phase bias between left and right superconducting reservoirs. The $\pm$ sign accounts for the "nature" of the bound state "seed" (a quasi-electron (+) or a quasi-hole(-)). Therefore, each $\pm$ set of bound states carries a current in opposite direction. These currents exactly cancel each other when the phase bias φ is a multiple of π. Otherwise an equilibrium (Josephson) current flows through the junction.

We can consider further two limiting cases: $L \ll \xi_N$ and $L \gg \xi_N$.

If $L \ll \xi_N$, Eq. (1.3) reduces to

$$-2\arccos(\epsilon_\pm/\Delta) \pm \varphi = 2n\pi. \tag{1.4}$$

Then only two degenerate levels exist at $\epsilon_+ = \epsilon_- = \pm\Delta\cos\varphi/2$.

Then in the limit $L \gg \xi_N$[5], we assume $L\,(k_e(\epsilon_\pm) - k_h(\epsilon_\pm)) = L\,k_F\epsilon_\pm/\mu$, such that

$$\epsilon_n^\pm = \frac{\hbar v_F}{2L}(\pi(2n+1) \pm \varphi). \tag{1.5}$$

The current flowing through the junction can be calculated from the thermodynamic potential of the system. In particular, the relation between the free energy $\mathcal{F}$ and the current reads

$$I = \frac{2e}{\hbar}\frac{\partial \mathcal{F}}{\partial \varphi}, \tag{1.6}$$

where φ is the phase bias across the junction.

For example, for a short junction, let us consider only the doubly degenerate levels of energies $\epsilon = \pm\Delta\cos(\varphi/2)$. Then, at zero temperature the negative energy state is doubly-occupied, and $\mathcal{F}(T=0) = -2\Delta(0)\cos(\varphi/2)$. Using Eq. (1.6), for $\varphi \in [-\pi, \pi]$, we obtain

$$I(\varphi) = N\frac{2e}{\hbar}\Delta(0)\sin\frac{\varphi}{2}, \tag{1.7}$$

where N is the number of independent channels of the contacts and $\Delta(0) = \Delta(T=0)$ [24]. Note that the CPR is 2π periodic, it is discontinuous at $\varphi = \pi[2\pi]$, see Fig. 1.3.a.

Thus, at $T = 0$, this relation departs from the usual Josephson relation of $S/I/S$ junctions $\propto \sin\varphi$ [25]. However, at finite temperature or with non-perfect interfaces, the CPR tends back toward the $\sin\varphi$ shape. This has been confirmed experimentally by [26], see Fig. 1.3.b.

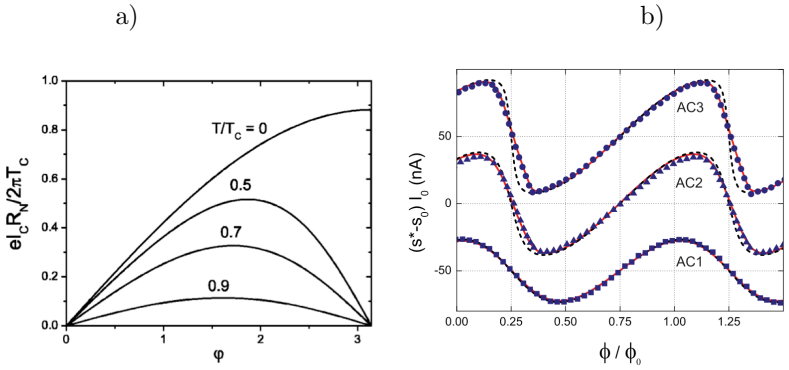

FIGURE 1.3: Current phase relation for a clean point contact a) Theoretical prediction at various temperature, from [27]. b) Experimental measurement for a point contact with three (AC1) and two (AC2, AC3) channels of different transmissions. Note the the evolution of the CPR from [26] a $\sin\frac{\varphi}{2}$ to a $\sin\varphi$ as temperature is raised or as the quality of the contact is lowered.

The idea is that the φ-dependence in the levels energy is the essence of the Josephson effect: a current can flow even at equilibrium without applying any voltage.

[5] actually $L < l_\phi$, where l_ϕ is the phase coherence length of the system.

Furthermore, for a long-junction, at $T = 0$, the current reads [28, 29]

$$I(\varphi) = \frac{2ev_F}{\pi L} \sum_{n>0} (-1)^{n+1} \frac{\sin n\varphi}{n}. \tag{1.8}$$

Thus, the CPR has a sawtooth shape, with sharp edges. At finite temperatures, the high harmonics are suppressed, and the current may reduce to a sinusoidal shape ($\propto \sin\varphi$).

Andreev bound states in 3 D

The multi-channel 1D case presented above does not account for a mixing between channels. What happens to the quantization of the Andreev bound states (ABS) in the real 3D case?

The difference with the quasi-1D presented in Eq. (1.7), is that we want to account for the incidence angle of a pair θ, see Fig. 1.4. Depending on θ, many paths with different lengths are available in the normal metal. Thus, the length Λ of a particular path is a continuous variable ranging from L to ∞. As an example, the path of length $\Lambda = L$ corresponds to the angle $\theta = 0$ in Fig. 1.4.a, while at $\theta = \pi/2$ the path is of infinite length. We may separate the propagation at zero and at finite energy to understand how the quantization stemming from Eq. (1.3) is changed. Namely, we find that

- at $\epsilon = 0$, Eq. (1.3) reads $-\pi \pm \varphi = 2n\pi$, thus for $\varphi \neq \pi$ there is no state at zero energy. However, it does not necessary imply that there is a gap in the energy spectrum.
- at any finite ϵ, we can always find an angle θ associated to a path of length Λ satisfying Eq. (1.3). Therefore, the spectrum is dense, and there is no gap.

Note that, the absence of states at $\epsilon = 0$ and the continuum above is called a pseudo-gap.

The diffusive $S/N/S$ junctions

From the ballistic to the diffusive limit, the situation is further changed. In particular, each impurity is a scattering center and even more paths are available. In particular, for

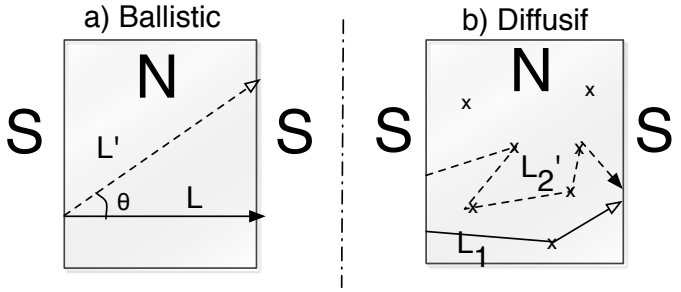

FIGURE 1.4: Andreev Bound states formation: a) in clean 3D samples: the length of a path depends on the incidence angle θ, it ranges from L to ∞ when $\theta = 0$ and $\theta = \pi/2$, respectively. b) in a dirty 3D sample (diffusive regime): each impurity is a diffusion center, the length of path is random.

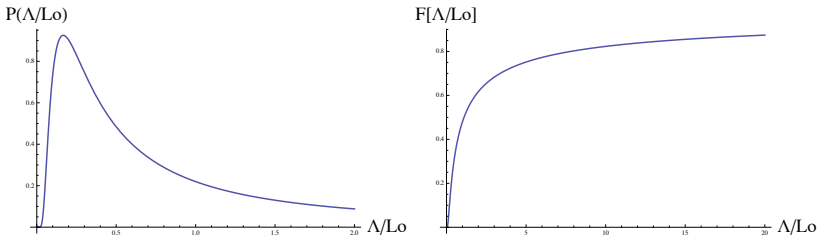

FIGURE 1.5: Length of a path, a) Probabilty distribution of the renormalized length of a path where $L_0 = L^2 v_F/D$. b) Cumulative distribution $F(\Lambda/L_0) = P(\Lambda \in [0, \Lambda])$.

a diffusive motion, the probability distribution for the length Λ of a path is given by [6]

$$P_L(\Lambda) = \frac{\sqrt{L_0}}{\sqrt{4\pi}\Lambda^{3/2}} \exp[-\frac{L_0}{4\pi\Lambda}], \tag{1.9}$$

where $L_0 = L^2 v_F/D = v_F/E_T$, ($E_T$ is the Touhless energy), see the plot in Fig. 1.4.c. Note that $P(\Lambda \in [0, L_0]) = 0.5$ and $P(\Lambda \in [0, 30L_0]) = 0.9$. As a result, most of the paths have a finite length see Fig. 1.4. The probability of infinite length, corresponding to the case $\theta = \pi/2$ in the ballistic case, is thus strongly reduced as compared with it. Inserting the length distribution in Eq. (1.3), we may conjecture that there is a continuum of states above a gap or mini-gap. The idea is that the lowest energy level arises from the contribution of the longest path and thus gives the amplitude of the mini-gap.

A proper derivation, using the Green function formalism, confirms this qualitative explanation. In particular, by solving the Usadel equation (see Chapter 2), we will see later that, the mini-gap depends on the phase bias as $E_g \simeq \min[\Delta, E_T] \cos(\varphi/2)$ [27, 30].

[6] The probability for a particle starting from $x = 0$ at $t = 0$ to reach $x = x_0$ at time t along one direction is given by $P_t(x_0) = \frac{1}{\sqrt{4\pi D t}} \exp[-x_0^2/(4Dt)]$, then the probability distribution of the time required to reach point x_0 or of first passage at x_0 is $P_{x_0}(t) = \frac{x_0}{t^{3/2}} \frac{\exp[-x_0^2/4Dt)]}{(4\pi D)^{1/2}}$. Then during a time t the electron propagates on $\Lambda = v_f t$, thus, $t = \frac{\Lambda}{v_F}$.

As a result, the current phase relation for a short $S/N/S$ junction is dominated by its first harmonic ($\propto \sin\varphi$) like in a $S/I/S$ junction.

1.1.3 Inverse proximity effect

Up to now, we considered only the induced correlation in a normal metal in contact with a superconductor. This "direct" proximity effect is due to the leakage of Cooper pairs in the adjacent layer. However, on the same time this leakage is a loss for the condensate, it weakens superconductivity close to the interface (inverse proximity effect). The inverse proximity effect happens on the coherence length ξ_S. As the typical size of a superconducting reservoir is much larger than ξ_S, we may usually neglect it. By contrast, for a thin superconducting film the effect of the inverse proximity effect is non-negligeable and should be included.

1.2 Proximity effect in ferromagnets: the interplay of ferromagnetism and superconductivity

As mentioned in the introduction, the proximity effect offers a unique opportunity to study the interplay between ferromagnetism and superconductivity.

In a ferromagnet, we assume that the magnetization is carried by ions (localized electrons). In a mean field approach, the spin of ions is "frozen" around its mean value and the exchange interactions between ions and itinerant electrons spin is given by

$$H_F = -\sum_{s,s'} \int \psi_s^\dagger(x)(\mathbf{h}(x).\boldsymbol{\sigma})_{s,s'}\psi_{s'}(x), \tag{1.10}$$

where the exchange field is $\mathbf{h}(x) = \sum_i J(x - x_i)\mathbf{S}_i$ where $\mathbf{S}_i$ is the spin on ions i and $J(x)$ is the exchange integral.

The Cooper pairs leaking in an adjacent ferromagnet feel this exchange interaction which acts on the spin of electrons forming a pair (paramagnetic limit).

It strongly impacts the proximity effect in ferromagnets. In particular, when the magnetization is homogeneous ($\mathbf{h}(x) = \text{const}$), the effective exchange field dephases the spin up and spin down electrons of a singlet pair and suppresses the superconducting correlations on a short length scale $\xi_F \ll \xi_N$, which we will derive in the following. The exchange interaction appears as the main source of decoherence rather than temperature. We will see that an inhomogeneous magnetization induces correlations between electrons of the

same spin. Such triplet correlations are insensitive to the presence of the exchange field restoring a long range proximity effect.

We first consider the homogeneous case, where the proximity effect is short range but yields a rich physics.

1.2.1 The π-junction

Similarly to the case of S/N/S junctions, we can measure the critical current through a homogenous ferromagnetic layer as a function of its thickness. The effect was predicted by the first time by Bulaevskii *et al.* [31] in a normal metal with magnetic impurities. Then, the current through an $S/F/S$ junction was first calculated by Buzdin *et al.* [32]. Many recent experiments confirmed the prediction [33–36].

Here we present the result of Obzonov *et al.* in a Nb/CuNi/Nb junction [37].

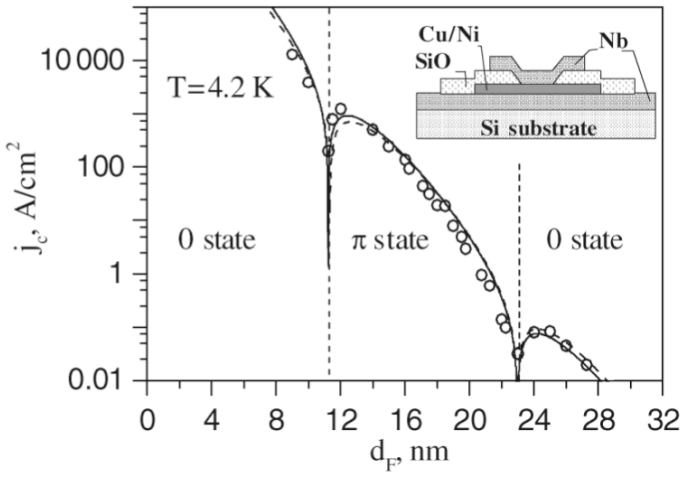

FIGURE 1.6: Critical current measurement from [37] on Nb/CuNi/Nb junction as a function of the CuNi ferromagnetic layer thickness.

As shown in Fig. 1.6, the critical current of the $S/F/S$ or π-junction, is oscillatory and exponentially decaying. As a function of the F layer thickness, it vanishes periodically between the region labelled by 0 and π, we will explain later this "labels".

Avoiding to deal with the complex Green function formalism, we now present the Demler *et al.* approach [38] in order to understand the oscillatory damped characteristic observed for the $\pi-$junction.

1.2.2 Homogeneous $S/F/S$ junction and the Demler picture

How does the singlet pairing state $|S\rangle$ penetrate a clean homogeneous ferromagnet? The singlet pair couples two electron with opposite momentum ($\pm p$) and opposite spin

$$|S\rangle = |\uparrow_p\downarrow_{-p}\rangle - |\downarrow_p\uparrow_{-p}\rangle. \tag{1.11}$$

When the singlet pair leaks into the ferromagnet, due to the exchange interaction the spin up electron of the singlet pair lowers its potential energy while the spin down electron raises it by the same amount. Because the total energy is conserved, this change in potential energy is compensated by a change in kinetic energy: the kinetic energy increases for the spin up electron and decreases for the spin down electron.

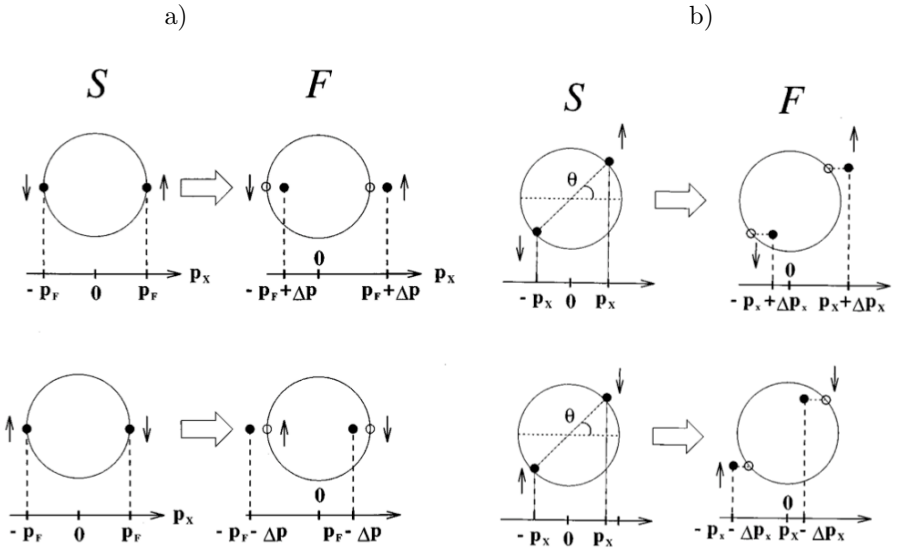

FIGURE 1.7: Proximity effect in a ferromagnet: leakage of a singlet pair from S to F a)1D case b) 3D case. Image from [38].

1D propagation in clean ferromagnet

For the propagation in a wire (1D) (see Fig. 1.7.a), the energy conservation principle for up and down electrons of initial momentum, $\boldsymbol{p} = \pm p_F \boldsymbol{e}_x$, reads

$$p_F^2/2m = (\pm p_F + \Delta p_{\pm\uparrow})^2/2m - \frac{h}{2}, \tag{1.12}$$

$$p_F^2/2m = (\pm p_F + \Delta p_{\pm\downarrow})^2/2m + \frac{h}{2} \tag{1.13}$$

where h is the exchange field, $\Delta p_{\pm\uparrow\downarrow}$ is the change in momentum as the electron enters F. Within the quasiclassical approximation ($\Delta p \ll p_F$), it yields to $\begin{cases} \Delta p_{\pm\uparrow} = \pm h/(2v_F) \\ \Delta p_{\pm\downarrow} = \mp h/(2v_F) \end{cases}$. Therefore, at a distance x from the perfect S/F interface, the initial singlet state $|S\rangle$ transforms as

$$|F(x)\rangle = e^{ix/\xi_F^c}|\uparrow_p\downarrow_{-p}\rangle - e^{-ix/\xi_F^c}|\downarrow_p\uparrow_{-p}\rangle, \tag{1.14}$$

where $\xi_F^c = 1/(\Delta p_{+\uparrow} + \Delta p_{-\downarrow}) = v_F/h$ is the ferromagnetic coherence length in the ballistic case (clean sample).

Essentially, $|F(x)\rangle$ is a superposition of singlet and triplet correlations with zero spin projection along the magnetization axes ($\boldsymbol{S} = 1, S_z = 0$)

$$|F(x)\rangle = \cos\left(\frac{x}{\xi_F^c}\right)|S\rangle + i\sin\left(\frac{x}{\xi_F^c}\right)|T_0(0)\rangle, \tag{1.15}$$

where $|T_0(\theta = 0)\rangle = |\uparrow_p\downarrow_{-p}\rangle + |\downarrow_p\uparrow_{-p}\rangle$ is the triplet pairing state with electrons of opposite spin along the magnetization axes (θ).

Interestingly, this 1D ballistic case illustrates the oscillatory behavior of the critical current! For instance, let us consider the $S/F/S$ junction where F is a ferromagnetic "wire" of length L. The singlet correlations from the left lead propagate towards the right lead and transform as $\psi_s^L(L) = \psi_s^L(0)\cos(2qL)$. In particular, at the right interface ($x = L$), it may induce a Josephson current [25] $I \propto \psi_s^L(L)\psi_s^R(L)\sin(\varphi_L - \varphi_R)$, namely,

$$I \propto \psi_s^R(0)\psi_s^L(0)\cos\left(L/\xi_F^c\right)\sin\left(\varphi_L - \varphi_R\right). \tag{1.16}$$

Note that the triplet correlations present at $x = L$ do not contribute to this current. Thus, the critical current may be cast in the form $I_c = I_0\cos\left(L/\xi_F^c\right)$, it is oscillating as a cosine and changes sign when $L = 2\pi\xi_F^c n$ for $n \in \mathbb{N}$. When $\cos\left(L/\xi_F^c\right) < 0$, the current phase relation may be rewritten as $I = |I_c|\sin\left(\varphi + \pi\right)$ with a positive value for critical current. This π-shift justifies the appelation "$\pi-$junction". Note that in the 0 and π regions, at a fixed phase bias, the current flows in opposite direction.

While this very simple case explains the oscillatory pattern of the critical current of the $S/F/S$ junction, it cannot explain its damped behavior. To carry on, we first turn to a 3D model and then include impurity scattering to describe dirty metals.

3D propagation in clean ferromagnet

Let us consider the propagation in 3D. The momemtum can now be decomposed as : $\boldsymbol{p} = p_x\mathbf{e}_x + p_y\mathbf{e}_y + p_z\mathbf{e}_z$, see Fig. 1.7.b.

Here, the energy conservation for a singlet pair leaking in the ferromagnetic reads: $\boldsymbol{p}^2/2m = (\boldsymbol{p}+\Delta\boldsymbol{p})^2/2m \pm h$. Within the quasiclassical approximation and because momentum is conserved in the direction parallel to the interface, we obtain: $\Delta p_x = h/v_F\cos\theta$, $\Delta p_y = 0$, $\Delta p_z = 0$, where θ is the angle of incidence of the singlet Cooper pair[7].

Let us now consider the propagation from one side to the other. The induced singlet correlations at a distance L are obtained by summing over all angles of incidence ($\frac{1}{4\pi}\int\int \sin\theta\, d\phi\, d\theta \ldots$), namely,

$$\psi_s(L) = 1/2\int \sin\theta d\theta \cos\left(Lh/(v_F\cos\theta)\right) = 1/2\int d(\cos\theta)\cos\left(Lh/(v_F\cos\theta)\right). \quad (1.17)$$

After integration, we obtain

$$\psi_s(L) = -\pi(L/\xi_F^c) + 2\cos\left(L/\xi_F^c\right) + (L/\xi_F^c)\mathrm{Sint}(L/\xi_F^c)), \quad (1.18)$$

where $\xi_F^c = v_F/h$ is the penetration in the clean limit and Sint is the sinus integral function. The induced singlet correlation $\psi_x(L)$ is plotted in Fig. 1.8.

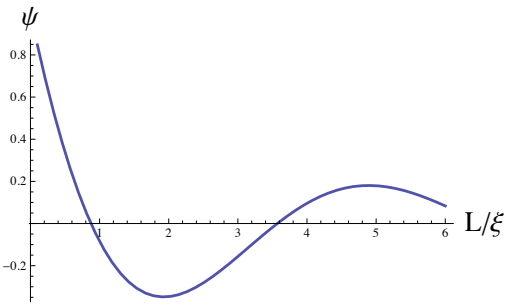

FIGURE 1.8: Amplitude of the singlet correlation as a function of L/ξ_c in the clean case→ ballistic motion. The penetration is oscillatory with an algebraic decay $\propto \xi_c/L$.

Therefore, for ballistic motions in 3D, the singlet correlations penetrate with a linear decay in the clean ferromagnet and oscillates with a typical length $\xi_F^c = v_F/h$.

What happens in a dirty ferromagnet? What is the effect of the multiple elastic scattering events on the Cooper pair coherence?

[7] the vector $\hat{p}$ on the unitary sphere reads $\hat{p} = (\cos\theta, \sin\theta\cos\phi, \sin\theta\sin\phi)$, θ and ϕ are the spherical coordinates

Average over disorder

To answer the above question, let us consider the case of a dirty ferromagnet in the diffusive limit, where D is the diffusion constant and $1/\tau$ is the elastic scattering rate.

In addition to the average over angles of incidence performed in the clean case, we need now account for the scattering on impurities and sum over all possible paths.

In the diffusive limit, the length of each path is a random variable Λ .The probability distribution of Λ is given by Eq. (1.9), namely

$$P_L(\Lambda) = \frac{\sqrt{L_0}}{\sqrt{4\pi}\Lambda^{3/2}} \exp[-\frac{L_0}{4\pi\Lambda}], \tag{1.19}$$

where $L_0 = L^2 v_F/D$ is the mean length of a path. Note that we already used this distribution for the proximity effect in the normal metal.

Introducing $\overline{\psi_s(L)}$ the averaged singlet correlation at a distance L from the interface, we find

$$\overline{\psi_s(L)} = 1/2 \int d(\cos\theta) \int d\Lambda\, P_L(\Lambda) \cos\left(\Lambda h/(v_F \cos\theta)\right), \tag{1.20}$$

which after integrating over the distribution of lengths (Λ) yields

$$\overline{\psi_s(L)} = \int d\theta\, \exp\left[-L/(\xi_F|\cos\theta|)\right] \cos\left[-L/(\xi_F|\cos\theta|)\right], \tag{1.21}$$

where $\xi_F^d = \xi_F = \sqrt{D/h}$ is the ferromagnetic penetration length (in the diffusive case).

In particular, assuming that the largest contribution in Eq. (1.21) arises from small θ angles, we may simplify Eq. (1.21) to

$$\overline{\psi_s(L)} \simeq \exp\left[-L/(\xi_F)\right] \cos\left[-L/(\xi_F)\right]. \tag{1.22}$$

Thus, in the dirty ferromagnet, the oscillatory behavior of singlets is modulated by an exponential decay! See figure 1.9.

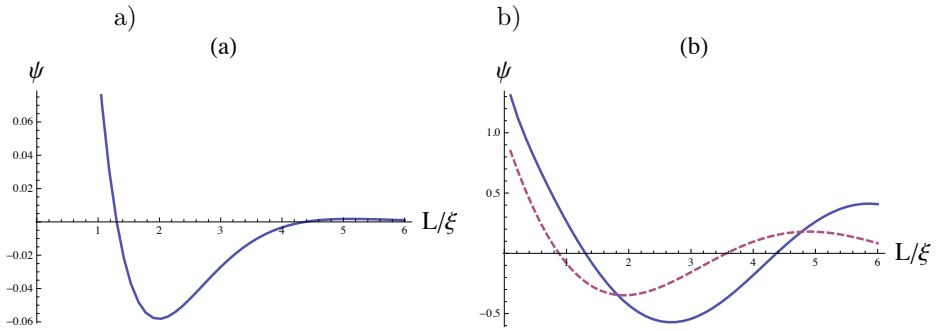

FIGURE 1.9: Penetration of singlet correlations in a ferromagnet. a) Penetration of singlet correlations as a function of L/ξ_F, the oscillations are exponentially damped. b) Representation of $\exp(L/\xi_F).\overline{\psi_s}(L/\xi_F))$ (blue line) and $\psi_s(L/\xi_F^c))$ (red dashed line) to compare the oscillatory behavior in both dirty and clean limit. It confirms that the extra decay in dirty metals is $\propto \exp(L/\xi_F)$.

1.2.3 Non-homogenous magnetization

In the previous section, we showed that a homogeneous magnetization generates triplet correlations between electrons of opposite spins. The latter get dephased by the presence of the exchange field and are exponentially suppressed with distance.

Let us now study the proximity effect in the presence of a non-homogeneous magnetization [15]. We consider an $S/F'/F$ structures where F'/F is a bilayer ferromagnet with non-colinear magnetization with

$$\boldsymbol{h}(y) = \begin{cases} h\,\mathbf{n} & \text{in } F' \\ h\,\boldsymbol{e}_z & \text{in } F, \end{cases} \tag{1.23}$$

where $\mathbf{n} = \cos\theta \boldsymbol{e}_z + \sin\theta \boldsymbol{e}_x$ and θ is the relative angle between the magnetizations,

Below, we depict the three-steps mechanism leading to the generation of triplet superconducting correlations between electrons of the same spin ($\boldsymbol{S} = 1, S_z = \pm 1$).

1. Singlet Cooper pairs $|S\rangle$ leak into F',
2. in F', the quantification axis for the spin is $\mathbf{n}$. As previously seen, $|S\rangle$ transforms as a mixture of singlet $|S\rangle$ and triplet ($\mathbf{S} = 1, S_\theta = 0$),where $|T_0(\theta) = (|\swarrow\nearrow\rangle + |\nearrow\swarrow\rangle)$, the θ-label refers to the magnetization direction in the xz-plane. Then, such superconducting correlations further leak in F.

3. In F, the magnetization is along $\mathbf{e}_z$. Thus, we project the pairing state on the $\mathbf{e}_z$ axes, using

$$|\nearrow\rangle \mapsto \cos\frac{\theta}{2}|\uparrow\rangle + \sin\frac{\theta}{2}|\downarrow\rangle, \tag{1.24}$$

$$|\swarrow\rangle \mapsto \cos\frac{\theta}{2}|\downarrow\rangle - \sin\frac{\theta}{2}|\uparrow\rangle. \tag{1.25}$$

We obtain

$$|\nearrow\swarrow\rangle = \cos^2\frac{\theta}{2}|\uparrow\downarrow\rangle - \sin^2\frac{\theta}{2}|\downarrow\uparrow\rangle + \sin\frac{\theta}{2}\cos\frac{\theta}{2}(|\downarrow\downarrow\rangle - |\uparrow\uparrow\rangle), \tag{1.26}$$

$$|\swarrow\nearrow\rangle = \cos^2\frac{\theta}{2}|\downarrow\uparrow\rangle - \sin^2\frac{\theta}{2}|\uparrow\downarrow\rangle + \sin\frac{\theta}{2}\cos\frac{\theta}{2}(|\downarrow\downarrow\rangle - |\uparrow\uparrow\rangle). \tag{1.27}$$

Therefore in the rotated spin frame, we find

$$|S\rangle \mapsto |S\rangle, \tag{1.28}$$

$$|T_0(\theta)\rangle \mapsto \cos\theta|T_0(0)\rangle + \sin\theta(-|\uparrow\uparrow\rangle + |\downarrow\downarrow\rangle), \tag{1.29}$$

Thus, if $\theta \neq 0, \pi$ triplet correlation between electrons with parallel spins ($\boldsymbol{S} = 1, S_z = \pm 1$) are induced in the second ferromagnetic layer F. Those correlations are insensitive to the presence of the exchange field in F and penetrate over a long-range in the ferromagnet. However, note that in order to generate a non-negligeable proportion of triplet pairs, the thickness of F' should be neither too long nor too short with respect to the ferromagnetic penetration length (ξ_F). We will discuss the optimal thickness of the F' layer in Chapter 3.

1.2.4 Long-range supercurrent through a tri-layer ferromagnet

After many theoretical predictions [10, 15, 39, 40], recently, such a long-range proximity effect through ferromagnets has been observed [13, 14, 41].

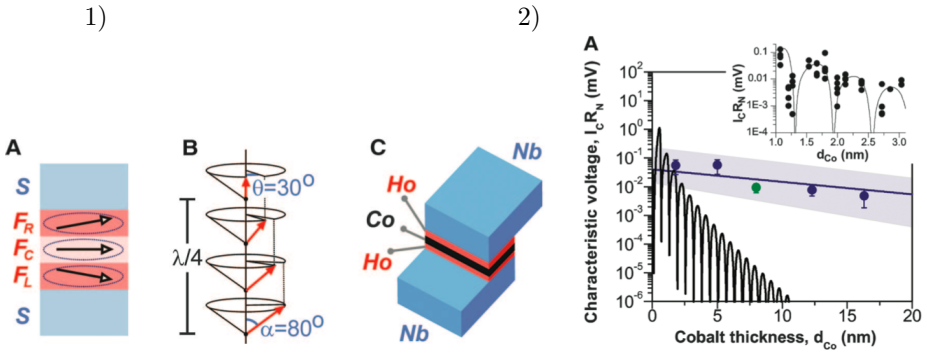

FIGURE 1.10: Experimental setup and results of Blamire *et al.* [13] 1 A) Theoretical model of the junction $S/F_L/F_C/F_R/S$, two singlet superconductors are connected through a non-collinear trilayer ferromagnet. 1B) Idealized holmium helical magnetization, the magnetic moment is rotating. 1C) Real device layout: 2 Nb electrodes are connected via a Ho-Co-Ho tri-layer. 2) Critical current measurement as a function of the cobalt layer thickness. Note the slow decay of experimental points as compared with the numerical simulation of a π-junction. The inset shows the exponential decay and oscillatory behavior of the critical current in absence of the holmium layer (Experimental), figures from [13].

The trilayer ferromagnet used by [13] consists of a cobalt layer sandwiched between two short layers of Holmium. The Holmium has the particularity to have a helical magnetization, such that the magnetization is not homogeneous. The critical current was measured with and without the extra holmium layer as a function of the Cobalt thickness (d_{Co}), see Fig. 1.10.

1. Without the Holmium, they recover the pattern of a π- junction with a short-range and oscillatory proximity effect, see the inset in Fig. 1.10.

2. With the extra Holmium layers, they measure a non-oscillatory long range proximity effect up to $d_{Co} = 10\xi_F$.

While the trilayer geometry was believed to be the minimal setup to observe a long-range proximity effect, in chapter 3, we show that it may also exist in bilayer geometry.

1.2.5 Inverse proximity effect

When discussing the proximity effect in superconducting/normal junctions, we mentioned, that while the leakage of Cooper pairs induces superconducting correlations, simultaneously it weakens superconductivity. This effect is even richer when dealing with superconductor/ferromagnet proximity effect. It has been predicted [42–45] that the critical temperature of a superconducting layer sandwiched between two ferromagnetic layers depends on their relative magnetization orientation: T_c is higher for an

antiparallel (AP) than for a parallel orientation (P). Note, however, that when the superconducting layer is of atomic thickness, the result is opposite, namely, $T_c^{AP} < T_c^P$ [45].

The explanation is that in the AP case, the mean exchange field seen by the Cooper pair is zero, due to the cancelation of the proximity effect from the left and right ferromagnetic leads, see Fig. 1.11. The first experimental evidences of the effect were obtained by Hauser (1969,[46]) using Indium films sandwiched between two ferromagnetic insulators and by Deutscher and Meunier [47], on an Indium film between two (metallic) oxydized FeNi layers.

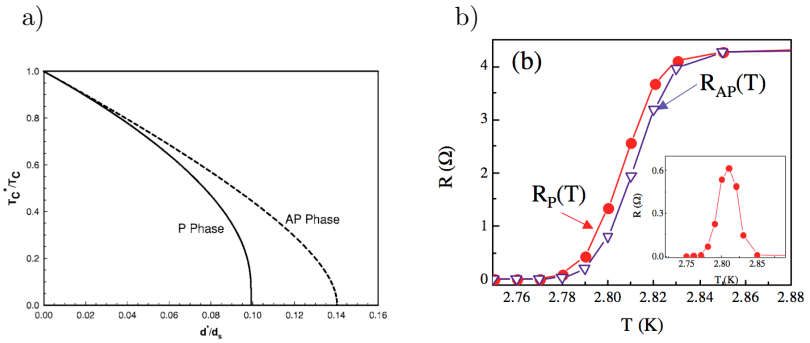

FIGURE 1.11: Critical temperature and magnetization of adjacent ferromagnetic layers. a) Calculated superconducting critical temperature as a function of the reduced half thickness of S d^*/d_S ($d^* \propto \xi_F$) in a $F/S/F$ trilayer [43]. b) Measurement of the resistivity (R) in the P and AP magnetizations on a Py/CuNi/Nb/CuNi/Py junction by Gu *et. al*[48]. R is larger in the P than in the AP case.

1.2.6 Singlet even-frequency versus triplet odd-frequency

1.2.6.1 Symmetries

Due to the Pauli principle, the wavefunction of a Cooper pair is anti-symmetric under the exchange of the electrons forming the pair. The wavefunction depending on space (orbital part), spin, and time (energy or frequency), we will consider below its symmetries with respect to all these quantities.

A singlet state is an anti-symmetric combination of electrons with opposite spin, therefore, the wavefunction is necessary either symmetric or antisymmetric in both space and time[9, 49]. By contrast, in a triplet state, the wave function is symmetric in spin, thus it is either antisymmetric in space (e.g. p-wave) and symmetric in time (even-frequency) or symmetric in space (s-wave, d-wave) and antisymmetric in time (odd-frequency).

In this thesis, we deal with the proximity effect in dirty metals, where, due to multiple impurity scatterings, the motion is mainly isotropic: the scattering suppresses all non s-wave pairing. As a result, the wavefunction of a pair is necassary symmetric in space and, a singlet state is even in frequency (ESE) while a triplet state is odd in frequency (OTE).

1.2.6.2 Modication of the density of states

Conventional superconductivity opens a gap in the density of states as the electrons condense in singlet pairs in a window of width Δ around the Fermi energy. In particular, the density of states (DoS) is

$$\nu(\epsilon) = \nu_0 \,\mathrm{Re}\,[(\mathrm{sign}(\epsilon))/\sqrt{\epsilon^2 - \Delta^2}], \tag{1.30}$$

it presents singlularities at $\epsilon = \pm\Delta$. When the superconductivity is induced via the proximity effect in a normal metal, the DoS of the normal metal features a reduced gap called minigap (E_g). The minigap can be large close by a transparent interface and dies on the large scale $\xi_N = \sqrt{D/T}$. Now, what happens when the metal is a ferromagnet? As aforesaid, the electrons feel the exchange interaction and the spin up and spin down excitations are Zeeman-split. We may distinguish different cases.

- The case of a small ferromagnetic node attached to a superconductor of typical size L, with $L \ll \xi_F$, is the simplest example[8] to start with. In particular, we expect the DoS to be

$$\nu_F(\epsilon) = \nu_0 \mathrm{Re}[1/2 \sum_{\pm} (\mathrm{sign}(\epsilon \pm h))/\sqrt{(\epsilon \pm h)^2 - E_g^2}], \tag{1.31}$$

  where E_g is the induced mini-gap. Due to the Zeeman interaction, up and down spin excitations are split, and the singularities shift at energies $E_g \pm h$ and $-E_g \pm h$, see Fig. 1.12 and Ref. [50]. While if $E_g > h$, a reduced gap survives ($\nu(0) = 0$), when $E_g < h$ the DoS is finite at zero energy, namely $\nu(0)/\nu_0 > 1$. Note that the case $E_g = h$ is resonant and the DoS features a peak a zero energy (ZEP)[51].

[8] It allows to neglect the spatial variation.

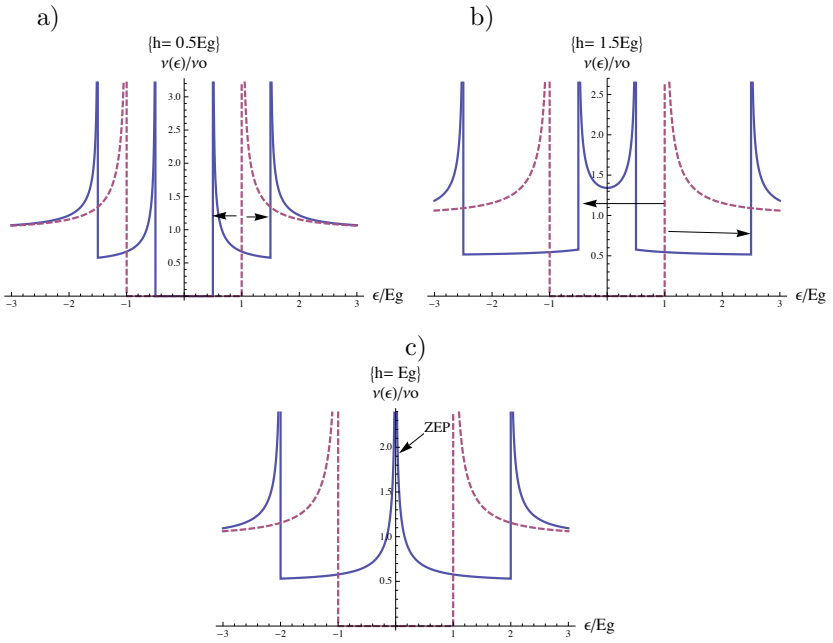

FIGURE 1.12: DoS in a small ferromagnet in contact with a superconductor, h is the exchange field in the ferromagnet and E_g is the induced minigap in the normal metal. The Dashed line represents the case $h = 0$ (normal metallic node), the singularities are at energies $|\epsilon| = E_g$, see [50]. a) $h < E_g$. b)$h > E_g$. c))$h = E_g$. The singularities are Zeeman split (arrows) and moves at energies $|\epsilon| = |E_g \pm h|$. Note that in case b) $h > E_g$, the DoS is finite at zero energy. Case c) is the resonant case, the DOoS features the ZEP (zero energy peak).

- When the length of the ferromagnet is of the order of ξ_F, as seen in the previous section, the wave function of singlet correlations is damped and oscillatory. The oscillation of singlet correlations is related to the generation (in anti-phase) of its triplet partner. It means that at some distance from the S/F interface, when the singlet correlations are minimal the triplet correlations are maximal and vice versa. At low energy, the density of states (DOS) follows these oscillations: a maximum of singlet correlations generates a dip, while a minimum (maximum for triplet correlations), gives a dome. Kontos *et al.* [52] have observed these oscillations via conductances measurements on two $Al/Al_2O_3PdNi/Nb$ junctions of different thicknesses of the PdNi layer, see Fig 1.13.

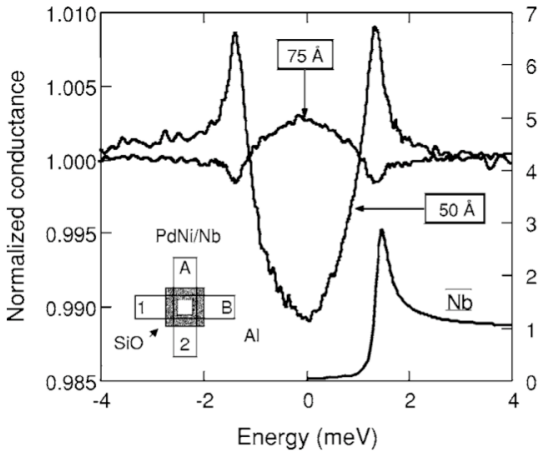

FIGURE 1.13: Differential conductance measurements by Kontos on Al/PdNi/Nb junctions, for two thicknesses of PdNi. For $d = 75A$ the density of states is peaked at zero energy.

To better illustrate the origin of the oscillations in the DoS measured by Kontos, we anticipate chapter 2 on quasi-classical Green functions and combine it with the qualitative results of Delmer presented in section (1.2.2). The quasiclassical Green function for diffusive metal is a matrix in Nambu (electron-hole space) and spin spaces , $\hat{g} = (g_0 + g_z\sigma_z)\tau_z + f_0 + f_z\sigma_z)\tau_x$[9]. In particular, $(g_0 + g_z\sigma_z)$ is the normal Green function and $(f_0 + f_z\sigma_z)$ is the anomalous part (f_0 and f_z are related respectively with singlet and triplet superconducting correlations). Additionally, g satisfies the normalization $\hat{g}^2 = 1$. Then, a simple calculation shows that $(g_0 \pm g_z)^2 = 1 - (f_0 \pm f_z)^2$, thus

$$g_0 = \frac{1}{2}\sum_{\pm}\sqrt{1 - (f_0 \pm f_z)^2}. \tag{1.32}$$

The advantage is that the low energy DoS ($\epsilon = 0$) is directly related to the normal Green function g_0 via

$$\nu(\epsilon = 0) = \nu_0 \mathrm{Re}[g_0(x, \epsilon = 0)], \tag{1.33}$$

where x is distance from the S/F interface.

We may now use the results of the Demler approach presented in section (1.2.2). In particular, Eq. (1.22) may be rewritten as

$$f_0(x) = \bar{\psi}_s(x) \simeq \frac{1}{2}\sum \exp\left[(1 \pm i)x/\xi_F\right], \tag{1.34}$$

[9] τ and σ are the Pauli matrices in the Nambu and spin spaces respectively. Here we have chosen the magnetization along the z direction

where, using Eq. (1.15) we see that the derivation of Eq. (1.22) intrinsically implies that: $\exp(1 \pm i)x/\xi_F \simeq f_0 \pm f_z$[10]. Additionally, in the limit $x \gg \xi_F$ the amplitude of induced correlations is small, we may expand at lowest order Eq. (1.32) to obtain

$$\nu(\epsilon = 0) \sim \nu_0(1 - \frac{1}{2}\cos(2x/\xi_F)e^{-2x/\xi_F}), \text{when } x \gg \xi_F. \tag{1.35}$$

The DoS is oscillatory, it is enhanced at zero energy when $x \sim (2n+1)\pi\xi_F/2$, correponding to the 75 A-long sample on Fig. 1.13) and gets a minimum when $x \sim 2n\pi\xi_F/2$ corresponding to the 50A long sample of Kontos .

The density of states for superconductor with all possible symmetries in spin, space and frequency has been further studied by [51, 53, 54]. In particular, they predict for a wide range of parameters (exchange field, transmission...) that when the triplet odd-frequency correlations are dominant, the density of states features a zero energy peak (ZEP), see Fig. 1.14.

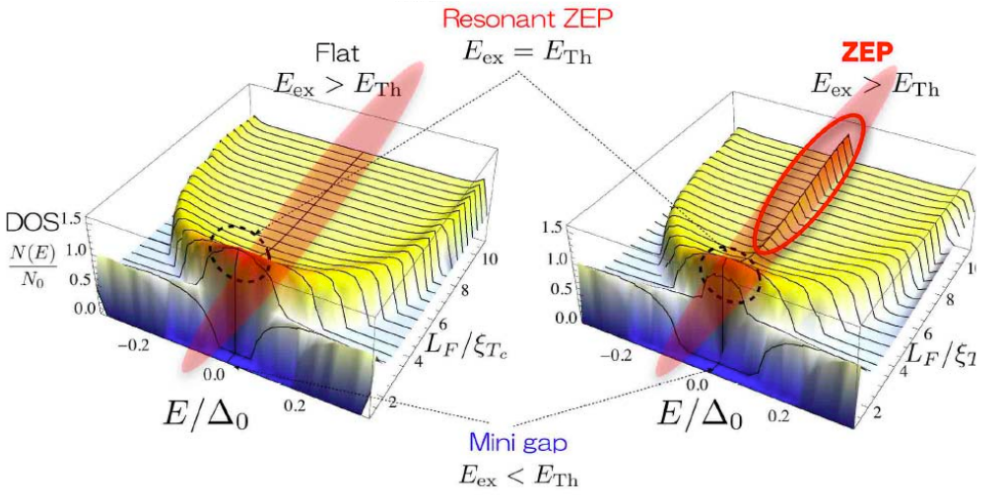

FIGURE 1.14: Zero Energy Peak [51]. Plot of the density of states induced in a ferromagnetic layer (S/F junction) as a function of the distance from the S/F interface (L_F). The left plot corresponds to the case of an homogeneous magnetization of the F layer, the ZEP dies exponentially like short-range triplets, whereas in the right plot shows the magnetization is inhomogenous, triplet correlations survives on a long range and generate a ZEP far from the interface.

1.2.7 Spin probe and Andreev reflection

In the Andreev reflection, an electron of spin up (resp. down) is reflected as an spin-down (resp. up) hole to enter a conventional superconductor, therefore, both spin bands

[10] More precisely, " $f_0 + f_z$" (resp. "$f_0 - f_z$") corresponds to the correlations in the $|\uparrow\downarrow\rangle$ state (resp. $|\downarrow\uparrow\rangle$ state), see (1.11).

contribute.

Up to now we neglected such splitting. How is the Andreev reflection modified in a ferromagnet when we include such spin band splitting and thus $\nu_\uparrow \neq \nu_\downarrow$[11]? Essentially, in half metals only one spin species is present, and thus the Andreev reflections are suppressed: the proximity effect vanishes. When the polarization is finite, we can compare the conductances of the F/N and F/S interfaces ($G_{F/N}$ and $G_{F/S}$) [20].

- For an F/N junction, the Landauer formula yields $G_{FN} = e^2/\hbar(N_\uparrow + N_\downarrow)$, $N_\downarrow$ and $N_\uparrow$ are the number of spin-down and spin-up channels.
- For a superconducting contact with a normal metal, the feature of Andreev reflection is that it doubles the conductance, indeed, one reflection = 2 electrons: $G_{SN} = 2e^2/\hbar(N_\downarrow + N_\uparrow)$ (note that here $N_\downarrow = N_\uparrow$).
- In the case of a ferromagnet, assuming $N_\downarrow < N_\uparrow$, since only $\tilde{N}_\downarrow = N_\downarrow - (N_\downarrow - N_\uparrow)$ spin down electron up can find a spin up partner, we obtain

$$G_{SF} = 2e^2/\hbar(\tilde{N}_\downarrow + N_\uparrow) = 4e^2/\hbar N_\uparrow \tag{1.36}$$

Therefore, if $P = (N_\downarrow - N_\uparrow)/(N_\downarrow + N_\uparrow)$ is the polarization, we obtained

$$G_{SF}/G_{FN} = 2(1 - P). \tag{1.37}$$

As a result, an Andreev spectroscopy (with a superconducting tip) realizes a probe to measure the polarization of a ferromagnet [55, 56].

1.3 Spintronics and superconductivity

1.3.1 Spintronics

1.3.1.1 From GMR to SRam devices

Spintronics emerged in the 1980s, with the discovery of spin dependent transport phenomena, in 1985 Johnson and Silsbee [57] observed the injection of spin polarized electrons at an F/N interface. In 1988, independently the groups of A. Fert [58] and P. Grunberg[59] discovered the giant magneto resistance effect (GMR). In addition to the

[11] Note that the assumption of the quasiclassical approximation is that $\frac{\delta\nu}{\nu_0} \sim \frac{h}{\epsilon_F} \ll 1$, where $\delta_\nu = \nu_\uparrow = \nu\downarrow$ and thus the approximation is $\nu_0 = \nu_\uparrow = \nu\downarrow$ where the band splitting is neglected.

charge of the electrons, spintronics aims at exploiting the spin and magnetic moment as additional degrees of freedom to encode and transfer information.

The GMR effect is observed by driving a current through a collinear bilayer ferromagnet. When the magnetizations are parallel (P) the resistance is lower than when they are antiparallel (AP). Nowadays, this effect is still widely used in the hard drive memories to write and read information. The data are recorded by magnetizing ferromagnetic domains via an external local field, e.g. the bit 0 corresponds to an up magnetization (↑) and the bit 1 corresponds to a down magnetization (↓). Then the data can be read by approaching a polarized head and measuring the resistance: low resistance means parallel magnetizations (P) between the head and the domain (read bit 0) while high resistance corresponds to AP magnetization (read bit 1). While this type of memory is non-volatile compared to RAM, the main drawback is the mechanical arm required to position the head during the writing and reading processes.

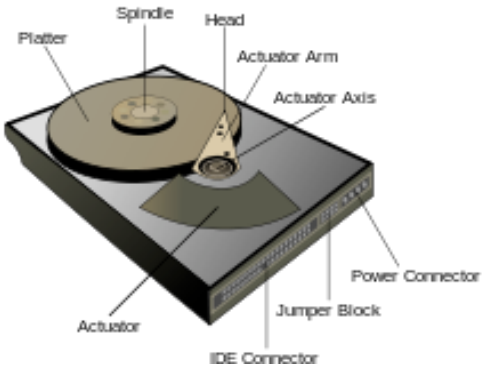

FIGURE 1.15: Hard drive

To suppress the mechanical arm, the idea is to use the spin transfer torque effect: a spin current exerts a torque on the magnetization and may thus revert it [60, 61]. While the external arm is replaced by an electrical contact on chip, the main difficulty is now to generate highly spin polarized currents. Such memories are called SRAM and are on their way to commercialization.

1.3.1.2 Ferromagnetic resonance and voltage generation

While a spin-current exerts a torque on the magnetization, the reverse effect has been predicted [62]. Namely a spin current can be dynamically produced by the precession of the magnetization. This effect is called spin-pumping.

The required precession of the magnetization is observed in a ferromagnet at ferromagnetic resonance (FMR). This effect is nowadays widely used to probe spin waves and

spin dynamics. The ferromagnetic resonance can be induced by shining light on a ferromagnet. The magnetization dynamics is well describe by the Landau-Lifshitz-Gilbert equation

$$\partial_t \boldsymbol{m} = -\gamma \boldsymbol{m} \wedge \boldsymbol{H}_e + \alpha \boldsymbol{m} \wedge \partial_t \boldsymbol{m} \tag{1.38}$$

where H_e is the external applied magnetic field, γ is the electron gyromagnetic ratio and α is a phenomenological damping parameter. In the absence of damping, an non-colinear external dc-field would drive the precession of the magnetization at frequency $\Omega = \gamma H_e$ for ever. The damping term tends to align the magnetization with the external field. The presence of an extra rf-field permits to maintain the precession. The relation between the resonant frequencies and amplitude of the dc-field have been calculated by Kittel [63, 64], they depend on the geometry of the sample. As an example, in the case of a film with parallel applied field, the Kittel formula reads $\Omega = \gamma\sqrt{H_e(H_e + ||\boldsymbol{m}||)}$.

How to measure this predicted FMR generated spin current? In the absence of direct spin probe, the idea was forward to use a second ferromagnet as an analyzer that converts the spin current into a charge current. Subsequently, it is was pointed out both theoretically [65] and experimentally [66, 67] that a single ferromagnet is enough to both generate and detect a spin current. Namely, Costache *et al.*[12] have performed voltage measurement on $N'/F/N$ junctions, where F is a ferromagnetic wire and N' and N are the left and right leads. They measured the voltage accross the junction as a function of the amplitude of the applied dc field and the rf frequency. For non-symmetric junctions, i.e. when N and N' are different, they record voltage peaks when the rf frequency matched the resonance frequency of FMR. Note than for symmetric junctions, the voltage peaks disappear. See Fig. 1.16.

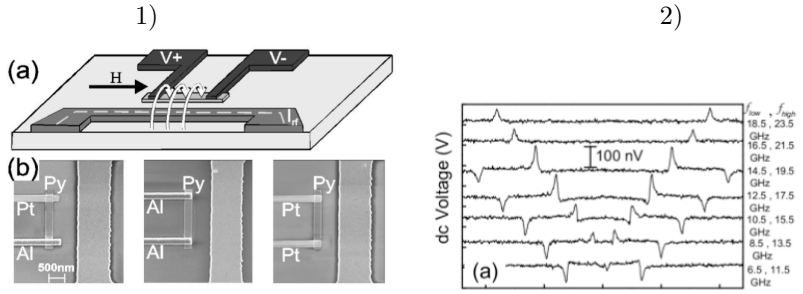

FIGURE 1.16: Voltage peaks at FMR 1a)Setup of Costache's experiment: the rf field is generated by an rf current (I_{rf}). 1b)They use two types of normal metal electrodes Al and Pt to fabricate and perform measurements on three junctions, : Al/Py/Pt , Al/Py/Al and Pt/Py/Pt. b)Voltage measurement as a function of the dc field amplitude for different rf frequencies on the asymmetric A/Py/Pt electrode. Picture taken from [66]

[12] Moriyama *et al.* have performed similar experiments [67]

The asymmetric spin accumulation in the electrodes due to the spin pumping effect is at the origin of the phenomenon. In addition, if the transmission of the majority and the minority spin are different, the difference in spin accumulation comes with a charge accumulation in an open circuit geometry. In an closed circuit geometry the charge accumulation yields a net charge current. For a symmetric junction, we can guess that the currents on each side compensate and the voltage peak disappears. Note that spin relaxation inhibits the spin accumulation and is damageable to the effect.

Thus the FMR is an alternatively way to the voltage induced GMR effect to produce a spin current.

1.3.2 Superconductivity and spintronics

Superconductors are attractive due to their dissipationless nature of the supercurrents. A current can flow without heating! At first sight, the ability to combine spintronics and superconductivity is thus promising to tackle the problem of heating. However, as suggested in the previous section due to the antagonist nature of superconductivity and ferromagnetism, the combination of spintronics and superconductivity might be even richer.

1.3.2.1 Spin valves

For example, an absolute spin valves effect and 100% polarization current can be obtained thanks to the proximity effect in a trilayer $S/N/F$ structure. In the normal metal, on one side the S superconductor induces a minigap (E_g) which is Zeeman split (h) due to the proximity of the ferromagnet on the other side. In particular, if $h < E_g$, in the energy window $[E_g - h, E_g]$ the quasiparticles are fully spin polarized allowing to achieve a 100% polarized current. Huertas and Nazarov [68] have proposed the extension to the absolute spin valve effect by coupling two $S/N/F$ trilayers junctions, see Fig. 1.17.

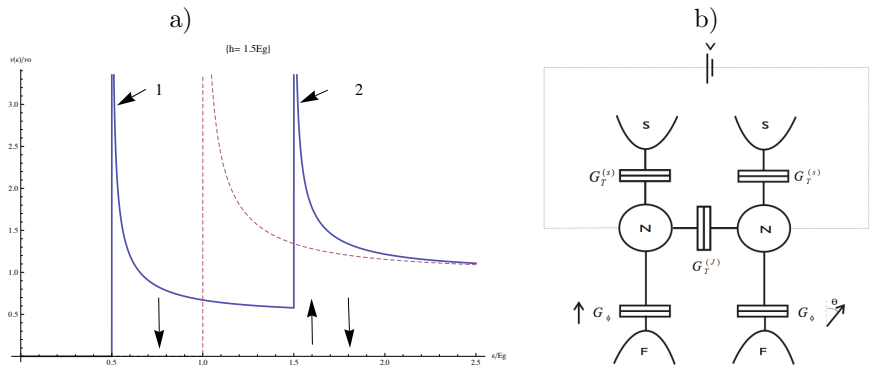

FIGURE 1.17: a) DOS of a normal metal sandwiched with between a superconductor and a ferromagnet ($S/N/F$ junction). Due the Zeeman splitting, between the two singularities (arrow 1 and 2) the quasiparticle are fully spin polarized. b) Coupled $F/N/S$ trilayers. For parallel magnetization the valve is open and the current 100% polarized. For anti-parallel the valve is closed.

Another type of spin valves has already been presented in the previous section: in $F/S/F$ junction the resistance is much lower in the AP case than in the P case.

Magnetic moment manipulation

As aforesaid, the magnetization strongly affects the symmetries and the penetration of induced superconducting correlations in ferromagnets. In particular, pure ferromagnetism and superconducting correlations with zero spin projection (along the magnetization axes) appear "incompatible". As a result, the latter correlations penetrate over a short range in homogeneous ferromagnet. Meanwhile, the opposite effect is true. As an example, Ref. [69] showed that, a singlet supercurrent flowing through an $F/N/F$ trilayer can be used to manipulate the magnetization direction of the ferromagnetic layers. Additionally, Ref. [70] predicted that superconducting triplet correlations can generate a magnetization orientation sensitive to the superconducting phase. Interestingly, the direct coupling between magnetization and supercurrent may thus be used to build new types of memories.

1.3.2.2 Spin pumping and Andreev Current

We have seen in the previous section that a ferromagnet under FMR conditions realizes a spin pumping mechanism. Due to interface effects, the spin current may induce a measurable charge current. Experimentally, Moriyama *et al.* [67] have measured dc voltage peaks at room temperature in a $N/F/N$ junction under FMR conditions. While one of the electrodes is made in Aluminum, we may wonder on the robustness of the

effect at low temperature below the superconducting transition. More precisely, can a spin-pumping mechanism in a ferromagnet induce a singlet supercurrent (without spin polarization) in the adjacent superconductor? We will address this question in chapter 5.

1.4 Conclusion

In this chapter, we described the phenomena related to the proximity effect in both a normal metal and a ferromagnet. In a ferromagnet, due to the presence of an exchange field, the proximity effect is very rich and offers a unique opportunity to study the interplay of ferromagnetism and superconductivity. In particular, the proximity effect in homogeneous ferromagnet is short-range and oscillatory, it may be compared with the predicted FFLO phase. By contrast, an inhomogeneous magnetization may generate long-range triplet pairs between electron of the same spin. To help the understanding of the triplet superconductivity, in chapter 3 and 4, we will look for specific signatures of induced triplet correlations in hybrid structures. Then, we showed that the combination of superconductivity and spintronics is promising for tomorrow electronic devices. Besides the use of spin valves, an alternative way to induce spin currents will be addressed in chapter 5.

In the next chapter, we will present the theoretical machinery to properly study the proximity effect in hybrid structures.

Chapter 2

Theoretical Tools

How to efficiently describe the motion of electrons in hybrid superconducting and ferromagnetic dirty junctions?

In this thesis, we chose to use the quasi-classical Green functions. We leverage the Keldysh formalism to treat out-of-equilibrium systems as it allows for a feasible full diagrammatic expansion. Why?

While Green functions carry only part of the full information on the wavefunction, they include the relevant information for expressing the one particle measurable quantities of interest such as currents, density of states ... [71]. Also, introducing the Nambu and spin field spaces, we can handle the electron-hole and spin correlations stemming from superconductivity and ferromagnetism. Additionally, we will see that the scattering on impurities is accounted in a self-energy, and for dirty sample, we will deal with a diffusion equation, namely the Usadel equation.

In a first part, we introduce the Green functions and derive the Keldysh formalism. Then in a second part, we focus on hybrid systems, and introduce our choice of field spinors in the Nambu and spin spaces. We derive step by step the quasiclassical limit (Eilenberger transport like equation), and then go to the diffusive limit (Usadel equation). Finally, we introduce the circuit theory which is powerful to describe the length of the junction is short compared the typical propagation lengths of correlations. The quasi-classical approximation assumes that the Fermi wavelength is the smallest energy scale of the system, while the diffusive limit considers that the mean free path between two impuritiy scatterings is much smaller than the size of the sample.

We use the convention, $\hbar = k_B = 1$.

2.1 Green function and equation of motion

2.1.1 Green functions

Let us start with the so-called greater and lesser Green functions,

$$G^{>}(1,1') = -i < \psi(1)\psi^{\dagger}(1') >, \tag{2.1}$$

$$G^{<}(1,1') = i < \psi^{\dagger}(1')\psi(1) > . \tag{2.2}$$

Here, $< ... >, = \mathrm{Tr}[\rho ...]$, where ρ is the density operator. While for a pure state, $\rho = |\psi >< \psi|$, for a system at thermal equilibrium $\rho = \exp(-\beta H)/\mathrm{Tr}[\exp(-\beta H)]$ where $\beta = 1/T$. These Green functions give the correlation between particles at $(1') = (x', t')$ and at $(1) = (x, t)$ with no conditions about the time ordering.

Due to this lack of causality[1] of the greater and lesser functions, we introduce the usual retarded and advanced Green functions

$$G^{R}(1,1') = -i\theta(t-t') < \{\psi(1), \psi^{\dagger}(1')\} >= \theta(t-t')\left(G^{>}(1,1') - G^{<}(1,1')\right) \tag{2.3}$$

$$G^{A}(1,1') = i\theta(t'-t) < \{\psi(1), \psi^{\dagger}(1')\} >= -\theta(t'-t)\left(G^{>}(1,1') - G^{<}(1,1')\right) \tag{2.4}$$

G^R is the retarded Green function. As it requires $t > t'$ it gives the amplitude of propagation of a particle from (x', t') to (x, t). By contrast, the advanced Green function G^A requires $t < t'$ and thus can be viewed as the amplitude of propagation of a hole from (x', t') to (x, t).

2.1.2 Observables

As we said, the single particle physical quantities of the system, e.g. the current or the density, can be expressed via the Green's function. Namely,

$$n(\mathbf{x}, t) = -i \sum_{\sigma_z} G^{<}(\mathbf{x}, t, \sigma_z, \mathbf{x}, t, \sigma_z), \tag{2.5}$$

$$j(\mathbf{x}, t) = \frac{e\hbar}{2m} \sum_{\sigma_z} \left(\frac{\partial}{\partial \mathbf{x}} - \frac{\partial}{\partial \mathbf{x}'}\right) G^{<}(\mathbf{x}, t, \sigma_z, \mathbf{x}', t, \sigma_z)\Big|_{x=x'} \tag{2.6}$$

$$+ i\frac{e^2}{m}\mathbf{A} \sum_{\sigma_z} G^{<}(\mathbf{x}, t, \sigma_z, \mathbf{x}, t, \sigma_z), \tag{2.7}$$

where $\boldsymbol{A}$ is the vector potential.

[1] No time ordering is present in $G^{>}$ and $G^{<}$.

2.1.3 The contour integral, dynamics of fields

In this section, our goal is to obtain the equation of motion governing the Green function in order to compute the dynamics or the thermal properties of the system under consideration.

Let us consider a system governed by the time dependent Hamiltonian $\mathcal{H} = H + H'(t)$, where

1. $H = H_0 + H_i$ is time independent. Here, H_0 is the free particle part and H_i contains the interactions between particles.
2. $H'(t)$ accounts for a time dependent perturbation. It is turned on at time t_0.

For times prior to the switching on perturbation $H'(t)$, the system is assumed at equilibrium, and the state of the system is described by the statistical distribution ρ_H such that $< \mathcal{O} >= \mathrm{Tr}[\rho_H \mathcal{O}]$ gives the value of an observable $\mathcal{O}$. Since the equilibrium distribution is stationary, the observable is constant, if $\mathcal{O}$ does not depend explicitely on time. After time t_0, the system is put out-of-equilibirum, and the observable may vary with time, namely

$$< \mathcal{O}_{\mathcal{H}}(t) >= \mathrm{Tr}[\rho_H \mathcal{O}_{\mathcal{H}}(t)], \tag{2.8}$$

where $O_{\mathcal{H}}(t)$ is an operator in the Heisenberg picture.

In particular, $< [\psi(1), \psi^\dagger(1')] >= \mathrm{Tr}\,[\rho_H [\psi_{\mathcal{H}}(1), \psi^\dagger_{\mathcal{H}}(1')]]$, where $\psi_{\mathcal{H}}$ is the field operator within the Heisenberg representation. However, we shall see that it is convenient to turn to the interaction picture of the field operator.

The operators in the Heisenberg picture, $O_{\mathcal{H}}(t)$, and in the interaction picture, $\mathcal{O}_H(t)$, are related via

$$\mathcal{O}_{\mathcal{H}}(t) = u^\dagger(t, t_0)\mathcal{O}_H(t)u(t, t_0), \tag{2.9}$$

with

$$u(t, t_0) = \mathcal{T}\ \exp\,[-i \int_{t_0}^{t} d\tau H'_H(\tau)], \tag{2.10}$$

where $H'_H(t)$ is the operator $H'(t)$ in the interaction picture and $\mathcal{T}$ is the usual time ordering operator.

To get a more compact and convenient expression, we introduce the contour c_t (see Fig. 2.1.a) and the associated time ordering operator T_c such that

$$\mathcal{T}_c(\psi(1)\psi^\dagger(1')) = \begin{cases} \psi(1)\psi^\dagger(1') & , t >_c t' \\ -\psi^\dagger(1')\psi(1) & , t <_c t \end{cases}, \tag{2.11}$$

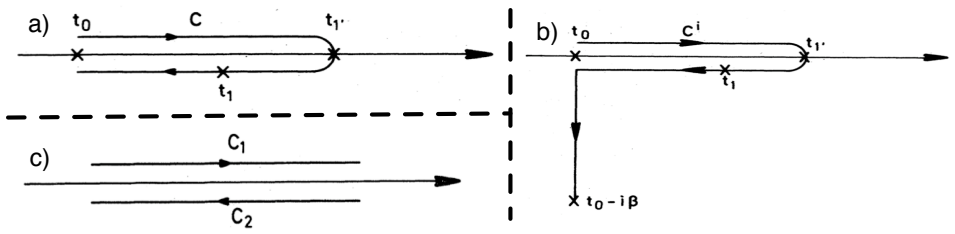

FIGURE 2.1: a) Close time path contour "c_t". b) Interaction contour "c_i". c) Keldysh contour "c". [71]

where $t <_c t'$ means that t is before t' on the contour c and vis versa. Such a trick permits to reexpress Eq. (2.9) as

$$\mathcal{O}_{\mathcal{H}}(t) = \mathcal{T}_c \exp\left[-i \int_{c_t} d\tau H'_H(\tau)\mathcal{O}_H(t)\right]. \tag{2.12}$$

It further gives with respect to the free-particle Hamiltonian H_0

$$\mathcal{O}_{\mathcal{H}}(t) = \mathcal{T}_c \exp\left[-i \int_{c_t} d\tau (H'_{H_0} + H^i_{H_0}(\tau))\mathcal{O}_{H_0}(t)\right]. \tag{2.13}$$

We now define the "contour-ordered" Green function:

$$G(1,1') = -i < \mathcal{T}_c \psi(1)\psi^\dagger(1') > . \tag{2.14}$$

It is related to the lesser and greater function via

$$G(1,1') = \begin{cases} G^>(1,1') & t >_c t' \\ G^<(1,1') & t <_c t' \end{cases}. \tag{2.15}$$

Using the relation $\exp[-\beta H_i] = \exp\left(-i \int_{c_i} d\tau H_i(\tau)\right)$, and from Eq. (2.13) we get

$$G(1,1') = -i \frac{\mathrm{Tr}\left[\exp[-\beta H_0]\mathcal{T}_c \exp\left[-i \int_{c_t+c_i} d\tau (H'_{H_0} + H^i_{H_0})(\tau)\psi(1)\psi^\dagger(1')\right]\right]}{\mathrm{Tr}\left[\exp[-\beta H_0] \exp[-\beta \int_{c_i} H^i_{H_0}]\right]}, \tag{2.16}$$

where $c + c_i$ is the contour depicted on Fig.2.1.b. Then we can extend the contour c such that it sweep forward and backward time from $-\infty$ to ∞. In order to work with a tractable form, we assume that correlations between particles due to the H^i in the far past (at $-\infty$) are not relevant, such that we can neglect the contribution of the contour

c_i [72, 73]. See [74] for a discussion about this approximation. Thus,

$$G(1,1') = -i\frac{\mathrm{Tr}\left[\exp(-\beta H_0)\mathcal{T}_c \exp\left[-i\int_c d\tau (H'_{H_0} + H^i_{H_0})(\tau)\psi(1)\psi^\dagger(1')\right]\right]}{\mathrm{Tr}[\exp -\beta H_0]}. \tag{2.17}$$

To obtain a tractable perturbative expansion of the contour integral, we will use the Wick's theorem. However, other methods due to Schwinger [75] that employ the functional derivative exist, see [76].

2.1.4 Wicks theorem and diagrammatic expansion

In a first step and as an example we consider the case of particles in an external classical field such that $H'(t) = \int dx V(x,t)\psi^\dagger(x,t)\psi(x,t)$. Then, the first order perturbative expansion of Eq. (2.17) is

$$G^{(1)}(1,1') = (-i)^2 \int_c dt_2 \int dx_2\, V(2)\mathrm{Tr}[\rho_0 \mathcal{T}_c\, (\psi^\dagger_{H_0}(2)\psi_{H_0}(2)\psi_{H_0}(1)^\dagger\psi_{H_0}(1'))], \tag{2.18}$$

where $(2) = (t_2, x_2)$. In particular, $G^{(1)}(1,1')$ is as a chain of 4 annihilation or creation operators weighted by the quadratic density ρ_{H_0}. Note that the nth order Green function $G^{(n)}(1,1')$ is a chain of $2n$ operators. Interestingly, Wick's theorem states[2]

$$< T_c(c(\tau_1)c(\tau_2)...c(\tau_n)) >= \sum_{\text{a.p.p}} \prod_{(q,q')} < \mathcal{T}_c\, c(\tau_q)c(\tau_{q'}) >, \tag{2.19}$$

where a.p.p is the sum over all possible permutations.

Then, Eq. (2.18) may be expressed as

$$G^{(1)}(1,1') = \int_c dt_2 \int dx_2\, G_0(1,2)V(2)G_0(2,1'), \tag{2.20}$$

where $G_0(1,1') = G^{(0)}(1,1')$ is the free particle propagator, it is diagrammatically represented in Fig. 2.2.a). Further, empowered by Wick's theorem, the full perturbative expansion can be written as a sum of Feynman diagramms, see Fig. 2.2.b). In addition, Fig. 2.2.c). shows that, the full pertubative expansion is enclosed in the corresponding left and right Dyson equations

$$G(1,1') = G_0(1,1) + \int d2\, G_0(1,2)V(2)G(2,1') \tag{2.21}$$

$$= G_0(1,1) + \int d2\, G(1,2)V(2)G_0(2,1'), \tag{2.22}$$

[2] for Gaussians or quadratic distribution function, e.g. $\rho_0 = \exp -\beta H_0$.

where $\int d2 = \int_c dt_2 \int x_2$.

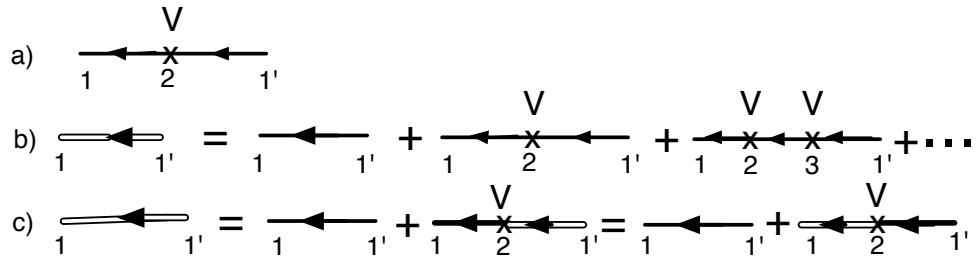

FIGURE 2.2: Feynamm diagramms. Here, double line arrow ≡ full propagator, single line arrow≡ free propagator, cross ≡ interaction vertex. a) Diagrammatic representation of $G^{(1)}(1,1')$. b) Full perturbative expansion (represented up to second order) in terms of the free propagator. c) Dyson equation representation of the full perturbative expansion.

More generally, when the perturbation is not point-like in space or time, e.g. to treat electron-phonon interaction, the Dyson equation reads

$$G(1,1') = G_0(1,1) + \int d2 \int d2'\, G_0(1,2)\Sigma(2,2')G(2',1') \tag{2.23}$$

$$= G_0(1,1) + \int d2 \int d2'\, G(1,2)\Sigma(2,2')G_0(2',1'), \tag{2.24}$$

where $\Sigma(2,2')$ is the self-energy. In the point like interaction case, the self energy takes on the simple form: $\Sigma(2,2') = \delta(2,2')V(2)$.

2.1.5 Dyson equation

The differentation of Eq. (2.23) yields the Dyson equation

$$\left(i\partial_{t_1} - H_0 - \Sigma(1,1')\right) \otimes G(1,1') = \delta(1,1'), \tag{2.25}$$

$$G(1,1') \otimes \left((i\partial_{t_1'} - H_0 - \Sigma(1,1')\right) = \delta(1,1'), \tag{2.26}$$

where $\Sigma(1,1')$ is the self-energy, note that for the classical field: $\Sigma(1,1') = \delta(1,1')V(1)$. By substracting Eq. (2.25) and (2.26), the Dirac functions cancel, and we gets the Dyson commutator

$$[i\partial_{t_1} - H_0 - \Sigma(1,1'),^{\otimes} G(1,1')] = 0 \tag{2.27}$$

where $\otimes$ is a convolution in both time and space.

2.1.6 Real time diagrammatic expansion : the R A K rules

While the contour integral allows for a the full diagrammatic expansion, it lacks physical insight. The idea is to switch back to a real-time formalism by splitting the contour in a forward and a backward paths[71], namely $\int_c = \int_{-\infty}^{\infty} dt \ldots + \int_{\infty}^{-\infty} dt \ldots = \int_{c(1)} - \int_{c(2)}$. The forward and the backward axis are labelled by 1 and 2, respectively.

Following this procedure, the contour ordered Green function gets mapped onto the Keldysh space where the (i, j) labels the axis of $(1, 1')$. As a result $G(1, 1')$ takes the matrix form

$$\hat{G}(1,1') = \begin{pmatrix} \hat{G}_{11} & \hat{G}_{12} \\ \hat{G}_{21} & \hat{G}_{22} \end{pmatrix}. \tag{2.28}$$

Further, because the G_{ij} matrix are not linearly independent, we perform linear operations in order to remove part of the redundancy. For instance, $G = L\left(\tau_3 \hat{G}\right) L^{\dagger}$ is triagonal and reads

$$G = \begin{pmatrix} G^R & G^K \\ 0 & G^A \end{pmatrix}. \tag{2.29}$$

Here τ_3 is the third Pauli matrix in the Keldysh space and $L = \frac{1}{\sqrt{2}} \begin{pmatrix} 1 & -1 \\ 1 & 1 \end{pmatrix}$. Moreover, $G^{R,A}$ are the retarded and advanced functions previously introduced. While G^R and G^A contain information about the quantum states of the system, $G^K = -i < [\psi(1), \psi^{\dagger}(1')] >$ is the Keldysh function, it encodes the dynamics or equivalently the occupations of states.

Moreover

$$G^K(1,1') = G^{>}(1,1') + G^{<}(1,1') = -i < [\psi(1), \psi^{\dagger}(1')] >, \tag{2.30}$$

$$G^R(1,1') - G^A(1,1') = G^{>}(1,1') - G^{<}(1,1') = -iA(1,1'). \tag{2.31}$$

A is the spectral weight function. Note that $A(\mathbf{x}, t, \mathbf{x}', t) = \delta(\mathbf{x} - \mathbf{x}')$ whatever the state of the system. We now write the diagrammatic expansion for the G matrix, using the example of a static potential.

We start from the contour ordered Green function ($\mathcal{G}$, to avoid the confusion with the matrix G), it obeys the Dyson equation

$$\mathcal{G}(1,1') = \mathcal{G}_0 + \int_c d\tau \int dx\, \mathcal{G}_0(1,2) V(x) \mathcal{G}(2,1'), \tag{2.32}$$

where $2 = (\tau, x)$, . Then,

- the time on the contour axis is split into the forward (label 1) and the backward axis (label 2), such that: $\int_c d\tau \cdots = \int dt_1 \cdots - \int dt_2 \ldots$.
- using Eq. (2.32), the (i,j) component of the real time matrix Green function $\hat{G}i,j$ obeys

$$\hat{G}_{i,j}(1,1') = (\hat{G}_0)_{i,j} + \int\int dt_2 dx_2\, (\hat{G}_0)_{i,1}(1,2)V(x)\hat{G}_{1,j}(2,1') - \int\int dt_2 dx_2\, (\hat{G}_0)_{i,2}(1,2)V(x)\hat{G}_{1,j}(2,1'), \quad (2.33)$$

which may be rewritten

$$\hat{G}_{i,j}(1,1') = (\hat{G}_0)_{i,j} + \int\int dt dx\, (\hat{G}_0)_{i,k}(1,2)\hat{V}_{k,k'}(x)\hat{G}_{k',j}(2,1'), \quad (2.34)$$

where $\hat{V}_{k,k'}(x) = V(x)\tau_3$ is the vertex of the static potential (the τ_3 being the third Pauli matrix in the real-time space). Finally, in the RAK space the vertex $\hat{V}$ transforms as $V = V(x)\mathbb{1}$ and we get the matrix form

$$G = G_0 + \int\int dt dx\, (G_0)(1,2)V(x)G(2,1'). \quad (2.35)$$

2.2 Equation of motion in hybrid superconducting ferromagnetic structures

2.2.1 Dyson equation

In this thesis, we are interest in hybrid superconducting and ferromagnetic systems. We account for ferromagnetism via the exchange interaction (see chapter 1, Eq. (1.10)) and treat superconductivity within the BCS model.

The hamiltonian of such hybrid junction takes on the generic form $H = H_0 + H_F + H_S$, where H_F and H_S describe respectively the exchange interaction in a ferromagnet and the superconductivity:

$$H_0 = \int dx \sum_{\sigma,\sigma'} \psi^\dagger_\sigma(x)\left(\left[\left(-\frac{\nabla^2}{2m} - \mu\right)\delta_{\sigma,\sigma'} + U_{\text{imp}}(x)\delta_{\sigma,\sigma'}\right]\psi_{\sigma'}(x)\right. \quad (2.36)$$

$$H_F = \int dx \sum_{\sigma,\sigma'} \psi^\dagger_\sigma(x)(-\mathbf{h}(x).\sigma_{\sigma,\sigma'})\psi_{\sigma'}(x) \quad (2.37)$$

$$H_S = \int dx \left[\Delta(x)\psi^\dagger_\uparrow(x)\psi^\dagger_\downarrow(x) + \text{h.c.}\right] \quad (2.38)$$

where U_{imp} is the impurity scattering potential.

The pair potential $\Delta(x)$ is solved self-consistently via:

$$\Delta(x) = \lambda < \psi_{\downarrow}(x)\psi_{\uparrow}(x) >, \tag{2.39}$$

where λ is the attractive pair potential.

Then to account for both spin and particle-hole correlations encountered in hybrid superconducting-ferromagnetic structure, the Green functions are expressed in terms of a field operator Ψ which is a 4-component spinor in the Nambu×spin space.

While many combinations of particle/hole and spin are possible to express Ψ and exist in the literature., we choose the following

$$\Psi = \begin{pmatrix} \psi_{\uparrow} \\ -i\psi_{\downarrow}^{\dagger} \\ \psi_{\downarrow} \\ i\psi_{\uparrow}^{\dagger} \end{pmatrix}, \text{ and } \Psi^{\dagger} = \begin{pmatrix} \psi_{\uparrow}^{\dagger}, & i\psi_{\downarrow}, & \psi_{\downarrow}^{\dagger}, & -i\psi_{\uparrow} \end{pmatrix}. \tag{2.40}$$

The time evolution of each component of Ψ obeys

$$i\partial_t\psi_{\uparrow} = \left(-\frac{\nabla^2}{2m} - \mu\right)\psi_{\uparrow} - \sum_{s'}\mathbf{h}(x).\sigma_{\uparrow,\mathbf{s}'}\psi_{s'} + i\Delta(-i\psi_{\downarrow}^{\dagger}), \tag{2.41}$$

$$i\partial_t\psi_{\downarrow} = \left(-\frac{\nabla^2}{2m} - \mu\right)\psi_{\downarrow} - \sum_{s'}\mathbf{h}(x).\sigma_{\downarrow,\mathbf{s}'}\psi_{s'} + i\Delta(i\psi_{\uparrow}^{\dagger}), \tag{2.42}$$

$$-i\partial_t\psi_{\uparrow}^{\dagger} = \left(-\frac{\nabla^2}{2m} - \mu\right)\psi_{\uparrow}^{\dagger} - \sum_{s'}(\mathbf{h}(x).\sigma_{\uparrow,\mathbf{s}'})^*\psi_{s'}^{\dagger} + \Delta^*(\psi_{\downarrow}), \tag{2.43}$$

$$-i\partial_t\psi_{\downarrow}^{\dagger} = \left(-\frac{\nabla^2}{2m} - \mu\right)\psi_{\downarrow}^{\dagger} - \sum_{s'}(\mathbf{h}(x).\sigma_{\downarrow,\mathbf{s}'})^*\psi_{s'}^{\dagger} - \Delta^*(\psi_{\uparrow}). \tag{2.44}$$

From these differential equations, the time evolution of the field operator Ψ can be written in a matrix form as

$$i\tau_z\partial_t\Psi(1) = \left(-\frac{\nabla^2}{2m} - \mu - \mathbf{h}(x).\boldsymbol{\sigma}\tau_z + i\hat{\Delta}(x)\right)\Psi(1) \tag{2.45}$$

where $\hat{\Delta} = \begin{pmatrix} 0 & \Delta \\ \Delta^* & 0 \end{pmatrix}\sigma_0$, where the σ_i and τ_j $(i,j = x,y,z,0)$ are the Pauli matrices in the spin and Nambu spaces, respectively.

In such a particle/hole and spin space, the real time or Keldysh Green functions reads

$$
\begin{aligned}
G^R(1,1') &= -i\,\theta(t-t') < \{\Psi(1), \Psi^\dagger(1')\} >, && (2.46)\\
G^A(1,1') &= i\,\theta(t'-t) < \{\Psi(1), \Psi^\dagger(1')\} >, && (2.47)\\
G^K(1,1') &= -i \ < [\Psi(1), \Psi^\dagger(1')] >, && (2.48)
\end{aligned}
$$

where

$$
\Psi(1)\Psi^\dagger(1') = \begin{pmatrix}
\psi_\uparrow(1)\psi^\dagger_\uparrow(1') & i\psi_\uparrow(1)\psi_\downarrow(1') & \psi_\uparrow(1)\psi^\dagger_\downarrow(1') & -i\psi_\uparrow(1)\psi_\uparrow(1') \\
-i\psi^\dagger_\downarrow(1)\psi^\dagger_\uparrow(1') & \psi^\dagger_\downarrow(1)\psi_\downarrow(1') & -i\psi^\dagger_\downarrow(1)\psi^\dagger_\downarrow(1') & -\psi^\dagger_\downarrow(1)\psi_\uparrow(1') \\
\psi_\downarrow(1)\psi^\dagger_\uparrow(1') & i\psi_\downarrow(1)\psi_\downarrow(1') & \psi_\downarrow(1)\psi^\dagger_\downarrow(1') & -i\psi_\downarrow(1)\psi_\uparrow(1') \\
i\psi^\dagger_\uparrow(1)\psi^\dagger_\uparrow(1') & -\psi^\dagger_\uparrow(1)\psi_\downarrow(1') & i\psi^\dagger_\uparrow(1)\psi^\dagger_\downarrow(1') & \psi^\dagger_\uparrow(1)\psi_\uparrow(1')
\end{pmatrix}. \quad (2.49)
$$

In particular, the order parameter can be extracted from the Keldysh function via

$$
\Delta(x) = \lambda <\psi_\downarrow(x)\psi_\uparrow(x)>= -\frac{\lambda}{8}\mathrm{Tr}[(\tau_x - i\tau_y)G^K(x,x). \quad (2.50)
$$

Similarly, the charge current reads

$$
j(x) = \frac{e}{4m}\mathrm{Tr}[(\nabla_x - \nabla_{x'})G^K(x,t,x',t)]|_{x'=x}. \quad (2.51)
$$

We may differentiate the RAK Green function relative to the creation operator $\Psi^\dagger$ (resp. annihilatrion operator Ψ) spinor operator acting at (x,t) (resp. (x',t')) to obtain the left (resp. right) equation of motion. Namely,

$$
\begin{aligned}
i\partial_t\tau_z G(1,1') &= \tau_z\delta(1,1') + \left[(-\frac{\nabla^2}{2m} - \mu) - \tau_z\mathbf{h}(x).\boldsymbol{\sigma} + i\hat{\Delta}\right] G(1,1'), && (2.52)\\
G(1,1')(-i\partial_{t'}\tau_z) &= \tau_z\delta(1,1') + G(1,1')\left[(-\frac{\nabla^2}{2m} - \mu) - \boldsymbol{h}(x).\boldsymbol{\sigma}\tau_z - i\hat{\Delta}\right]. && (2.53)
\end{aligned}
$$

Then in order to symmetrize the left and right equations, we introduce $\bar{G} = \tau_z G$ such that Eq. (2.52) transforms as

$$
\begin{aligned}
i\partial_t\tau_z\bar{G}(1,1') &= \delta(1,1') + \left[(-\frac{\nabla^2}{2m} - \mu) - \tau_z\mathbf{h}(x).\boldsymbol{\sigma} + i\tau_z\hat{\Delta}\tau_z\right]\bar{G}(1,1'), && (2.54)\\
\bar{G}(1,1')(-i\partial_{t'}\tau_z) &= \delta(1,1') + \bar{G}(1,1')\left[(-\frac{\nabla^2}{2m} - \mu) - \mathbf{h}(x).\boldsymbol{\sigma}\tau_z - i\hat{\Delta}\right]. && (2.55)
\end{aligned}
$$

Since $\tau_z\hat{\Delta}\tau_z = -\hat{\Delta}$, by substracting the left and right equation of motion, we cancel the Dirac and obtain the well-known Dyson commutator for Keldysh×Nambu×spin space,

$$\left[G_0^{-1} - \Sigma, {}^o\, \bar{G}\right] = 0, \tag{2.56}$$

where $G_0^{-1}(1,1') = i\partial_t\delta(t-t') + (\frac{\nabla^2}{2m} + \mu)$ and $\Sigma(1,1') = \mathbf{h}(x).\boldsymbol{\sigma}\tau_z - i\hat{\Delta}(x)$ and the o denotes convolution in time.

2.2.2 Symmetries

The use of symmetry can often greatly simplify the problems. We derive below the most common symmetries for the Green function in the Keldysh×Nambu×spin spaces.

1. Between the RAK functions:

$$\begin{aligned}\bar{G}^A(x,t,x',t') &= \tau_z\, i\theta(t'-t)\mathrm{Tr}[\{\psi(1),\psi^\dagger(1')\}]/Z = \tau_z(-i\theta(t'-t)\mathrm{Tr}[\{\psi^\dagger(1),\psi(1')\}]/Z)^\dagger \\ &= \tau_z(-i\tau_z\theta(t'-t)\mathrm{Tr}[\{\psi(1'),\psi^\dagger(1)\}]/Z)^\dagger\tau_z.\end{aligned}$$

   Therefore,

$$\bar{G}^A(x,t,x',t') = \tau_z(\bar{G}^R(x,t,x',t'))^\dagger\tau_z \tag{2.57}$$

   Similarly we obtain,

$$\bar{G}^K(x,t,x',t') = -\tau_z(\bar{G}^K(x,t,x',t'))^\dagger\tau_z, \tag{2.58}$$

$$\bar{G}^>(x,t,x',t') = -\tau_z(\bar{G}^<(x',t',x,t))^\dagger\tau_z. \tag{2.59}$$

2. Retarded Green function: The component in spin and Nambu of the spinor satisfies: $\psi^\dagger_{ns} = -i(-1)^{n+s}\psi_{\bar{n}\bar{s}}$. Where n corresponds to the nambu index and s to the spin index, the notation $\bar{n}$ changes an electron in hole and vis versa, more precisely $\Psi = (\,\psi_{11},\psi_{21},\psi_{21},\psi_{22})$.

   In the Nambu× spin spinor, the symmetries between i,j component read

$$\begin{aligned}\bar{G}^R_{ns,n's'} &= -i\theta(t-t')(-1)^{n+1} < \{\psi_{ns}(x,t),\psi^\dagger_{n's'}(x',t')\} > \\ &= \left[i\theta(t-t')(-1)^{n+1} < \{\psi^\dagger_{ns}(x,t),\psi_{n's'}(x',t')\} >\right]^* \\ &= \left[-i\theta(t-t')(-1)^{\bar{n}+1}(-1)^{n'+s+s'+n} < \{\psi_{\bar{n}\bar{s}}(x,t),\psi^\dagger_{\bar{n}'\bar{s}'}(x',t')\} >\right]^* \\ &= \left[(-1)^{n'+s+s'+n}G^R_{\bar{n}\bar{s},\bar{n}'\bar{s}'}\right]^*.\end{aligned}$$

Thus,

$$\bar{G}^R(x,t,x',t') = \tau_y\sigma_y(\bar{G}^R(x,t,x',t'))^*\tau_y\sigma_y. \tag{2.60}$$

3. In time and space:

$$\begin{aligned}
\bar{G}^R_{ns,n's'} &= -i\theta(t-t')(-1)^{n+1} < \{\psi_{ns}(x,t), \psi^\dagger_{n's'}(x',t')\} > \\
&= -i\theta(t-t')(-1)^{n+1}(1)^{n+n'+s+s'} < \{\psi^\dagger_{\bar{n}\bar{s}}(x,t), \psi_{\bar{n}'\bar{s}'}(x',t')\} > \\
&= i\theta(t-t')(-1)^{\bar{n}'+1}(-1)^{s+s'} < \{\psi_{\bar{n}'\bar{s}'}(x',t'), \psi^\dagger_{\bar{n}\bar{s}}(x,t)\} > \\
&= (-1)^{s+s'}G^A_{\bar{n}'\bar{s}',\bar{n}\bar{s}}.
\end{aligned}$$

Thus,

$$\bar{G}^R(x,t,x',t') = -\sigma_y(\bar{G}^A(x',t',x,t))^t\sigma_y, \tag{2.61}$$

Finally, combining Eqs. (2.57) and (2.61), we obtain

$$\bar{G}^R(x,t,x',t') = -\tau_z\sigma_y(G^R(x',t',x,t))^*\sigma_y\tau_z. \tag{2.62}$$

2.2.3 The averaged Green function over disorder

Generally, metals are not perfect critalline structures and contain defaults or impurities on which electrons scatter.

In our model, we incorporate the elastic electron-impurity scattering U_{imp} through the following Hamiltonian

$$\hat{U}_{\text{imp}} = \int dr\, \Psi^\dagger_{H_0}(r)U_{\text{imp}}(r)\Psi_{H_0}(r) \tag{2.63}$$

where $U_{\text{imp}} = \sum_{i=1}^N u(r-R_i)$ and R_i gives the position of impurities. Within the Born approximation, the diffusion is isotropic and point-like: $u(r) = u_0\delta(r)$.

Moreover, in disordered metal, impurities are generally randomly distributed, and the potential $V(r)$ can be described by a stochastic variable with $< U_{\text{imp}}(r) >= 0$ and $< U_{\text{imp}}(r)U_{\text{imp}}(r') >= u_0^2\delta(r-r')$. In such a situation, it proves useful to work with the averaged (over impurities) Green function $< G(1,1') >_{\text{dis}}$. The scattering over impurities gets incorporated in a self energy Σ_{imp} where we conserve the non-crossing diagrams (diffusion approximation[3]), see Fig. 2.3 , it yields $\Sigma_{\text{imp}}(1,1') = \delta(x-x') <$

[3]The ratio of the weight between crossing and non-crossing diagrams is of the order of $1/k_Fl \ll 1$, where l is the mean free path. Note that taking into account the $1/k_Fl$ correction leads to the weak localization.

$U(x)G(x,t,x,t')U(x) >_{\rm dis}$. It is local in space and reads

$$\Sigma_{\rm imp}(1,1') = \frac{1}{2\pi\nu\tau} < \bar{G}(1,1') >_{dis} \delta(x-x') \tag{2.64}$$

where τ plays the role of collision time and is related to the concentration of impurity via $n_i u_0^2 = 1/2\pi\nu\tau$, ($n_i = N/V$ where V is the volume).

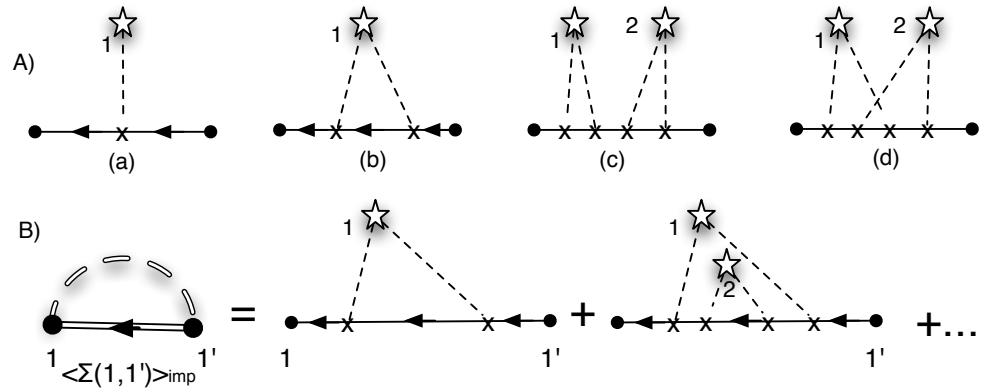

FIGURE 2.3: A) Examples of first and second order diagrams, a) single scattering, b) 2 scattering on the same impurity, c) and d) 4 scatterings on two impurities,(d) is a crossed-diagramm. After averaging over disorder, (a) disappears. B) Impurity scattering self-energy, we conserve only the non-crossing diagrams.

As a result, the averaged Green function obeys the following Dyson commutator

$$\left[\bar{G}_0^{-1} + \delta(t-t')\mathbf{h}(x).\boldsymbol{\sigma}\tau_z - \delta(t-t')\Sigma_{imp}(x) + i\delta(t-t')\hat{\Delta}, ^o < \bar{G}(1,1') >_d\right] = 0, \tag{2.65}$$

where $\bar{G}_0^{-1} = i\partial_t\delta(t-t')\tau_z + \delta(t-t')\left(\frac{\nabla^2}{2m} + \mu\right)$.

2.3 Quasiclassical approximation

2.3.1 Eilenberger equation

The full Green function contains information about microscopic details such as the Fermi wavelength, that might be not relevant for low energy transport equations. Indeed the Fermi wavelength is much smaller than the typical scales associated with impurity scattering and superconductivity. Additionally, for superconductivity, the energy width is of the order of the binding energy Δ, thus it is much smaller than the typical Fermi energy.

Following this idea, Eilenberger in 1968 proposed the quasiclassical approximation, which is now widely used [77]. The main assumption behind is that the Fermi wavelength is the smallest length scale or equivalently that the Fermi energy E_F is the largest energy scale.

The first step is to turn to Wigner coordinates in order to separate the motion of the center of mass from the fast oscillating contribution. Namely, we use the reduced coordinates

$$\begin{cases} x = x_1 - x_1', & ,X = (x_1 + x_1')/2 \\ t = t_1 - t_1', & T = (t_1 + t_1')/2 \end{cases}, \tag{2.66}$$

where (X, T) are the coordinates of the center of mass.

Then we Fourier transform $< G(1, 1') >_{dis}$ with respect to the Wigner coordinate x,

$$< \bar{G}(\boldsymbol{p}, X, t, t' >_{dis} = \int dx < \bar{G}(x, X, t, t' >_{dis} \, e^{-ix.\boldsymbol{p}}. \tag{2.67}$$

Again, as only electrons close to the Fermi surface participate in transport, we can suppose that $\boldsymbol{p} \simeq \boldsymbol{p}_F$. Consequently $|\nabla_X| \ll | \boldsymbol{p}| \simeq |\boldsymbol{p}_F|$ yields

$$\nabla^2_{1,1'} = -\boldsymbol{p}^2 \mp i\boldsymbol{p}\,\nabla_X + 1/4\nabla^2_X \simeq -\boldsymbol{p}^2 \mp i\boldsymbol{p}\,\nabla_X. \tag{2.68}$$

Accordingly, the Dyson commutator can be re expressed

$$[i\partial_t\delta(t-t')\tau_z + \mathbf{h}(X).\boldsymbol{\sigma}\tau_z + i\hat{\Delta}(X) - \Sigma_{imp}(X), < \bar{G} >_{dis}] + i\frac{1}{m}\boldsymbol{p}.\nabla_X < \bar{G} >_{dis} = 0. \tag{2.69}$$

Note that in addition we assumed $\Delta(X \pm x/2) \simeq \Delta(X)$,$\mathbf{h}(X \pm x/2) \simeq \mathbf{h}(X)$. Indeed, as mentioned in chapter 1, $\xi_S, \xi_N, \xi_F \gg \lambda_F$. We now introduce the quasi-classical Green function $\hat{g}$. It takes advantage on the the peaked properties of $\bar{G}(\boldsymbol{p}, X, t, t') \propto \delta(|\boldsymbol{p}| - \boldsymbol{p}_F)$,

$$\hat{g}(\hat{p}, X, t, t') = \frac{i}{\pi}\int d\xi_p < \bar{G}(\boldsymbol{p}, X, t, t') >_{dis} . \tag{2.70}$$

$\hat{g}(\hat{p}, X, t, t')$ depends now only on the units vector $\hat{p}$ such that $\boldsymbol{p} \simeq p_F\hat{p}$.

Accordingly, the quasiclassical Green function $\hat{g}(\hat{p}, X, t, t')$ obeys

$$[i\partial_t\delta(t-t')\tau_z + \mathbf{h}(x).\boldsymbol{\sigma}\tau_z + i\hat{\Delta} - \Sigma_{imp}(x), ^o\, \hat{g}] + iv_F(\hat{p}.\nabla_X)\hat{g} = 0. \tag{2.71}$$

The self energies can be expressed using the quasi-classical Green function. Since $\int d^3p/(2\pi)^3 = \int \frac{p^2}{2\pi^2}dp\frac{d\Omega}{4\pi}$, in addition$\int \frac{p^2}{2\pi^2}dp \simeq \int \frac{p_F m}{2\pi^2}d\xi_p \simeq \nu_0 \int d\xi_p$, we write

$$\Sigma_{imp} = -\frac{i}{2\tau}\int \frac{d\Omega}{4\pi}\hat{g}(\hat{p}, X, t, t'). \tag{2.72}$$

Similarly, the superconducting order parameter reads

$$\Delta = i\frac{\lambda\nu_0}{16}\int\int \frac{d\Omega}{4\pi}d\epsilon \mathrm{Tr}[(\tau_x - i\tau_y)\hat{g}^K], \tag{2.73}$$

where $\hat{g}^K$ is the Keldysh component of $\hat{g}$.

Finally, the Eilenberger equation reads

$$-iv_F(\hat{p}.\nabla)\hat{g} = [\frac{i}{2\tau} < \hat{g} > +A, \hat{g}], \tag{2.74}$$

where $A(1,1') = i\partial_t\delta(t-t')\tau_z + \delta(t-t')\left(\mathbf{h}(x).\boldsymbol{\sigma}\tau_z + i\hat{\Delta}(x)\right)$.

2.3.2 Properties of $\hat{g}$

The solution of the Eilenberger equation is not yet unique. To obtain a unique solution, it has to be supplemented by normalizations. In the normal state, Σ is diagonal since no electron-hole correlation exists, and we can choose for an homogeneous system $g_N^{R/A} = \pm\tau_z$.

For an arbitrary state, we first solve the Eilenberger equation and then consider the same normalization as in the normal case. Let us begin in the Nambu space (for the moment we consider only electron hole correlations), then $\hat{g}_S^{RAK}$ can be decomposed on the τ_i Pauli matrices, $\hat{g} = a\tau_0 + b\tau_x + c\tau_y + d\tau_z$. By taking the trace over the Eilenberg equation, we obtain $(\hat{p}.\nabla)\mathrm{Tr}\left[\hat{g}(x)\right] = \mathrm{Tr}\left[[A, \hat{g}(x)]\right] = 0$, thus $\mathrm{Tr}\left[\hat{g}(x)\right] = \text{const}$. Since we can go continuously from the normal to the superconducting state, it yields

$$\mathrm{Tr}\left[\hat{g}_S\right] = \mathrm{Tr}[\hat{g}_N] = 0. \tag{2.75}$$

Consequently, $a = 0$ and $\hat{g}^2 = b^2 + c^2 + d^2$ is a scalar which might depend on space. In addition, the Eilenberger equation gives $(\hat{p}.\nabla)(\hat{g}^2) = (\hat{p}.\nabla\hat{g})\hat{g} + \hat{g}(\hat{p}.\nabla\hat{g}) = [A, \hat{g}^2] = 0$.

Thus similarly, we obtain

$$\hat{g}^2(x) = \text{const} = \hat{g}_N^2 = 1. \tag{2.76}$$

To conclude as we chose $\hat{g}^{R/A} = \pm\tau_z$ to be the solution in the normal case, the Eilenberger equation needs to be supplemented by Eqs. (2.75) and (2.76), namely,

$$\hat{g}^2 = 1 \text{ and } \mathrm{Tr}\,[\hat{g}] = 0. \tag{2.77}$$

Properties

Thus, the quasiclassical Green function in the Keldysh is triangular and reads

$$\hat{g} = \begin{pmatrix} \hat{g}^R & \hat{g}^K \\ 0 & \hat{g}^A \end{pmatrix} \tag{2.78}$$

where $\hat{g}^R$, $\hat{g}^A$, and $\hat{g}^K$ are respectively the retarded, advanced and, Keldysh components.

- The normalization $\mathrm{Tr}\,[\hat{g}] = 0$ gives $\mathrm{Tr}\,[\hat{g}^{R/A}] = 0$.
- Then, applying the condition $\hat{g}^2 = 1$ to Eq. (2.78), we obtain

$$(\hat{g}^{R/A})^2 = 1, \tag{2.79}$$

$$\hat{g}^R\hat{g}^K + \hat{g}^K\hat{g}^A = 0. \tag{2.80}$$

  Thus, due to Eq. (2.80), the Keldysh component can always be cast in the form

$$\hat{g}^K(t,t') = g^R(t,t')\hat{\varphi}(t,t') - \hat{\varphi}(t,t')g_A(t,t'), \tag{2.81}$$

  where $\hat{\varphi}(t,t')$ plays the role of a distribution function. In particular, at thermal equilibrium, $\hat{\varphi}$ depends only on the time difference $(t-t')$, and its Fourier transform reads $\hat{\varphi}(E) = \tanh(E/2T) = f(E)$, where T is the temperature.

Charge current

Within the quasi-classical approximation, the charge current can be rewritten as

$$\boldsymbol{j}(x) = \frac{e\nu_0 v_F}{8}\int d\epsilon \int \frac{d\Omega}{4\pi}\hat{p}.\mathrm{Tr}\,[\tau_z\hat{g}^K(x,\hat{p},\epsilon)]. \tag{2.82}$$

2.4 Diffusive limit

2.4.1 Usadel equation

In the dirty limit, due to many scattering events, the mean free path is short, and the motion is mainly isotropic [78]. Therefore, one can solve the Eilenberger equation by expanding the Green function on the spherical harmonics. Up to first orde this yields $\hat{g} = g_0(x) + \hat{p}.\vec{g} + ...$ where $|\vec{g}| \ll g_0$. The functions $\hat{p}$ are the first spherical harmonics (on the unit sphere), namely $\hat{p} = (\cos\theta, \sin\theta\cos\phi, \sin\theta\sin\phi)$ with $(\theta, \phi) \in [0, \pi] \times [0, 2\pi]$. In addition, they obey the normalization $\int d\Omega/4\pi p_i p_j = \delta_{i,j} 1/3$.

It is easy to check that the normalization conditions for the quasiclassical Green function yield $g_0^2 = 1$ and $\{g_0, \hat{p}.\vec{g}\} = 0$. Then the Eilenberger equation (2.74) reads

$$-iv_F\hat{p}.\nabla(g_0 + \hat{p}.\vec{g})(x) = \frac{i}{\tau}g_0\hat{p}.\vec{g} + [A, g_0 + \hat{p}.\vec{g}]. \tag{2.83}$$

Then we proceed as follows:

1. Averaging Eq. (2.83) over angles ($\int d\Omega$) yields

$$\sum_i \frac{v_F}{3}\partial_i g_i = i[A, g_0]. \tag{2.84}$$

2. The projection of the first order spherical harmonics ($\int d\Omega/4\pi\hat{p}_i ...$) gives

$$v_F\partial_i g_0 = -\frac{1}{\tau}g_0 g_i - i[A, g_i] \sim -\frac{1}{\tau}g_0 g_i, \tag{2.85}$$

   where $i = 1, 2, 3$. The last approximation assumes that the energy associated to disorder dominates.

   Then since $g_0^2 = 1$ we obtain

$$v_F g_0\partial_i g_0 = -\frac{1}{\tau}g_i. \tag{2.86}$$

3. By combining the last equalities we obtain the Usadel equation, namely

$$D\nabla(g_0.\nabla g_0) = -i[A, g_0], \tag{2.87}$$

   where $D = v_F^2\tau/3$ is the diffusion constant.

Charge current

Thus, using Eq. (2.82), may be re expressed as

$$\boldsymbol{j}(x) = -\frac{e\nu D}{8}\int d\epsilon \mathrm{Tr}[v_F \tau_z g_0 \nabla g_0]. \tag{2.88}$$

2.4.2 Symmetries

To simplify the notation in the following, we will omit the subscript and denote the Usadel Green function by g. For the following, g is actually g_0. We use the symmetries presented in section (2.2.2) and adapt them in the diffusive limit.

1. $$g^A(x,t,t') = -\tau_z (g^R(x,t',t))^\dagger \tau_z, \tag{2.89}$$

   yielding in the stationary case

   $$g^A(x,\epsilon) = -\tau_z (g^R(x,\epsilon)^\dagger \tau_z. \tag{2.90}$$

2. $$g^R(x,t,t') = -\tau_y\sigma_y (g^R(x,t,t'))^* \tau_y\sigma_y, \tag{2.91}$$

   yielding in the stationary case

   $$g^R(x,-\epsilon) = -\tau_y\sigma_y (g^R(x,\epsilon))^* \tau_y\sigma_y. \tag{2.92}$$

2.5 Boundary conditions

The Usadel equation arises from the simplification of the Gor'kov equation using the quasiclassical approximation within the diffusive limit. Hence, clearly, such equation cannot properly describe the equation of motion close to interfaces where the direction of propagation is definitely of first importance and where the typical size of potential variation can be very short ($\sim \xi_F$). Neverthless, one can avoid this problem by solving the previous equations far enough from the interface and then match the solution on each side using appropriate boundary conditions. Far enough means at a few λ_F for the Eilenberger equation and at a distance larger than the mean free path for the Usadel equation. The matching conditions were first derived by Zaitzev (1984,[79]) and later by Kuprianov and Lukichev (1988, [80]) and rely on some spectral current conservation principles.

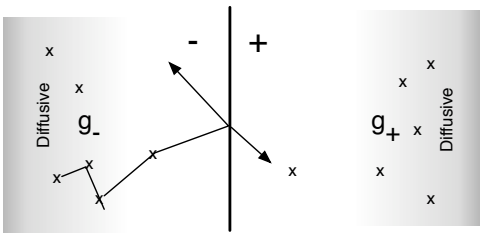

FIGURE 2.4: 2boundary

Let us consider the interface that separates the + from the − region in Fig. 2.4 . $g_\pm$ solves the Usadel equation in the bulk of the + and − region far from the interface. In the vicinity of the interface, the motion is not diffusive but ballistic, however the boundary conditions match directly the Usadel Green functions. The boundary conditions are obtained by requiring the conservation of the spectral current. Namely,

$$2\sigma_\pm(g\partial g)_\pm = G[g_+, g_-]. \tag{2.93}$$

Here $\sigma_\pm$ are the bulk conductivity in the + and − regions, ∂ is the partial derivative along the direction perpendicular to the interface and G is the conductance of the interface. Note that this relation is not restricted to low tranparent or tunnel interface, it is valid for any conductances. However we can exhibit some limiting cases for these boundary conditions

1. If the electric contact at the interface is very good ($G \gg G_\pm$), we obtained the continuity conditions

$$g_- = g_+ \text{ and } \sigma_-(\partial_{\boldsymbol{x}} g_-) = \sigma_+(\partial_{\boldsymbol{x}} g_+). \tag{2.94}$$

2. Further the limiting case $\sigma_- \gg \sigma_+$ generates the rigid boundary conditions. In particular, it reduces to $g_+ = g_-$. Such a relation holds for the coupling of a "metallic island" of finite mean level spacing to a reservoir with a quasi-continuum of levels. Due to its large size, while the reservoir is almost unaffected by the metallic island, it can strongly modify the properties of the metallic island.

3. If $G \ll \sigma_\pm/L_\pm$ where $L_\pm$ is the length of the ± region, we obtain the tunnel condition. Thus, the lowest energy scale is the associated with interfaces conductance where

$$2\sigma_\pm(g\partial g)_\pm = G[g_+, g_-]. \tag{2.95}$$

2.5.1 Spin dependent interfaces

Up to now we have only described spin independent interfaces. In a ferromagnet, this description might be incomplete due to the band splitting between majority and minority spin species. As a example, in chapter 1, we mentioned that the Andreev reflexion is changed, and can be used to measure the polarization of a ferromagnet.

For the transport in a diffusive medium [81] the spin-dependent interface may lead to

1. different conductance for the two spin species ($G_\uparrow \neq G_\downarrow$), this leads to the definition of $G_m = G_\uparrow - G_\downarrow$
2. different phase shift while passing the interface for the two spin species ($\phi_\uparrow \neq \phi_\downarrow \Rightarrow G_\phi^\pm$). This spin-dependent scattering phase might lead to, e.g. a shift in the spatial oscillation of the phase in a ferromagnet, or even generate correlations between equal spin.

In the tunnel limit, the spin-dependent conductances supplement the tunnel contact presented above, they write

$$2\hat{I}_- = 2\sigma_-(g\nabla g)_- = G[g_+, g_-] + G_m[\{\sigma_z\tau_z, g_+\}; g_-] + iG_\phi^-[\sigma_z\tau_z, g_-], \tag{2.96}$$

$$2\hat{I}_+ = 2\sigma_+(g\nabla g)_+ = G[g_+, g_-] - G_m[\{\sigma_z\tau_z, g_-\}; g_+] - iG_\phi^+[\sigma_z\tau_z, g_+]. \tag{2.97}$$

Note that, these tunnel conditions hold for $G_m \ll G$. However the "phase shift" conductance may be arbitrary, both $G > G_\phi$ and $G < G_\phi$ can be realized.

2.6 The dot approximation

Let us consider the simple case of a metallic wire of length L connected to a left and right reservoir via interfaces of finite conductance G. Then, the Usadel equation for the Green function in the wire can generally be written as

$$iD\nabla(g\nabla g) = [A, g]. \tag{2.98}$$

The "properties" of A determine the length scale for variation of the Green function g in the metallic wire. For a normal metal $\xi_N = \sqrt{T/D}$ such that if $L \ll \xi_N$, can assume that g is almost constant along the wire. For a superconducting metal the typical variation length is ξ_S. For a ferromagnet, in presence of superconducting correlations, in the channels with zero spin projection along the magnetization axes the length scale of

variation is ξ_F, whereas for triplet correlations with parallel spin it is ξ_N. For $L \ll \xi_i$ ($i = N, S$ or F depending on the junction), we can assume $g \simeq g(0) \simeq g(L) \simeq 1/L \int_0^L g(y)dy$. Using this approximation, we can eliminate the spatial dependence by integrating the Usadel equation along the wire, namely

$$iD[(g\nabla g)_R - (g\nabla g)_L] = [A, \int dy\, g(y)]. \tag{2.99}$$

To carry on, we now introduce the Zaitsev boundary conditions [79] supplementing the Usadel equation

$$\begin{cases} G_0 L g\nabla g|_L = G_L/2[g_L, g], \\ G_0 L g\nabla g|_R = -G_R/2[g_R, g], \end{cases} \tag{2.100}$$

where G_0 is the bulk conductance in the wire, and $G_{R/L}$ are the conductances of the left and the right interface. Then, Eq. (2.99) can now be rewritten as

$$\frac{1}{2}[G_L g_L + G_R g_R, g] - i\frac{G_0 L^2}{D}[A, g] = 0, \tag{2.101}$$

where g is taken to be constant in space. For a metallic wire of volume V, the equation can be rewritten in terms of the mean level spacing δ in the wire, namely

$$-i\frac{2\pi G_Q}{\delta}[A, g] + [G_L g_L + G_R g_R, g] = 0, \tag{2.102}$$

where, $G_Q = e^2/\hbar$, $G_0 = \frac{e^2 D(\nu_0 V)}{L^2}$ and $\delta = \frac{1}{\nu_0 V}$.

This procedure can be generalized to consider more complicated nanostructures within the circuit theory formalism.

2.7 Generalization to circuit theory

The circuit theory is a finite element technique which decomposes the nanostructure in nodes and connectors [82]. A node can either be a lead or an intermediate metallic island or layer while a connector refers to the interface between two nodes. The Green function g takes on a constant value g_i in the ith node, and obeys

$$-i\frac{2\pi G_Q}{\delta_i}[A_i, g_i] + \sum_j \hat{I}_{i,j} = 0, \tag{2.103}$$

where δ_i is the mean level spacing in node i and $\hat{I}_{ij}$ is the spectral leackage current from node i to j. Within the Zaitsev boundary conditions (2.93), the leakage current reads

$$\hat{I}_{ij} = G_{ij}[g_j, g_i], \tag{2.104}$$

where G_{ij} is the conductance of the connector between i and j. In addition, for a node which can be either normal, ferromagnetic or superconducting, we obtain

$$A_i = \left(\partial_t \tau_z + \boldsymbol{h}_i.\boldsymbol{\sigma}\tau_z + i\Delta_i(\cos\varphi_i\tau_x - \sin\varphi_i\tau_y)\right)\delta(t-t'), \tag{2.105}$$

where $\boldsymbol{h}_i$ is the effective exchange field while, Δ_i and φ_i are respectively the amplitude and the phase of the superconducting order parameter in node i.

2.8 Equilibrium and Matsubara Green functions

2.8.1 Relation between RAK Green function at equilibrium

When the system is in equilibrium, the density operator is given by $\rho = e^{-\beta H}$. Using the cyclic property of the trace we find

$$< \psi_H(x,t)\psi_H^\dagger(x',t') > = < \psi_H^\dagger(x',t')\psi_H(x,t+i\beta) >, \tag{2.106}$$

where $< \cdots > = \mathrm{Tr}[e^{-\beta H}\ldots]/Z$ and $Z = \mathrm{Tr}[e^{-\beta H}]$.

Then the lesser and greater Green function are related via

$$G^<(x,t+i\beta,x',t') = -G^>(x,t,x',t'). \tag{2.107}$$

As in any stationary cases, at thermal equilibrium the correlation function depends only on the time difference $t-t'$, consequently one can introduce its Fourier transform as

$$G(x,t,x',t')) = G(t-t',x,x') = \int d\epsilon\, e^{-i\epsilon(t-t')}G(\epsilon,x,x'). \tag{2.108}$$

Finally, Eq. (2.107) yields the famous relation

$$G^K(\epsilon,x,x') = \tanh\frac{\epsilon}{2T}\left(G^R(\epsilon,x,x') - G^A(\epsilon,x,x')\right) \tag{2.109}$$

2.8.2 The Matsubara functions

Since the Keldysh and the advanced Green function can be expressed via the retarded function, all the observables can be expressed in terms of the retarded Green function.

We will see below that it is mathematically convenient to turn to a representation where time and frequencies are imaginary. A similar mathematical trick is made in electrical circuits when dealing with complex numbers while the current and voltage are real... While such a mathematical trick is very powerful, it lacks physical reality.

For a time independent Hamiltonian, the unitary time evolution operator is $U(t) = e^{-iHt}$ and thus solves $i\partial_t U = HU$. Further when the system is at equilibrium, the density operator is $\rho = e^{-\beta H}/Z_0$ and solves $\partial_\beta \rho = -H\rho$. In order to treat the time evolution and the equilibrium density on the same footing, one can turn to imaginary times where $t \mapsto -i\tau$. Within the imaginary time mapping, one can redefine, the Heisenberg operator evolution: $A(\tau) = e^{H\tau} A e^{-H\tau}$. Consequently, one can define the imaginary time or Matsubara Green function as

$$\mathcal{G}_{12}(\tau, \tau') = - < \mathcal{T}_\tau(\psi_1(x,\tau)\psi_2^\dagger(x',\tau') >, \tag{2.110}$$

where $\mathcal{T}_\tau$ is the "imaginary" time ordering operator. For fermions if $\tau < \tau'$, $\mathcal{T}_\tau(\psi_1(x,\tau)\psi_2^\dagger(x',\tau')) = -\psi_2^\dagger(x',\tau')\psi_1(x,\tau)$. Furthermore,

$$\mathcal{G}_{12}(\tau, \tau') = \mathcal{G}_{12}(\tau - \tau'), \tag{2.111}$$

and according to Eq. (2.107)

$$\mathcal{G}_{12}(\tau + \beta) = -\mathcal{G}_{12}(\tau). \tag{2.112}$$

Since the Matsubara function is 2β-periodic it can be expanded in Fourier series such that

$$\mathcal{G}_{12}(\tau) = \frac{1}{\beta} \sum_n e^{-i(2n+1)\pi/\beta} \mathcal{G}_{2n+1} \tag{2.113}$$

where

$$\mathcal{G}_{2n+1} = \int_0^\beta d\tau \mathcal{G}_{12}(\tau) \tag{2.114}$$

The Fourier transform of the Matsubara function is defined as $\mathcal{G}(i\omega_n) = \mathcal{G}_{2n+1}$ where $\omega_n = (2n+1)\pi/\beta$. We can prove via the use of Lehmann representation that the Matsubara function and the retarded function derives from the same analytic continuation in the upper and lower complex plane $\mathcal{G}_{12}(z)$. In particular,

$$\mathcal{G}_{12}(i\omega_n \to \omega + i\eta) = G_{12}^R(\omega). \tag{2.115}$$

In the lower half plane, a similar relation holds with the advanced green function,

$$G_{12}^{A}(\omega) = \mathcal{G}_{12}(i\omega_n \to \omega - i\eta). \tag{2.116}$$

Further, the integral over the real axis may be expressed as a sum over Matsubara poles on the imaginary axis, e.g.

$$\int d\epsilon\, f(\epsilon) \tan\frac{\epsilon}{2T} = 2\pi T i \sum_{\omega_n>0} f(\omega_n), \tag{2.117}$$

where f is an arbitrary analytic function.

2.8.3 quasi-classical and diffusive approximation

In particular, the mapping between quasiclassical RAK and Matsubara functions reads

$$\begin{cases} g^R(\omega) = g(-i(\omega + i\eta)) & \text{upper half plane,} \\ g^A(\omega) = g(-i(\omega - i\eta)) & \text{lower half plane,} \end{cases} \tag{2.118}$$

where $g(\omega)$ is the Matsubara function.

In particular, since in equilibrium $g^K(x,\epsilon) = \tan\frac{\epsilon}{2T}(g^R(\epsilon,x) - g^A(\epsilon,x)) = \tan\frac{\epsilon}{2T}(g(-i\omega) + \tau_z g^\dagger(-i\omega)\tau_z)$ where $\omega = (2n+1)\pi T$ are the Matsubara frequencies.

then $\int d\epsilon f \times g^K = i\pi T \sum_{\omega>0} f \times g(\omega)$.

To obtain the equation governing the Matsubara function in the diffusive limit in the upper complex plane, we do the mapping: $\epsilon \to -i\omega$ such that

$$D\nabla(g\nabla g) = [(\omega + i\boldsymbol{h}.\sigma)\tau_z + \hat{\Delta}], g(\omega)]. \tag{2.119}$$

The extension of the boundary conditions are straightforward. At the interface between region $-$ and $+$, they read

- $\begin{cases} g_+(\omega) = g_-(\omega) \\ \sigma_+ \partial g_+(\omega) = \sigma_- \partial g_-(\omega) \end{cases}$ for a transparent interface
- $\sigma_+(g\nabla g)_+ = G[g_+, g_-]$ for a dirty interface.

2.9 Conclusion

In this chapter, we have derived the Usadel equation and its boundary conditions to treat hybrid superconducting and ferromagnetic junctions. The current can be easily expressed in terms of the diffusive Green function. Note that while the quasi-classical formalism describes well superconductivity, it puts on the same footing spin up and spin down electrons in a ferromagnet. Therefore assuming $h \ll E_F$ it only describes weakly polarized ferromagnets. However, it can be extended to half metal, where only one spin species is present, e.g. $\nu_\uparrow = 0$ and $\nu_\downarrow = \nu_0$ [83, 84].

In chapter 3, we will use the Usadel equation for the Matsubara Green functions. In chapter 4, we still study equilibrium properties and use mainly the circuit theory. Finally, in chapter 5 we will treat out-of-equilibrium properties and thus work in the full Keldysh⊗spin⊗ Nambu space within the circuit theory.

Chapter 3

Superharmonic current phase relation through a bilayer ferromagnet

In this chapter, we study the Josephson current through a long ferromagnetic bilayer in the diffusive regime. For non-collinear magnetization and when one of the layer is short (thikness $\sim \xi_F$), we find that the current phase relation is dominated by its second harmonic. As we will explain below, it corresponds to the long-range propagation of two triplet pairs of electrons.

3.1 Motivation: long-range triplet pairing

As discussed in chapter 1, in an homogeneous ferromagnet in contact with a superconductor, superconducting correlations are induced in the singlet and triplet channels with zero spin projection along the magnetization direction. This proximity effect is short range due to the dephasing, by the exchange field, occurring between spin up and spin down electrons. In presence of an inhomogeneous magnetization, triplet correlations between electrons of the same spin are also induced. Since no dephasing occurs in this last triplet channel, it allows for a long range proximity effect. This long range effect has been recently observed by Blamire and Birge groups via critical current measurements on trilayer ferromagnetic Josephson junctions[13, 14].

Here, we are interested in whether three layers are necessary to observe the effect. Recently, it has been predicted that a long range proximity effect may also develop in ballistic bi-layer junctions [85, 86]. More precisely, Trifunovic [85] has studied the

current phase relation of a $S/F/S$ ballistic junction with a single spin-dependent interface, equivalent to a short non-colinear ferromagnetic layer. He considers the transport mechanisms involving one or two Cooper pairs, generating the first harmonic (I_1) and the second harmonic (I_2), respectively. More generally, the CPR may be expanded as $I(\varphi) = \sum_i I_i \sin(i\varphi)$. Interestingly, the second harmonic may be decomposed as $I_2 = I_{2s} + I_{2l}$. Thus, it has two contributions: the first originates from two normal Andreev reflections at each interface, it transports two pairs with opposite spins (I_{2s}), while the second stems from two anomalous Andreev reflection at the spin-dependent interface and two normal Andreev reflection at the other interface (I_{2l}). The anomalous reflection, at the spin-dependent interface, is peculiar: it reflects a electron into a hole of the same spin, see Fig. 3.1. As a result, it coherently propagates two pairs with the same spin.

I_1 and I_{2s} are both short range, since the presence of the exchange field in F dephases pairs with opposite spin. By contrast, I_{2l} coherently transports two pairs with parallel spins through F, since no dephasing occurs, its contribution is long range. This prediction is confirmed by the numerical calculations of Trifunovic. In particular, he finds that for a long junction the current in the low temperature limit is dominated by the long range second harmonic.

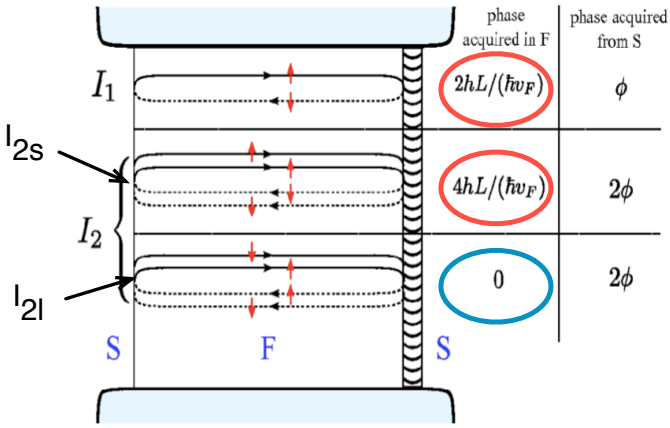

FIGURE 3.1: Coherent transport of one (I_1) and two pairs ($I_2 = I_{2s} + I_{2l}$). I_1 and I_{2s} consist of respectively one and two Andreev reflections at each interfaces. Due the acquired dephasing (circled in red), they are short range. By contrast, I_{2s} consists of two normal and two anomalous reflections, it is long range as the phase acquired in F is null. The solid (resp. dotted) line represents the electron (resp. hole) propagation in the F layer. Picture taken from [85]

Note that [86] predicted that for a non-collinear bilayer clean junction, when the thicknesses of the layers are the same, due to interference effect, surprisingly the long-range proximity effect exists in the first harmonic.

The question that arises is: what happens in experiments performed with metals in the diffusive regime (dirty) like in Refs. [13, 14]? Does this superharmonic long range contribution survives the diffusive limit?

In the following, we study the robustness of the long-range second harmonic to disorder by consider the current through a bilayer ferromagnetic diffusive Josepshon junction.

3.2 Diffusive $S/F_L/F_R/S$ junction

Let us consider a Josephson junction formed of two superconducting leads contacted through two ferromagnetic layers in series, of respective thicknesses d_L and d_R, see Fig. 3.2. The F layers are assumed to have the same properties but with different orientation of their magnetization.

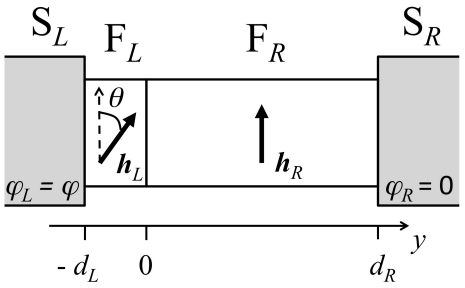

FIGURE 3.2: $S/F_L/F_R/S$ junction. Two superconducting leads are connected through a bilayer ferromagnetic layer.

We use the quasiclassical diffusive theory where g is the 4×4 matrix in Nambu$\times$ spin spaces (see chapter 2).

g obeys the normalization condition: $g^2 = 1$ and $\mathrm{Tr}\,[g] = 0$ and solves the non-linear Usadel equation [78],

$$-D\partial g \partial g + [(\omega + i\boldsymbol{h}(y).\boldsymbol{\sigma})\tau_z, g] = 0, \tag{3.1}$$

where y is the coordinate along the junction, τ_i, σ_j are the Pauli matrices in Nambu and spin spaces, and $\omega = (2n+1)\pi T$ is a positive Matsubara frequency ($n \geq 0$). The orientation of the exchange are characterized by a tilt angle, such that

$$\boldsymbol{h}(y) = \cos(\theta(y))\mathbf{e}_x + \sin(\theta(y)))\mathbf{e}_y, \text{ where } \theta(y) = \begin{cases} \theta & \text{, for } d_L < y < 0 \\ 0 & \text{, for } 0 < y < d_R \end{cases} \tag{3.2}$$

Note that the orbital effect is neglected by assuming that the magnetic flux through the junction is smaller than the quantum flux. Eq. (3.1) has to be supplemented by specific boundary conditions at each interface:

- We consider the rigid boundary conditions at the interfaces with the S reservoirs, namely $g(d_L) = g_L$ and $g(d_R) = g_R$, where g_L and g_R are the equilibrium Green function in the left and right superconducting reservoirs. Namely,

$$g_{L/R} = \frac{\omega\tau_z + \Delta(\cos\varphi_{L/R}\tau_x - \sin\varphi_{L/R}\tau_y)}{\sqrt{\omega^2 + \Delta^2}}, \tag{3.3}$$

  where Δ is the amplitude of the order parameter for both reservoirs while $\varphi_{L/R}$ is the superconducting phase in each reservoir. For convenience, we choose $\varphi_L = \varphi$ and $\varphi_R = 0$. The phase bias across the junction is thus φ.

- We consider the continuity relation at the F_L/F_R interface by assuming it is perfectly transparent. Thus, $g(0-) = g(0+)$ and $\partial g(0-) = \partial g(0+)$.

Finally the supercurrent is related to the Green function g via

$$I = \pi\nu_0 eDTA \sum_{\omega>0} \mathrm{Im}\,\mathrm{Tr}[\tau_z g \partial g], \tag{3.4}$$

where ν_0 is the density of states per spin at the Fermi level, and A is the cross section of the junction. Due to current conservation, Eq. (3.4) can be evaluated at any position.

3.2.1 parametrization

To proceed further, we parametrize the Green function introducing the anomalous Green function F in the spin space. Namely,

$$g = \begin{pmatrix} \sqrt{1 - F\tilde{F}} & F \\ \tilde{F} & -\sqrt{1 - \tilde{F}F} \end{pmatrix} \tag{3.5}$$

where $\tilde{F} = \sigma_y F^* \sigma_y$. This parametrization is convenient because as we show below, it automatically satisfies the normalization conditions $\mathrm{Tr}[g] = 0$ and $g^2 = 1$, and the required symmetry $g(\omega) = \sigma_y\tau_z(g(\omega))^*\sigma_y\tau_z$.

Let us first check the normalization of g.

$$\mathrm{Tr}[g] = \mathrm{Tr}\sqrt{1-F\tilde{F}} - \mathrm{Tr}\sqrt{1-\tilde{F}F} \tag{3.6}$$

$$g^2 = \begin{pmatrix} 1 & \sqrt{1-F\tilde{F}}F - F\sqrt{1-\tilde{F}F} \\ \tilde{F}\sqrt{1-F\tilde{F}} - \sqrt{1-\tilde{F}F}\tilde{F} & 1 \end{pmatrix} \tag{3.7}$$

Using the Taylor expansion $\sqrt{1-M} = \sum_n c_n M^n$, we can write

1. $\mathrm{Tr}\sqrt{1-F\tilde{F}} = \sum c_n \mathrm{Tr}[(F\tilde{F})^n]$. Using the cyclic property of the Trace operator we get

$$\mathrm{Tr}\,\underbrace{(F\tilde{F}F\tilde{F}..F\tilde{F}F\tilde{F})}_{2n} = \mathrm{Tr}\,\underbrace{(\tilde{F}F\tilde{F}F\tilde{F}..F\tilde{F}F)}_{2n}, \tag{3.8}$$

   which gives

$$\sum c_n \mathrm{Tr}[(F\tilde{F})^n] = \sum c_n \mathrm{Tr}[(\tilde{F}F)^n] = \mathrm{Tr}\sqrt{1-\tilde{F}F}. \tag{3.9}$$

   As a result, $\mathrm{Tr}[g] = 0$.

2. Moreover, since

$$\sqrt{1-F\tilde{F}}F = \sum c_n (F\tilde{F})^n F = \sum c_n F(F\tilde{F})^n = F\sqrt{1-\tilde{F}F}, \tag{3.10}$$

   we obtain $g^2 = 1$.

Then, $\tilde{F} = \sigma_y F^* \sigma_y$ supports the desired symmetry $g(\omega) = \sigma_y \tau_z (g(\omega))^* \sigma_y \tau_z$.

With the parametrization (3.5), the Usadel equation transforms as an equation on F,

$$-D\partial\left[\sqrt{1-F\tilde{F}}\partial F - \sqrt{1-\tilde{F}F}\partial\tilde{F}\right] + \{\omega + i\boldsymbol{h}.\boldsymbol{\sigma}, F\}, \tag{3.11}$$

and the current takes on the simple form

$$I = 2\pi T e\nu DA \sum_{\omega>0} \mathrm{Im}\,\mathrm{Tr}[F\partial\tilde{F}]. \tag{3.12}$$

Indeed, $\mathrm{Tr}[\tau_z g\partial g] = \mathrm{Tr}[-1/2\partial(F\tilde{F}) + F\partial\tilde{F} + 1/2\partial(\tilde{F}F) - \tilde{F}\partial F = \mathrm{Tr}[F\partial\tilde{F} - \tilde{F}\partial F]$.

3.2.2 Linearization close to T_c

At this stage, solving the non-linear Usadel equation is very challenging. While it is numerically solvable, here we want to obtain an analytical solution. Thus, we need to further simplify it.

In the vicinity of the superconducting transition the gap vanishes as $\Delta \sim \sqrt{T_c(T_c - T)}$, hence Δ/ω, $\Delta/T_c \ll 1$ are small parameters we can use to perform a perturbative expansion. The idea is to solve Eq. (3.11) perturbatively around the normal state solution where superconducting correlations are absent ($F = 0$). This perturbative expansion allows to transform the non-linear equation in a hierarchy of solvable linear equations.

To this end, we expand the F matrix in the small parameter Δ/ω, namely $F = (\Delta/\omega)F^{(1)} + (\Delta/\omega)^3 F^{(3)} + ...$ and then solve the Usadel equation order by order. Note that the Δ/ω expansion of the F matrix contains only odd power in Δ/ω. This symmetry is inherited from the singlet superconducting reservoir where the anomalous function is $F_S = \Delta/\sqrt{\omega^2 + \Delta^2} = \sum c_{2n+1}(\Delta/\omega)^{2n+1}$.

Similarly, the supercurrent can be expanded in powers of Δ/T_c. Using Eq. (3.12), I contains only even powers and reads

$$I = I^{(2)} + I^{(4)} + ... = I_1 \sin\varphi + I_2 \sin 2\varphi + ... \tag{3.13}$$

In particular, to compute the $2n$th order contribution of the charge current, we need the $F^{(i)}$ correlation matrices up to order $2n-1$. While the first harmonic I_1 is related with the amplitude of propagation of one pair, I_2 accounts for the coherent transport of two pairs. The leading contribution to the first harmonic is thus in $I^{(2)}$ whereas it is in $I^{(4)}$ for the second harmonic.

3.2.3 Second order charge current: short range contribution

As aforesaid, the second order contribution, $I^{(2)}$, corresponds to the transport of one Andreev pair through the ferromagnetic bilayer. Due to spin conservation at the interface two electrons of the same spin cannot be converted into a Cooper pair which pairs two electrons with opposite spin. As a result, a long range triplet pair cannot enter alone the singlet condensate and contribute to the first harmonic. We can thus guess that the amplitude of I_1 is exponentially decaying with the length of the bilayer.

To confirm this statement, we first compute the first order anomalous function $F^{(1)}$ induced in the bilayer. It obeys

$$-D\partial^2 F^{(1)} + 2\omega F^{(1)} + i\{\boldsymbol{h}.\boldsymbol{\sigma}, F^{(1)}\} = 0. \tag{3.14}$$

Upon performing a unitary transformation , $\mathcal{F}^{(1)}(y) = e^{i\sigma_y\theta(y)/2}F^{(1)}(y)e^{-i\sigma_y\theta(y)/2}$, the solution in each layer is of the form $\mathcal{F}^{(1)} = \mathcal{F}_0^{(1)} + \mathcal{F}_z^{(1)}\sigma_z + \mathcal{F}_x^{(1)}\sigma_x$, where

$$\mathcal{F}^{(1)}_{L/R,s} = A_s^{L/R}e^{-p_s y} + B_s^{L/R}e^{p_s y}, \tag{3.15}$$

with $s = \pm, x$ and $\mathcal{F}_\pm^{(1)} = \mathcal{F}_0^{(1)} \pm \mathcal{F}_z^{(1)}$. Here, $\mathcal{F}_\pm^{(1)}$ with $p_\pm = \sqrt{2(\omega \pm ih)/D}$ correspond to the induced short-range singlet et triplet correlations. In the limit, $h \gg T_c$, we get roughly $p_\pm \simeq (1 \pm i)/\xi_F$ such that the penetration length is $\xi_F = \sqrt{D/h} \ll \xi_N$.

By contrast, the triplet correlations with parallel spin, $\mathcal{F}_x^{(1)}$, propagate through the ferromagnetic region with $p_x = \sqrt{\omega/D}$. Their penetration length is thus $\xi_N = \sqrt{D/T}$ like in normal metal. It is long range.

The coefficients $A_s^{L/R}$ and $B_s^{L/R}$ entering Eq. (3.15) are determined by the boundary conditions. Assuming $d_R \gg \xi_F$, we find, up to an exponentially small correction, that $A_\pm^R = e^{-i\varphi}a_\pm$, $B_\pm^R = e^{-p_\pm d_R}$ and $A_x^R e^{-p_x d_R} = -B_x^R e^{p_x d_R} = ie^{i\varphi}a_x$, with

$$a_+ = a_-^* = \frac{\alpha - \beta}{|\alpha|^2 + |\beta|^2}, \tag{3.16}$$

$$a_x = \frac{\tan\theta}{2\sinh p_x d}\mathrm{Im}[(p_+ d_L + 1)a_+], \tag{3.17}$$

and

$$\alpha = \cos^2\frac{\theta}{2}e^{p_- d_L} + \frac{\sin^2\frac{\theta}{2}}{2\cos\theta}(p_- d_L + 1)\frac{\cosh p_- d_L \sin p_x d_R}{\sinh p_x d}, \tag{3.18}$$

$$\beta = \sin^2\frac{\theta}{2}(\cosh p_+ d_L - i\sinh p_+ d_L) - \frac{\sin^2}{2\cos\theta}(p_- d_L + 1)\frac{\cosh p_+ d_L \sin p_x d_R}{\sinh p_x d}, \tag{3.19}$$

where $d = d_L + d_R$ is the total length of the junction.

Note that the ratio d_L/ξ_F can be arbitrary as long as $\xi_N \gg d_L$.

3.2.3.1 First harmonic

The second order charge current reads

$$I = 2\pi T_c e\nu DA\sum_{\omega>0}\mathrm{Im}\,\mathrm{Tr}[F^{(1)}\partial\tilde{F}^{(1)}]. \tag{3.20}$$

The expression of Eq. (3.20) at the right interface is simple: since $F^{(1)}(d_R) = 1$, only the expression of $\partial F_0^{(1)}(d_R)$ is necessary. For instance,

$$\begin{aligned}\mathrm{Im}\,\mathrm{Tr}[\xi_F F \partial \tilde{F}] &= \mathrm{Im}\sum_{\pm}\sqrt{2}e^{\mp i\pi/4}[e^{i\varphi}a_{\mp}e^{\mp i(d_R/\xi_F)}]e^{-d_R/\xi_F} - 1 \\ &= 2\sqrt{2}\sin\varphi e^{-d_R/\xi_F}\mathrm{Re}[e^{i\pi/4-id_R/\xi_F}a_+]. \quad (3.21)\end{aligned}$$

As a result, $I^{(2)} = I_1 \sin\varphi$, where the amplitude of the first harmonic, I_1, reads

$$I_1 = \frac{\pi G\Delta^2}{e\sqrt{2}T_c}\frac{d}{\xi_F}e^{-d/\xi_F}\Upsilon_1\left(\frac{d_L}{\xi_F},\frac{d_R}{\xi_F},\theta\right). \quad (3.22)$$

Here $G = 2e^2\nu DA/d$ is the conductance of the junction in the normal state and Υ_1 is a scaling function with

$$\Upsilon_1\left(\frac{d_L}{\xi_F},\frac{d_R}{\xi_F},\theta\right) = \sum_{\omega>0} 8\,\mathrm{Re}\,[e^{i\pi/4-id_R/\xi_F}a_+]. \quad (3.23)$$

We obtain the predicted short range nature of the first harmonic, namely $I_1 \propto e^{-d/\xi_F}$. Additionally, while $\mathcal{F}_x^{(1)}$ is non-zero for $\theta \neq 0$, it does not contribute to this first harmonic as it would not conserve the spin!

The scaling function is a function of the thickness of both the left and right ferromagnets and of the relative angle θ between the magnetization of both layers. It is represented in Fig. 3.3. Its absolute value is of the order of 1 and its sign oscillates, thereby displaying the transitions between the 0-state when $I_1 > 0$ and π-state when $I_1 < 0$. Hence, this result follows at least qualitatively measurements performed on $S/F/S$ junction.

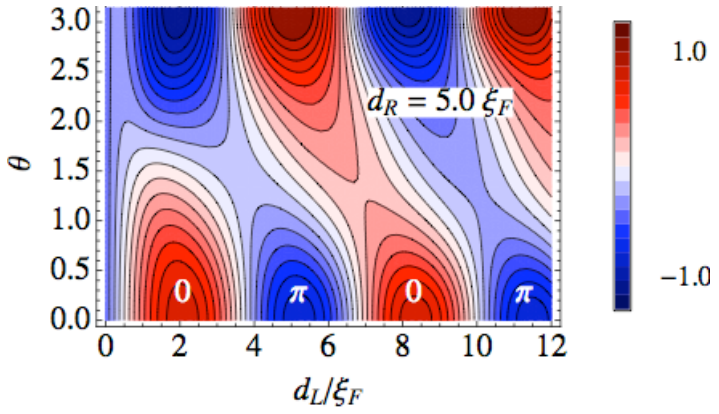

FIGURE 3.3: Dependence of the short-range first harmonic I_1 of the current phase relation on the thickness d_L/ξ_F and the angle θ at fixed $d_R/\xi_F = 5$. Here I_1 is measured in units of $I_{10} = \pi G\Delta^2 d/(\sqrt{2}eT_c\xi_F)e^{-d/\xi_F}$.

3.2.3.2 Limiting cases

Simple analytic expressions can be found for Υ in various regime:

- Case of parallel alignment ($\theta = 0$), it represents a monolayer of length d: we get $a_\pm = 1$ yielding

$$\Upsilon_1 \sim \sin(d/\xi_F + \pi/4). \tag{3.24}$$

  It reproduces well the case of a long mono-domain $S/F/S$ junction with $d \gg \xi_F$[87]. The formula works at arbitrary lengths, and gives a good qualitative prediction. However, to fit the experimental measurements for short junctions ($d < \xi_F$) we need to account in the model for the scattering on magnetic impurities [88].

- When $d_L \ll \xi_F$ obviously the first magnetic is so short that one can extend the previous conclusion to arbitrary angle: the relation (3.24) is valid at any angle as long as $d_L \ll \xi_F$.

- In the opposite limit corresponds to $d_L \gg \xi_F$, namely both magnetic layers are thick compared with the ferromagnetic coherence length. Here the cases of parallel and antiparallel magnetization exhibit special features with almost no angle dependence, namely

$$\Upsilon_1 = \begin{cases} \sqrt{2}\sin\left(d + \pi/4\right)/\xi_F & \theta = 0 \\ \sqrt{2}\cos\left(d_L/\xi_F\right)\cos\left(d_R/\xi_F\right) & \delta\theta < \theta < \pi - \delta \\ \sqrt{2}\cos\left(d_L - d_R\right)/\xi_F & \theta = \pi \end{cases}. \tag{3.25}$$

  The crossover region between the singular values and the central plateau happens on a scale $\delta\theta \sim \xi_F/\min[d_L, d_R]$. Notice that for $\theta \in [\delta\theta, \pi - \delta\theta]$, the value of Υ_1 does not depend on θ (flat).

  Eq. (3.25) generalizes the results obtained for $d_L = d_R$ by [89, 90]: the peculiarity of this case is that for antiparallel magnetization the oscillations disappear. If $\theta \neq 0$ the oscillation persits but without the 0 to π- transition as $\Upsilon_1 > 0$.

Because the first harmonic is exponentially small, we turn to higher orders to exhibit a long-range contribution, stemming from the coherent transport of two triplet pairs with parallel spin.

3.3 Higher order charge current and long range triplet contribution

The fourth order contribution $I^{(4)}$ contains a small correction to the first harmonic $\propto \sin\varphi$ (I_1^c) , but also contains a second harmonic $\propto \sin 2\varphi$ (I_2).

In collinear structures, no long-range correlations are induced. Hence I_2 is short range $\propto e^{-2d/\xi_F}$. Thus its contribution is important for thicknesses near the $0-$ to $\pi-$ transition, when I_1 vanishes[91, 92].

For non-collinear structures the contribution of long-ranged triplet pairs appears. Indeed two triplet pairs can enter the singlet condensate without breaking any symmetry. More generally, an even number of triplet pairs (with equal superposition of $S_z = \pm 1$) can transform into an even number of singlet pairs. Hence, I_2 is a superposition of a short range I_2^s and a long range I_2^l contributions corresponding to the coherent transport of two short-ranged pairs and two long-ranged pairs, respectively.

We will concentrate below on the long-range contribution and show that there is a range of thicknesses for the left and right layers where $I_2^l \gg I_1$.

For concreteness, we assume $d_R \gg d_L$ and we choose to evaluate the current in the middle of the right layer. Indeed, in the limit $d_R \gg \xi_F$, the amplitude of short-range correlations in the middle of the layer is vanishingly small ($\propto e^{-d_R/\xi_F}$), and only long-range triplet pairs survives. As a result, the current formula (up to exponentially small corrections) reads

$$I_l^{(4)} = 2\pi T_c e\nu DA \sum_{\omega>0} \mathrm{Im}\,\mathrm{Tr}[F_{R,x}^{(1)}\partial\tilde{F}_{R,x}^{(3)} + F_{R,x}^{(3)}\partial\tilde{F}_{R,x}^{(1)}]_{y=d_R/2}, \tag{3.26}$$

where $I_l^{(4)} = I_2^l \sin(2\varphi)$. Actually, Eq. (3.26) is valid as long as it is evaluated far enough from the interface where terms of the form $[F_{R,\pm}^{(1)}\partial\tilde{F}_{R,\pm}^{(3)}]_y$ are exponentially small. The advantage of evaluating the current in the middle of the right layer is that only $F_{R,x}^{(3)}(y)$ is necessary. Using Eq. (3.1), we find that $F_{R,x}^{(3)}(y)$ obeys

$$-D\partial^2 F_{R,x}^{(3)} + 2\omega F_{R,x}^{(3)} = \frac{D}{2}\partial\left\{[(F_{R,x}^{(1)})^2 + F_{R,+}^{(1)}F_{R,-}^{(1)}]\partial\tilde{F}_{R,x}^{(1)} + [F_{R,+}^{(1)}\partial\tilde{F}_{R,+}^{(1)} + F_{R,-}^{(1)}\partial\tilde{F}_{R,-}^{(1)}]F_{R,x}^{(1)}\right\}. \tag{3.27}$$

The r.h.s. is as a source term for the triplet correlations, it translates the singlet to triplet conversion process, e.g. $F_{R,+}^{(1)}F_{R,-}^{(1)}\partial\tilde{F}_{R,x}^{(1)}$ ...

In addition, in order to compute the second harmonic, we need only to retain the terms $\propto e^{-i\varphi}$, as . To this end, we write $F_{R,x}^{(3)} = f_x^{(3)}e^{-i\varphi} + \Psi_{R,x}^{(3)}$ where the last term does not

contain any term in $e^{-i\varphi}$. The function $f_x^{(3)}$ obeys a differential equation derived from Eq. (3.27) by conserving on the r.h.s. the terms proportional to $e^{-i\varphi}$ only. Such terms arise from the contribution $F_{R,+}^{(1)}F_{R,-}^{(1)}\partial\tilde{F}_{R,x}^{(1)}$ and yield

$$-D\partial^2 f_x^{(3)} + 2\omega f_x^{(3)} = -\frac{2Dq}{\xi_F}\frac{\Delta^3}{\omega^3}a_x e^{2(y-d_R)/\xi_F}. \tag{3.28}$$

A general solution that satisfies both Eq. (3.28) and the boundary condition $f_x^{(3)}(d_R) = 0$ at the right interface reads

$$f_x^{(3)} = \frac{p_x\xi_F}{2}\frac{\Delta^3}{\omega^3}a_x\left\{e^{2(y-d_R)/\xi_F} - \cosh p_x(d_R-y)\right\} + C\sinh p_x(d_R-y). \tag{3.29}$$

Here C is a constant which can be determined from the boundary conditions at the interface between the left and right ferromagnets. It turns out that it does not contribute to the current and, thus, will not need to be determined. Finally, Eq. (3.26) yields

$$I_2 = 4\pi e\nu ADT\sum_{\omega>0}\frac{\Delta^4}{\omega^4}p_x^2\xi_F a_x^2, \tag{3.30}$$

which evaluates to

$$I_2 = \frac{\pi G\Delta^4}{192eT_c^3}\frac{\xi_F}{d_R}\Upsilon_2(\frac{d_L}{\xi_F},\theta)\times\begin{cases}1, & d_R\ll\xi_N\\ \frac{384d^2}{\pi^4\xi_N^2}e^{-2d_R\xi_N} & d_R\gg\xi_N\end{cases}. \tag{3.31}$$

The first limit corresponds to $p_x d_R \ll 1$ where we set in Eq. (3.30) $p_x d_R = 0$. By contrast, the second limit correspond to a long right layer, namely $p_x d_R \gg 1$, as a result the sum is a hierarchy of exponentially small terms where the first term dominates as $\propto e^{-2d_R/\xi_N}$.

As anticipated, the second harmonic is long-ranged, it depends on the length d_R/ξ_F only as a power law. The suppression factor ξ_F/d_R is due to the conversion of parallel-spin triplet pairs into singlet pairs which takes place on a distance ξ_F from the F/S interface only. The triplets/singlets conversion happening deeper in the sample are dephased on a length ξ_F before reaching the reservoir and cannot contribute to the charge current. As a result, only a potion ξ_F/d_R of all the two-pairs recombination processes are efficient.

The dependence of the function Υ_2 appearing in Eq. (3.31) on the tilt angle θ and the thickness of the left layer is shown in Fig. 3.4.

Υ_2 is maximal for lengths $d_L \sim \xi_F$ and angles $\theta \sim \pi/2$. As expected, it vanishes for collinear structures, $\theta \to 0, \pi$ of arbitrary length. In non-collinear structures, it simplifies

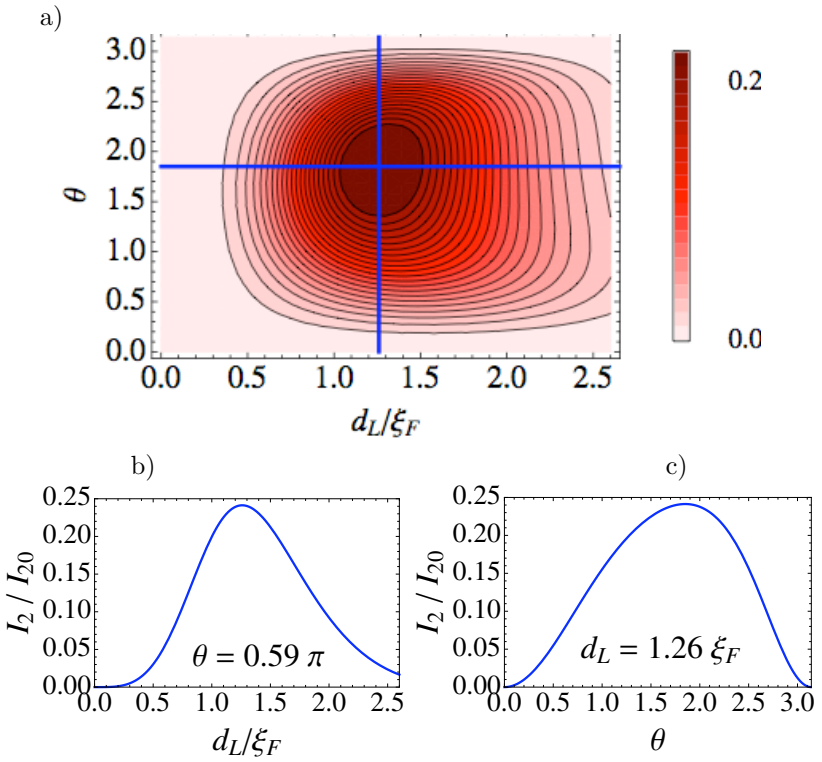

FIGURE 3.4: Dependence of the long-range second harmonic I_2 of the current phase relation on the thickness d_L/ξ_F and the angle θ. Here, I_2 is measured in units of $\pi G\Delta^4\xi_F/(192eT_c^3 d_R)$. The plots b) and c) are taken along the cuts indicated by the blue lines in a), at $\theta = 0.59\,\pi$ and $d_L/\xi_F = 1.26$, respectively. Both cuts include the maximal value $I_2^{\max} \sim 0.24 I_{20}$.

to $\Upsilon_2 \approx (d_L/\xi_F)^4 \sin^2\theta$ for a short left layer, $d_L \ll \xi_F$, while it vanishes exponentially for a long layer $d_L \gg \xi_F$, namely,

$$\Upsilon_2 = \frac{4\sin^2\theta(\cos\frac{d_L}{\xi_F}\cos^2\frac{\theta}{2} - \sin\frac{d_L}{\xi_F})^2 e^{-2\frac{d_L}{\xi_F}}}{(\sin^2\theta + a_\theta\frac{\xi_F}{d_L})^2}. \tag{3.32}$$

Here, a_θ is only relevant in the vicinity of $\theta = 0$ or π, where $a_0 = 2$ and $a_\pi = 1$.

As the second harmonic is long-ranged (in contrast with the first harmonic), we expect it to dominate I_1 as soon as d_R exceeds a few times ξ_F. In particular, for an optimal thickness $d_L \sim \xi_F$ we find the ratio $I_2/I_1 \sim (\Delta/T_c)^2(\xi_F/d_R)^2 e^{d_R/\xi_F}$, valid close to T_c. The effect is expected to be robust as temperature is lowered enhancing the ratio I_2/I_1. To demonstrate such statement, the possibility would be to solve the Usadel equation numerically. More generally, odd and even harmonics will be short and long range respectively. We interpret the algebraic reduction $\propto \xi_F/d_R$ in the second harmonic I_2, as the need for triplets to recombine on a distance ξ_F from the right F/S interface.

As a generalization of the case $n = 1$, we conjecture that the amplitude of 2nth even harmonic $I_{2n} \propto \sin(2n\varphi)$ to come with a small factor $(\xi_F/d_R)^n$. We guess that the current phase relation would be dominated by the second harmonic at any temperature.

3.4 Measurability

Let us discuss the measurability of our prediction. The long-range proximity effect has been observed in trilayers [13, 14], where already the first harmonic is long-ranged. The amplitude of the second harmonic for the bilayer is predicted to be smaller by a factor ξ_F/d_R as compared to the first harmonic in tri-layers. Thus, we believe that it should be within the sensitivity of present-day experiments when the metallic contact are good. Its specific current phase relation may be detected by a direct measurement of the currrent phase relation [93] or through the appearance of fractional Shapiro steps in the current-voltage characteristic under microwave irraditations[36].

Note that our prediction relies on the coherent propagation of parallel-spin triplet pairs with opposite spin directions. Therefore, I_2 should be proportional to $1 - P^2$, where P is the spin polarization of conduction electrons in the ferromagnet ($|P| \ll 1$ in the quasiclassical theory we used). In particular, the effect should be robust in ferromagnets with intermediate spin polarization, while it would be suppressed in half-metals where $|P| \to 1$.

3.5 Conclusion

We predict that the current phase relation through a diffusive ferromagnetic bilayer Josephson junction with noncollinear magnetizations is dominated by a superharmonic contribution $\propto \sin(2\varphi)$ when one of the layers has a thickness comparable with the ferromagnetic penetration length while the other is much thicker. Measuring the dependence of the Josephson current on the thicknesses of the layers and the angle between the magnetization of the layers would provide further evidence for the long-range triplet proximity effect.

Note that, anticipating the next chapter, the second harmonic can be viewed as the minimal Josephson current that can flow between a conventional even-frequency superconductor and an effective odd-frequency superconductor generated by the long-range proximity effect at the extremity of the long bilayer. Detecting the π-periodicity of the current phase relation would be a strong indication of the odd-frequency nature of the long-range proximity effect.

Chapter 4

Critical current signature of odd-frequency correlations

Contacting a bilayer ferromagnet with a conventional singlet even-frequency superconductor allows for the realization of an effective triplet odd-frequency superconductor. In this work we investigate the Josephson effect between superconductors with opposite symmetries, namely triplet odd-frequency versus singlet even-frequency. In particular, we study the peculiar temperature dependence of the critical current flowing between two triplet odd-frequency superconducting leads through a conventional singlet even-frequency superconductor. We show that the temperature dependence of the critical current under quite general conditions presents a maximum at the superconducting transition of the weak superconductor. It is a signature of the competition between odd/odd[1] and odd /even[2] Josephson couplings.

4.1 Motivation: evidence of odd-frequency triplet correlations

In the last chapter we predicted that a long-range triplet proximity effect can develop in a bilayer ferromagnet with non-collinear magnetization, i.e. $S/F_L/F_R/S$ junction. When the junction is asymmetric, e.g. when the F_L layer is short and the F_R layer is long, the proximity effect due to short-range singlet or triplet pairs is suppressed. Instead a superharmonic Josephson relation is generated by the long-range propagation of an even number of triplet pairs with parallel spins that recombine in singlet pairs in the vicinity of the F_R/S interface.

[1] triplet odd-frequency/ triplet odd-frequency Josephson coupling.
[2] triplet odd-frequency/singlet even-frequency Josephson coupling.

Such a multilayer junction ($S/F_L/F_R/S$) can be mapped to a simple S_T/S Josephson junction where $S_T \equiv S/F_L/F_R$ is an "effective" source of pure triplet correlations (the bilayer F_R/F_L acts as both a triplet generator and filter). From a symmetry point of view, S_T is a triplet odd-frequency superconductor while S is conventional singlet even-frequency superconductor (see chapter 1). Therefore the S_T/S Josephson junction realizes an odd/even-frequency Josephson coupling[3]. The absence of odd harmonics in its current phase relation is simply due to the symmetry mismatch between S and S_T. Essentially, a triplet pair cannot transform as a singlet pair but two triplet pairs can be converted in two singlet pairs without breaking symmetries. The superharmonicity is a clear signature of the even/odd-coupling, experimentally it would confirm the existence of odd-frequency triplet pairs.

Such results can be compared with the experiments on the tri-layer ferromagnetic junctions [13, 14][4]. These tri-layers junctions exhibit a long range proximity effect and produce an effective S_T/S_T junction that realizes an effective odd/odd-frequency coupling. Since both superconducting leads share the same symmetry, the current phase relation is not peculiar ($I \propto \sin\varphi$). This means these experiments do support the reality of triplet correlations, they do not exhibit any signature of the odd-frequency triplet nature of long range correlations. By contrast the superharmonic current phase relation of the bilayer junction exhibits such odd-frequency triplet nature. However due to the difficulties of measuring current phase relations, it is desirable to find alternative systems where odd-frequency signatures can be captured.

In this chapter , we explore the competition between odd/even-frequency coupling and even/even-frequency coupling. To this end, we study the temperature dependence of the critical current in a $S_T/S/S_T$ junction where a conventional superconductor of bare critical temperature T_c is sandwiched between two effective odd-frequency triplet superconductors of critical temperature T_c'. The triplet reservoirs are assumed to be in a subgap regime, $T_c \ll T_c'$. Experimentally the $S_T/S/S_T$ junction may be realized in a $S'/F/F/S/F/F/S'$ where the bare critical temperature of S' is much higher than the one of S, the setup is shown schematically in Fig. 4.1. We call the effective critical temperature of S is T_c^*.

Above its effective critical temperature T_c^*, the superconducting island (S) is normal metallic, an effective odd/odd-frequency coupling builds up. Like in an $S/N/S$ junction, the triplet pairs flow from one lead to the other via virtual Andreev pairs in the normal island. At temperatures below T_c^*, S is superconducting. Quasi-particles above the

[3]The notation odd/even is a short cut of triplet odd-frequency /singlet even-frequency Josephson coupling. In the diffusive case, the orbital part of the superconducting correlations is necessary symmetric. Thus, singlet superconductor are necessary even-frequency while triplet superconductors are necessary odd-frequency.

[4] The trilayer used in [13, 14] are Nb/Ho/Co/Ho/Nb or Nb/PdNi/Co/PdNi/Nb

gap coexist now with the underlying singlet even-frequency condensate. On top of the existing odd/odd-frequency coupling, an odd/even-frequency Josephson junction (JJ) sets up at each interface.

In particular we will show that the current associated with the odd/odd- and the odd/even- Josephson couplings compete. Beside a peculiar current-phase relation, the critical current as a function of temperature contains signatures of this competition. In particular, it presents a maximum at finite temperature, for a wide range of parameters.

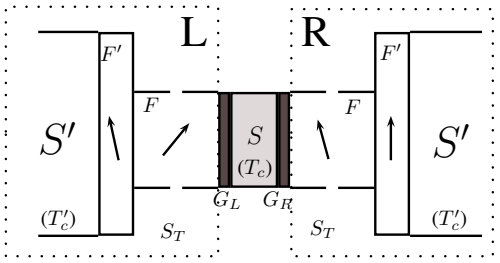

FIGURE 4.1: Effective $S_T/S/S_T$ junction.

The outline of the chapter is as follows: in the first part, we derive the Green function of our effective odd-frequency reservoir (S_T) and in the second part we compute the current in the $S_T/S/S_T$ junction using the circuit theory.

4.2 Description of the odd-frequency reservoirs (S_T)

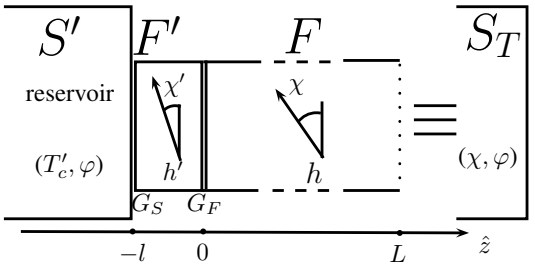

FIGURE 4.2: (Magnetizations lie in the xy-plane, perpendicular to the direction of propagation) Geometry of the effective S_T reservoir: a superconducting reservoir (critical temperature T_c') in contact with a bilayer ferromagnet of length $l + L$. $\boldsymbol{h}$ (resp. $\boldsymbol{h}'$) is the exchange field in F(resp. F'), and $\theta = \chi - \chi'$ is the tilt angle between the exchange fields.

Let us consider the effective triplet reservoir (S_T) depicted in Fig. 4.2 . Along the z-axes, a conventional superconductor S' is attached to a non-collinear bilayer ferromagnet F'/F: $S_T \equiv S'/F'/F$. In order to neglect any orbital effects, the magnetizations of both

layers lie in the perpendicular xy- plane such that the exchange field in F' and F read

$$\boldsymbol{h}' = h'(\cos\chi'\,\mathbf{e}_x + \sin\chi'\,\mathbf{e}_y) \text{ in } F', \tag{4.1}$$

$$\boldsymbol{h} = h(\cos\chi\,\mathbf{e}_x + \sin\chi\,\mathbf{e}_y) \text{ in } F. \tag{4.2}$$

$\xi'_F = \sqrt{D/h'}$ and $\xi_F = \sqrt{D/h}$ are the ferromagnetic coherence lengths in F' and F respectively, while $\theta = \chi - \chi'$ is the relative angle between F and F' magnetization directions.

Here, F' generates the $S_{\chi'} = 0$ triplets. Thus, its length needs to be short ($l \lesssim \xi'_F$). By contrast, F generates triplet pairs with all different spin projections . To filter out only the long-range components it needs to be much longer than ξ_F ($L \gg \xi_F$).

4.2.1 Effective triplet reservoir Green function

Within the quasiclassical theory, we call $g_{F'}$ and g_F the Green functions in the F' and F layers. Then, the Green function of the effective odd-frequency reservoir is related to the correlation developing at the right edge of the F layer, namely $g_T = g_F(L)$.

Assuming $l \ll \xi_F$ and within the circuit theory, described in chapter 2, the F' layer is a ferromagnetic node of mean level spacing δ'. The Green function in the F' node ($g_{F'}$) is assumed constant and obeys

$$[\frac{2\pi G_Q}{\delta'}(\omega + ih'\sigma_{\chi'})\tau_z + \frac{1}{2}(G_S\, g_S + G_F\, g_F), g_{F'}] = 0, \tag{4.3}$$

where G_S (resp. G_F) is the conductance of the S'/F' (resp. F'/F) interface, $\sigma'_\chi = \cos\chi'\sigma_x + \sin\chi'\sigma_y$, and g_S is the Green function in S'. Assuming that $T'_c \gg \omega, T...$ we consider the superconducting lead in its subgap regime. Thus, $g_S = \tau_\varphi$, where φ is the superconducting phase of S' and, $\tau_\varphi = \cos\varphi\tau_x - \sin\varphi\tau_y$. In particular, we intrinsically assume that $\xi_S \sim \sqrt{D/T'_c} \ll \xi'_F$.

Additionally, by assuming that F' is well coupled to S' ($G_S \gg G_F$), we neglect the leakage current at the F'/F interface such that $g_{F'}$ reads

$$g_{F'} = \frac{(\omega + ih'\sigma_{\chi'})\tau_z + \gamma_S\tau_\varphi}{\sqrt{(\omega + ih'\sigma_{\chi'}))^2 + \gamma_S^2}}. \tag{4.4}$$

Here, $\gamma_S = (G_S/G_Q)\delta'/(4\pi)$ is the induced minigap in F'. Note that a superconductor subject to an external Zeeman field is described by the same Green function with $\gamma_S = \Delta > h' = E_Z$. However, if the external Zeeman field is stronger than Δ ($\gamma_S = \Delta < h' =$

E_Z), superconductivity is destroyed. Thus, the advantage of using an F'/F bilayer is the possibility of realizing both $\gamma_S > h'$ and $h' > \gamma_S$ by tuning, e.g. the transparency of the S'/F' interface.

Remarks on the density of states in F'

Note that the density of states in F' depends on the relative value of h' and γ_S. When $h' < \gamma_S$, the minigap survives and the singularities at $\epsilon = \gamma_S$ in the case of a normal layer split at $\epsilon = \gamma_S \pm h$. At the special case $h' = \gamma_S$, the gap closes and one of the singularity sits at $\epsilon = 0$. Then, when $h' > \gamma_S$ a minigaplike structures opens around $\epsilon = h'$. The comparison with numerical calculations of the Usadel equation [94] shows that the node approximation is qualitatively good, except for the predicted singularities which should smear for a layer of finite thickness as the Touhless energy is reduced. Since a node is a zero dimensional region, its Touhless energy is the largest energy scale, as a consequence the circuit theory neglect the finite size effects.

Having determined $g_{F'}$, let us now consider the long ferromagnetic layer F. Since $L \gg \xi_F$ we cannot directly make use of the circuit theory.

Close to the F'/F interface there is a mixture of short range and long range correlations. The rapidly oscillating nature of the short-range correlations prevents us from directly using the circuit theory. However, at a few ξ_F from the F'/F interface these short-range correlations are suppressed, only non-oscillating long range triplet correlations survive. Then, for $\xi_N \gg z > \xi_F$, we can assume $g_F(z) = g_T = \text{const}$, where z is the distance from the F'/F interface. Hence if $\xi_F \to 0$ we get throughout the layer, $g_F(z) = g_T$, it means that only long-range triplet correlations may exist. Thus, in a circuit theory approach the F layer is a ferromagnetic node with $\xi_F \to 0$ which equivalently corresponds to the limit $h \to \infty$. Consequently, g_T obeys

$$[\omega\tau_z + ih\sigma_\chi\tau_z + \gamma_F g_{F'}, g_T] = 0\,, \text{with } h \to \infty, \tag{4.5}$$

where $\gamma_F = (G_F/G_Q)\delta_F/(4\pi)$ and δ_F is the mean level spacing in the ferromagnetic node F.

In the reference frame where the exchange field is along the z- direction, Eq. (4.5) reads

$$[ih\sigma_z\tau_z + \tilde{A}, \tilde{g}_T] = 0, \tag{4.6}$$

where $\tilde{A} = \omega\tau_z + \gamma_F\tilde{g}_{F'}$ and $\tilde{g}_{T,F'} = R.g_{T,F'}.R^\dagger$ with $R = e^{i\frac{\chi}{2}\sigma_z}$.

We now derive a general solution for Eq. (4.6).

Keeping in mind the normalization $\tilde{g}^2 = 1$, when h is large, $\tilde{g}$ can be expanded perturbatively in the small parameter $1/h$, namely $\tilde{g} = \tilde{g}^{(0)} + (1/h)\tilde{g}^{(1)} + \ldots$.

We now introduce the decomposition $\tilde{A} = \tilde{A}_\perp + \tilde{A}_\parallel$, with $[\tilde{A}_\parallel, \sigma_z\tau_z] = 0$ and $\{\tilde{A}_\perp, \sigma_z\tau_z\} = 0$. Similarly, we write $\tilde{g}$ as $\tilde{g}^{(n)} = \tilde{g}_\parallel^{(n)} + \tilde{g}_\perp^{(n)}$. The idea is that $\tilde{g}$ can be decomposed in a long-range ($\tilde{g}_\parallel$) and a short range ($\tilde{g}_\perp$) part when subjected to a strong exchange field along $\hat{z}$.

Additionally, we further decompose $\tilde{A}_\parallel$ as $\tilde{A}_\parallel = \bar{A}_\parallel + \tilde{J}\sigma_z\tau_z$, where J can be absorbed by the large h value ($h - i\tilde{J} \sim h$) in Eq. (4.6).

In the leading order in h, Eq. (4.6) yields $\tilde{g}_\perp^{(0)} = 0$, and the normalization condition reads $(\tilde{g}_\parallel^{(0)})^2 = 1$.

In the next order, Eq. (4.6) yields

$$2\sigma_z\tau_z\tilde{g}_\perp^{(1)} + [\bar{A}_\parallel + \tilde{A}_\perp, \tilde{g}_\parallel^{(0)}] = 0, \tag{4.7}$$

while the normalization condition reads $\{\tilde{g}_\perp^{(1)} + \tilde{g}_\parallel^{(1)}, \tilde{g}_\parallel^{(0)}\} = 0$. It is solved by $\tilde{g}_\parallel^{(0)} = \bar{A}_\parallel/\sqrt{\bar{A}_\parallel^2}$ (note that $\bar{A}_\parallel^2$ is scalar), $\tilde{g}_\perp^{(1)} = -(1/2)\sigma_z\tau_z[\tilde{A}_\perp, \tilde{g}_\parallel^{(0)}]$, and $\tilde{g}_\parallel^{(1)} = 0$.

As a result, transforming back to the laboratory frame and taking the limit $h \to \infty$, Eq. (4.5) can be simplified to

$$[\omega\tau_z + \gamma_F g_{F'}^{\parallel}, g_T] = 0, \tag{4.8}$$

where $g_{F'}^{\parallel} = \alpha(\omega)\tau_z + i\beta(\omega)\sigma_\chi\tau_\varphi$, with

$$\alpha(\omega) = \frac{1}{4}\mathrm{Tr}(\tau_z g_{F'}) = \frac{1}{2}\sum_\pm \frac{(\omega \pm ih')}{\sqrt{(\omega \pm ih')^2 + \gamma_S^2}} \tag{4.9}$$

$$\beta(\omega) = -i\frac{1}{4}\mathrm{Tr}(\sigma_\chi\tau_\varphi g_{F'}) = -i\sin\theta\frac{1}{2}\sum_\pm \frac{\pm\gamma_S}{\sqrt{(\omega \pm ih')^2 + \gamma_S^2}} \tag{4.10}$$

Here, $\beta(\omega)$ describes the amplitude of the induced triplet correlations and $\theta = \chi - \chi'$ is the relative angle between F and F' magnetizations.

Essentially, to obtain Eq. (4.8) we have suppressed the short range superconducting correlations in $g_{F'}^{\perp}$.

Finally, the Green function for our effective triplet reservoirs can be written

$$g_T = \cosh\vartheta\tau_z + i\sinh\vartheta\sigma_\chi\tau_\varphi, \tag{4.11}$$

where

$$\cosh\vartheta(\omega) = \frac{\omega+\gamma_F\alpha(\omega)}{\sqrt{(\omega+\gamma_F\alpha(\omega))^2-(\gamma_F\beta(\omega))^2}}, \tag{4.12}$$

$$\sinh\vartheta(\omega) = \frac{\gamma_F\beta(\omega)}{\sqrt{(\omega+\gamma_F\alpha(\omega))^2-(\gamma_F\beta(\omega))^2}}. \tag{4.13}$$

The Green function of the triplet reservoir is thus described by a single angle $\vartheta(\omega)$ which depends however on all the parameters $(h', \gamma_S, \gamma_F, \theta)$. In addition, φ is the superconducting phase, and χ is the magnetization direction of the triplet reservoirs. Note that $\cosh\vartheta$ corresponds to the normal Green function and encodes the density of states, whereas $\sinh\vartheta$ corresponds to the anomalous Green function, describing the induced triplet correlations. As $\beta \propto \sin\theta$, we see that, as expected, the triplet correlations vanish for collinear F'/F layers ($\theta = 0$), while they are maximal for perpendicular magnetizations ($\theta = \pi/2$).

Let us now analyze the form of g_T in more details.

Both $\cosh\vartheta(\omega)$ and $|\sinh\vartheta(\omega)|$ are real, monotonous and decreasing as a function of Matsubara frequencies. Fig. 4.3 depicts the general behavior of $|\sinh\vartheta(\omega)|$ for different values of γ_S and γ_F.

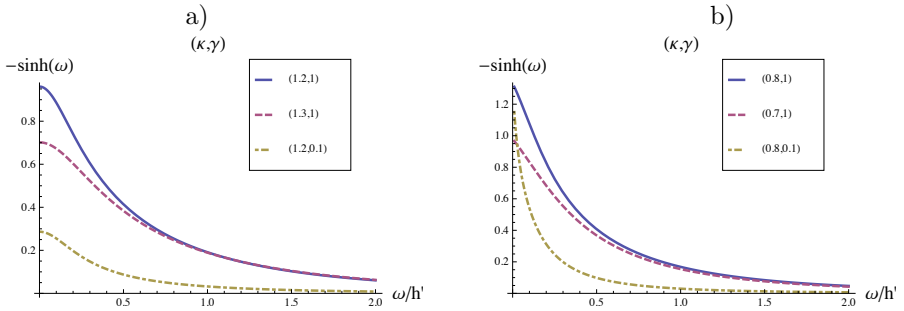

FIGURE 4.3: Plot of $\sinh\vartheta(\omega)$ for differents values of $(\kappa, \tilde{\gamma})$, where $\kappa = \gamma_S/h'$ and $\tilde{\gamma} = \gamma_F/h'$:
a) for $(\kappa = 1.2, \tilde{\gamma} = 1)$ (full line), $(1.3, 1)$ (Dotted line), $(1.2, 0.1)$ (dashed line)
b) for $(\kappa = 0.8, \tilde{\gamma} = 1)$ (full line), $(0.7, 1)$ (Dotted line), $(0.8, 0.1)$ (dashed line)

In order to extract the cutoff energy for triplet correlations as well the density of states of our odd-frequency reservoir, we now study the asymptotic behavior of $g_T(\omega)$ as a function of the dimensionless quantities $\tilde{\omega} = \omega/h'$, $\kappa = \gamma_S/h'$ and $\tilde{\gamma} = \gamma_F/h'$ for some

limiting cases. As a reminder, $\gamma_S = G_S/(4\pi G_Q)\delta'$ and $\gamma_F = G_F/(4\pi G_Q)\delta_F$, with $G_S \gg G_F$.

In particular, we will define two energy scales E_c' and E_c satisfying $E_c' < E_c$.

4.2.2 Asymptotic behavior

4.2.2.1 Case $\gamma_F \gg h', \gamma_S$.

We first consider the case where γ_F is the largest energy scale, in particular it means that $\delta' \gg \delta$. The last requirement may be satisfied if the volume of the F layer is much smaller than the volume of F'.

For $\omega \ll \gamma_F$, we neglect the finite conductance of the F'/F interface, and work with the simplified form for the triplet Green function $\tilde{g}_T$. Namely,

$$\tilde{g}_T(\tilde{\omega}) = \frac{\alpha\tau_z + i\beta\sigma_\chi\tau_\varphi}{\sqrt{\alpha^2-\beta^2}}, \tag{4.14}$$

1. At low frequencies, α and β are singular at $\kappa = 1$ ($\gamma_S = h'$), therefore, we study separately the cases $\kappa < 1$ and $\kappa > 1$. However, in both cases we may define the same energy scale $E_c' = \frac{|\kappa^2-1|}{\max[1,\kappa]}h'$.

   (a) Case $\kappa > 1$. For $\tilde{\omega} \ll E_c'$, we get

   $$\cosh\vartheta(\tilde{\omega}) = \frac{\kappa}{\sqrt{\kappa^2-1}}\left(1 - \frac{\tilde{\omega}^2}{(\kappa^2-1)^2}\right), \tag{4.15}$$

   $$\sinh\vartheta(\tilde{\omega}) = -\frac{1}{\sqrt{\kappa^2-1}}\left(1 - \frac{\kappa^2\tilde{\omega}^2}{(\kappa^2-1)^2}\right) \tag{4.16}$$

   Note that in the limit $\kappa \gg 1$, the amplitude of triplet correlations is very small ($\sinh\vartheta_0 \sim \frac{1}{\kappa} \to 0$).

   (b) Case $\kappa < 1$. For $\tilde{\omega} \ll E_c'$,

   $$\cosh\vartheta(\tilde{\omega}) = \frac{1}{\sqrt{1-\kappa^2}}\left(1 - \frac{\kappa^2\tilde{\omega}^2}{(1-\kappa^2)^2}\right), \tag{4.17}$$

   $$\sinh\vartheta(\tilde{\omega}) = -\frac{\kappa}{\sqrt{1-\kappa^2}}\left(1 - \frac{\tilde{\omega}^2}{(1-\kappa^2)^2}\right). \tag{4.18}$$

   Then, in the limit $\kappa \to 1$, while the Taylor coefficients diverge, the range of validity of the perturbative expansion shrinks to zero ($\tilde{\omega} \ll E_c' \simeq |\kappa^2 - 1| \to 0$). Thus, we additionally consider the intermediate frequency range where $|\kappa^2 - 1| \ll \tilde{\omega} \ll 1$, we obtain

$$\cosh\vartheta = \frac{1}{\sqrt{2\tilde{\omega}}} + \frac{\sqrt{\tilde{\omega}}}{2\sqrt{2}} + \dots, \tag{4.19}$$

$$\sinh\vartheta = -\frac{1}{\sqrt{2\tilde{\omega}}} + \frac{\sqrt{\tilde{\omega}}}{2\sqrt{2}} + \dots \tag{4.20}$$

which is valid for both $\kappa > 1$ and $\kappa < 1$.

2. At large frequencies, when $\tilde{\omega} \gg 1, \kappa$,

$$\cosh\vartheta \simeq 1, \tag{4.21}$$

$$\sinh\vartheta \simeq -\frac{\kappa}{\tilde{\omega}^2}. \tag{4.22}$$

The high energy cutoff for the anomalous Green function is thus $E_c = \sqrt{h'\gamma_S}$. Note that at large κ, $\int d\tilde{\omega} \sinh\vartheta(\tilde{\omega}) \sim 1$, thus triplet correlations exist on a large frequency window but with a small amplitude, we guess that it leads to small current.

4.2.2.2 Extension to intermediate and low conductances, $\gamma_F < h'$

In order to see how the finite conductance of the F'/F interface affects the asymptotic behavior, we now consider arbitrary values for γ_F.

At low Matsubara frequencies, $\omega \ll E_c'$, where E_c' is to be redefined, we obtain:

1. When $\kappa > 1$, at low frequencies, the normal Green function, $\cosh\vartheta$, may be expanded as $\cosh\vartheta \sim c_0^+ + c_2^+\tilde{\omega}^2 + \dots$. For all frequencies, we find that $c_0^+ > 0$ and $c_2^+ < 0$, however the expression of the coefficients is not trivial.

   While , in the previous section, we considered the case $\tilde{\gamma} \gg 1$, here we consider the opposite case, namely, $\tilde{\gamma} \ll 1$,

$$\cosh\vartheta = 1 + o(\tilde{\gamma}) \tag{4.23}$$

$$\sinh\vartheta = -\frac{\tilde{\gamma}\kappa}{(\kappa^2-1)^{3/2}}\left(1 - \frac{2+3\kappa^2}{2(\kappa^2-1)^2}\tilde{\omega}^2\right) + o(\tilde{\gamma}), \tag{4.24}$$

   In particular, we may conjecture that energy scale E_c' is not changed as compared with the previous section. However, the amplitude of the triplet correlations is strongly reduced ($\propto \tilde{\gamma}$).

2. When $\kappa < 1$,

$$\cosh\vartheta = \frac{1}{\sqrt{1-\kappa^2}}\left(1-\frac{\kappa^2}{\tilde{\gamma}\sqrt{1-\kappa^2}}\omega-\frac{\kappa^2(3(\kappa^2-1)+2\tilde{\gamma}^2)}{2\tilde{\gamma}^2(1-\kappa^2)^2}\tilde{\omega}^2\right), \quad (4.25)$$

$$\sinh\vartheta = -\frac{\kappa}{\sqrt{1-\kappa^2}}\left(1-\frac{\kappa}{\tilde{\gamma}\sqrt{1-\kappa^2}}\omega+\frac{\kappa(-2+\kappa^2+\kappa^4+2\tilde{\gamma}^2)}{2\tilde{\gamma}^2(1-\kappa^2)^2}\tilde{\omega}^2\right) \quad (4.26)$$

which is valid for arbitrary values of $\tilde{\gamma}$. This time E_c' is changed, namely $E_c' = \min[\tilde{\gamma}\frac{\sqrt{1-\kappa^2}}{\kappa^2}, \frac{1-\kappa^2}{\kappa}]h'$.

For the following, we introduce the coefficients c_i^- such that $\cosh\vartheta = c_0^- + c_1^-\tilde{\omega} + c_2^-(\tilde{\omega})^2$.

Fig. 4.4.b. shows the $\tilde{\gamma}$ dependence of $c_2^- = \frac{\partial^2\cosh\vartheta}{\partial^2\omega}|_{(\omega=0)}$.

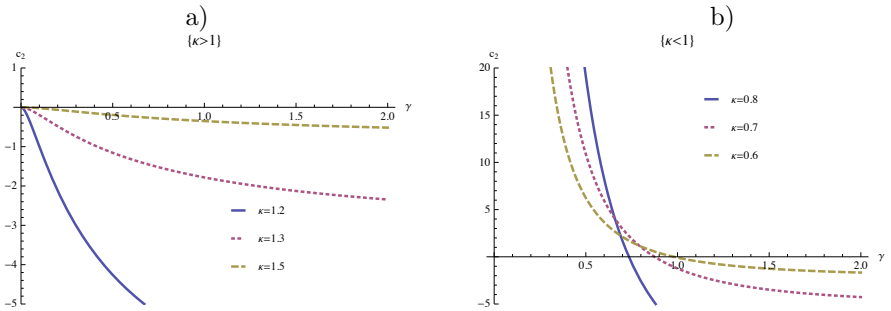

FIGURE 4.4: Plot of the second derivative of $\frac{\partial^2\cosh\vartheta}{\partial^2\omega}|_{(\omega=0)} = c_2^{\pm}$, as a function of $\tilde{\gamma} = \gamma_F/h'$ for different values of κ (a)$\kappa > 1$, and b)$\kappa < 1$). A positive sign is the feature of zero energy peak in the density of states.

At high frequencies, $\omega \gg E_c = (h\gamma_S\gamma_F)^{1/3}$, we obtain $\sinh\vartheta \simeq -\frac{\tilde{\gamma}\kappa}{\tilde{\omega}^3}$. Hence, E_c is a high-energy cutoff for the triplet correlations.

4.2.3 Density of states

We are now in a position to evaluate the DoS in the triplet reservoirs. In particular, it is expressed in terms of the normal Green function,

$$\nu(\epsilon) = \nu_0\frac{1}{4}\mathrm{Re}\,[\mathrm{Tr}[\tau_z g_T(-i\epsilon_+)]] = \nu_0\mathrm{Re}\,[\cosh\vartheta(-i\epsilon+0^+)] \quad (4.27)$$

We are mainly interested by the low energy DoS, in particular we ask the question: Does the effective odd-frequency superconductor present a zero energy peak (ZEP)[51, 54]?

Using the low energy expansion performed in the last section, we obtain

$$\nu(\epsilon) = c_0^{\pm} - c_2^{\pm}(\epsilon/h')^2 + \ldots, \text{ for } \epsilon \ll E_c'. \quad (4.28)$$

Hence the density of states presents a peak at zero energy only if $c_2^{\pm}$ is positive, which happens when $\kappa < 1$ and $\tilde{\gamma} < \sqrt{3/2(1-\kappa^2)}$, see Figs. 4.5 and 4.6. Otherwise, the low-energy DoS is only finite. Note that, in the resonant case $\gamma_S = h'$, the low energy DoS behaves as $\nu(\epsilon \ll E_c) \propto 1/\sqrt{\epsilon}$, thus it does feature the ZEP .

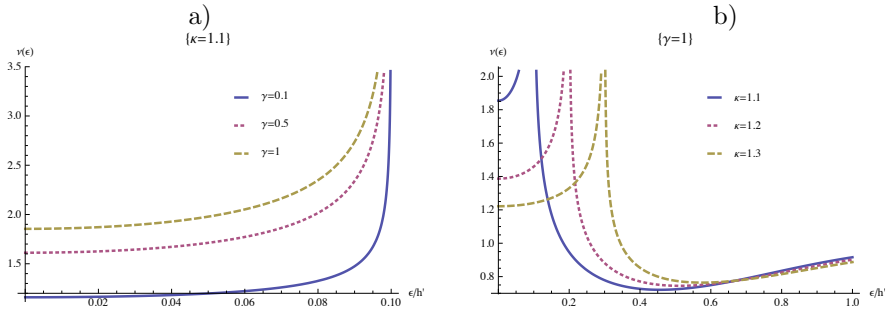

FIGURE 4.5: Density of states as a function of κ and $\tilde{\gamma}$ for $\kappa > 1$. The density at zero energy is > 1 but never presents a ZEP.

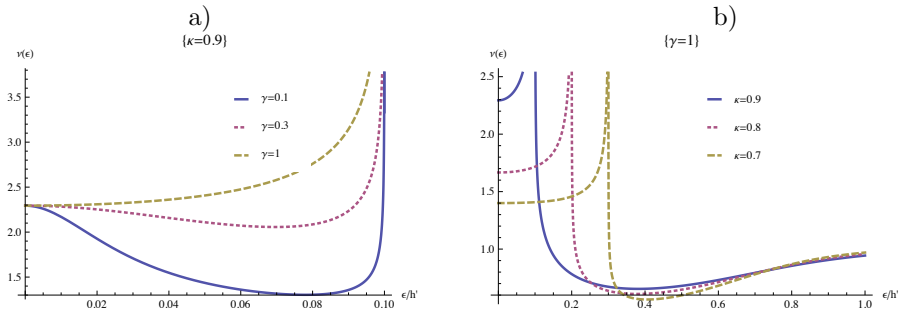

FIGURE 4.6: Density of states as a function of κ and $\tilde{\gamma}$ for $\kappa < 1$. Observe the ZEP at low $\tilde{\gamma}$. The condition for ZEP is : $\tilde{\gamma} < \sqrt{3/2(\kappa^2-1)}$.

At higher energies, the DoS presents singularities when $\epsilon = |\gamma_S \pm h'|$, see Figs. 4.6 and 4.5.

Relevance of our model

We may wonder how relevant is our model of the effective triplet reservoir S_T at describing a bilayer $S/F'/F$. As a reminder, to obtain an analytical expression for g_T, at all temperatures, and avoid a numerical analysis, we subdivided the junction in finite elements (circuit theory). To this end, we considered interfaces of finite transparencies, and reduced each ferromagnetic layer to a node[5]. As well to simplify, we assumed the conventional superconducting lead in the subgap regime and considered interfaces of

[5] In particular, the thickness of the first ferromagnetic layer was assumed short $l \ll \xi_{F'} = \sqrt{D/h'}$. As well to filter out singlet correlations, we assumed the effective exchange field in the second node to be the largest energy scale ($h \to \infty$).

finite transparency. By contrast, the perfect effective triplet reservoir would have good interfaces and using the result of the last chapter, we may wish $l \approx \xi_{F'}$ to have a large triplet correlations amplitude. Furthermore, while the case $\kappa > 1$ ($\gamma_S > h'$) may be realized by applying an external magnetic field to a bulk superconductor adjacent to a long ferromagnet, the second case, namely $\kappa > 1$ is more realistic to describe the ferromagnetic bilayer, where the exchange field is usually much higher than the critical temperature ($h' \gg T_c'$). As an example, a weakly ferromagnetic alloy such as PdNi used by [14] has a Curie temperature of 175K (it yields $h' \gg \gamma_S$, where $\kappa \ll 1$). However the Holmium used in [13] has a smaller T_c around 16K thus, would correspond to $h' \lesssim \gamma_S$[6].

The pertinence of our model for g_T may be tested by comparing it with a numerical calculation of the density of states in similar setups [51, 54].

In particular, Ref. [51] considered a similar $S/F'/F$ hybrid junction, see Fig 4.7.a. In the case $T_c' > h'$, they performed a numerical method to solve the full Usadel equation in order to relate the magnitude of a ZEP and the fraction of odd-frequency triplet pairs. They consider a bilayer ferromegnetic S/F junctions, where the thickness of the first layer corresponds to the case, $\kappa > 1$.

- For a non-collinear bilayer ferromagnet, the computed DoS presents for a wide range of parameters the ZEP ($\kappa > 1$). The ZEP is attributed to the presence of long-range triplet pairs (as it is absent in the homogeneous case), see Fig. 4.7.b. As a comparison, for $\kappa < 1$, in our model, we found a ZEP when $\gamma_F < 3/2\sqrt{h'^2 - \gamma_S^2}$. However the comparison is difficult, as they consider $T_c' \sim h'$ and a good F/F' interface, while we consider the case $T_c' \gg h'$ and a non-perfect F'/F interface.
- By contrast with our result, the DoS of [51] exhibits only a smeared singularity at $\epsilon \simeq h' - \gamma_S$ on the plotting range. In our case, the absence of smearing of the singularities is attributed to the absence of finite size effect intrinsic to the zero dimensional approximation made when converting a ferromagnetic layer to a node.

To conclude while our model may describe both $\kappa < 1$ and $\kappa > 1$. Experimentally, only the case $\kappa < 1$ is realizable with a bilayer ferromagnet, the alternative case may be realized by applying an external field on a superconducting film[7]. In addition, while the singularities in our model are not well described, we believe that the low energy description is qualitatively good. Although, while the DoS presents badly described singularities. With respect to Matsubara frequencies, g_T is continuous. Thus, we believe

[6] To counterbalance the fact that we consider the superconducting in the subgap regime, we consider $\gamma_S \approx T_c'$ and $T_c' < h'$ which would describe a more realistic superconducting lead well coupled to the short ferromagnetic layer F'.

[7] We will see in the next section, that the current is not very changed from one case to the other.

that the tranport properties (equilibrium currents) derived by summing on the imaginary axes (Matsubara) will be qualitatively good.

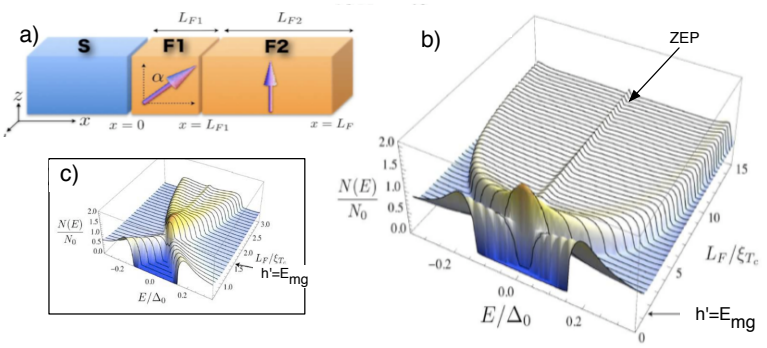

FIGURE 4.7: Numerical analysis of the DoS in $S/F_1/F_2$ junction from [51]. a) Model for their junction. b) DoS as a function of $L_F = L_{F1} + L_{F2}$ for $L_{F_1} \simeq 1.5\xi_F$ ($h'/T_c = 0.1$, $\xi_F \simeq 3\xi_{T_c}$ and $\alpha = \pi/2$). The ZEP (arrow) is characteristic of the presence of triplet long-range. c) Magnified low energy DoS, note the closing of the gap and the resonance at $h' = E_{mg}$.

4.3 $S_T/S/S_T$ junction

We are now in a position to study the $S_T/S/S_T$ junction presented in the introduction:

- S is a superconductor of bare temperature T_c and typical size $L \ll \xi_N$.
- $S_T \equiv S'/F/'F$ are the effective odd-frequency superconducting leads described in the previous section. For simplicity, we assume they have the same properties, namely $\vartheta = \vartheta_L = \vartheta_R$. However, they may have different superconducting phase $\varphi_{L/R}$ and magnetization axes $\chi_{L/R}$. In particular, we choose $\varphi_L = -\varphi_R = \varphi/2$ and $\chi_R = -\chi_L = \chi/2$ such that φ is the phase bias of the junction and χ is the relative angle between the magnetization axes. Then, their respective Green function reads

$$g_{L/R} = \cosh\vartheta\tau_z + i\sinh\vartheta\sigma_{\chi_{L/R}}\tau_{\phi_{L/R}}. \tag{4.29}$$

We now use the circuit theory[8] to describe the properties of the junction (see Chapter 2).

In the language of circuit theory, S is a superconducting node of mean level spacing δ which is connected to the left and right odd-frequency leads via connectors of respective

[8] we consider $L \ll \xi_N$ where L is the typical size of the superconducting node

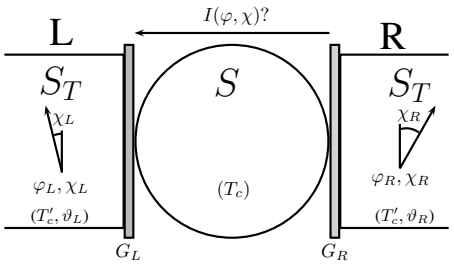

FIGURE 4.8: The effective $S_T/S/S_T$ junction the superconducting node (S) is sandwiched between two triplet reservoirs (S_T). $\varphi_{L/R}$ and $\chi_{L/R}$ are the phase and the magnetization direction of left (L) and right (R) reservoirs.

conductances G_L and G_R, see Fig. 4.8. Then, g is the Green function in the node S. It satisfies the normalization $g^2 = 1$ and obeys

$$[\omega\tau_z + \Delta\tau_\phi, g] + \hat{I}_L + \hat{I}_R = 0. \tag{4.30}$$

Here $\hat{I}_{L/R} = 1/2\gamma_{L/R}[g_{L/R}, g]$ are the spectral leakage currents at the left and right connectors, where $g_{L/R}$ are the Green functions of the L and R leads defined above and $\gamma_{L/R} = G_{L/R}/G_Q\delta$. In addition, Δ and ϕ are the amplitude and phase of the superconducting order parameter in the node, they satisfy the self-consistent equation

$$\ln\frac{T_c}{T} = 2\pi T\sum_{\omega>0}\left(\frac{1}{\omega} - \frac{e^{-i\phi}}{4\Delta}\mathrm{Tr}\left[\tau_-(g+g^\dagger)\right]\right), \tag{4.31}$$

where $\tau_- = (\tau_x - i\tau_y)/2$. Note that to determine the phase we can alternatively consider the free energy of the junction and minimize it.

Finally, the charge current flowing through the junction is expressed via the spectral leakage current at left or right interfaces

$$I_{L/R} = -\pi T\sum_{\omega>0}\mathrm{Im}[\mathrm{Tr}[\tau_z\hat{I}_{L/R}]. \tag{4.32}$$

Because the charge in the node is conserved, the charge current obeys $I = I_R = -I_L$.

4.3.0.1 Free energy of the junction (E_J)

For a better understanding of the underlying mechanism, it is interesting to extract the free energy of the junction E_J. In particular, E_J depends on both ϕ, the phase in the

node, and $\varphi_{L/R}$ the phase in the L/R reservoir and satisfies

$$\frac{\partial E_J}{\partial \varphi_{L/R}} = I_{L/R}, \tag{4.33}$$

and,

$$\frac{\partial E_J}{\partial \phi} = I_L + I_R. \tag{4.34}$$

Additionally, in equilibrium, the Josephson energy should be minimum with respect to ϕ, namely, using Eq. (4.34) we obtain

$$I_L + I_R = 0, \tag{4.35}$$

$$\frac{\partial I_L + I_R}{\partial \phi} > 0. \tag{4.36}$$

Note that Eq. (4.35) is simply the current conservation. This condition is included in the imaginary part of Eq. (4.31).

In the first part, for better readability and understanding, we consider the weak coupling regime. In the second part, we derive the exact solution for comparison and extension of the weak-coupling results.

4.3.1 Weak coupling limit

4.3.1.1 Perturbative expansion

In the weak coupling limit, $\gamma_{L/R} = G_{L/R}/G_Q\delta$ are the smallest energy scales in the system. Therefore, using $\gamma_{L/R}$ as small parameters, it is possible to perform a perturbative expansion of g around its bulk value g_0. To this end, we write: $g = g_0 + g_1 + \ldots$ where $g_0 \gg g_1$. Consequently, the charge current can be rewritten in the form: $I_{L/R} = I^{(1)}_{L/R} + I^{(2)}_{L/R} + \ldots$, where $I^{(i)}_{L/R}$ is expressed in terms of g_{i-1},

$$I^{(i)}_{L/R} = G_{L/R}\pi T \sum_{\omega>0} \mathrm{ImTr}[\tau_z[g_{i-1}, g_{L/R}]]. \tag{4.37}$$

Using Eq. (4.37), the Josephson energy E_J may also be expanded as $E_J = E_J^{(1)} + E_J^{(2)} + \ldots$.

Bare Green function

Let us start with the Green function of the bare node g_0. It solves Eq. (4.30) for $\gamma_{L/R} = 0$[9] and thus, it reads

$$g_0 = \frac{\omega\tau_z + \Delta_0\tau_\phi}{\sqrt{\omega^2 + \Delta_0^2}}, \tag{4.38}$$

where $\Delta_0(T)$ and ϕ are the amplitude and the phase of the superconducting order parameter, respectively. Whereas $\Delta_0(T)$ is determined by the self-consistency equation

$$2\pi T \sum_\omega \frac{1}{\omega} - \ln\frac{T_c}{T} = 2\pi T \sum_\omega \frac{1}{\sqrt{\omega^2 + \Delta_0^2}}, \tag{4.39}$$

ϕ is free for the bare node. The $U(1)$ symmetry is broken once the node is coupled to the reservoirs.

Then inserting g_0 in Eq. (4.32), we find $I^{(1)}_{L/R} = 0$ and thus $E^{(1)}_J = \text{const}$ (at any temperature): no Josephson coupling exists at first order. This is due to symmetry mismatched: a triplet pair from one reservoir may not transform as a singlet pair of S and generate a first order Josephson coupling.

We thus need to study higher orders to reveal a non-zero Josephson coupling. As an example, the recombination of two triplet pairs in two singlet Cooper pairs is authorized and will contribute to a second order Josephson coupling.

First order correction g_1

The first order expansion of Eq. (4.30) gives

$$[\omega\tau_z + \Delta_0\tau_\phi, g_1] = [g_0, \frac{\gamma_L g_L + \gamma_R g_R}{2} + \Delta_1\tau_\phi], \tag{4.40}$$

where Δ_1 is the first order correction to Δ_0. In addition, the normalization reads

$$\{g_0, g_1\} = 0. \tag{4.41}$$

Then as a solution of both Eqs. (4.40) and (4.41), g_1 reads

$$g_1 = \frac{1}{\sqrt{\omega^2 + \Delta_0^2}} \left(\frac{\gamma_L g_L + \gamma_R g_R}{2} + \Delta_1\tau_\phi - g_0 \frac{1}{2} \left\{ \frac{\gamma_R g_R + \gamma_L g_L}{2} + \Delta_1\tau_\phi \, , g_0 \right\} \right). \tag{4.42}$$

Equivalently, g_1 may be expressed as

[9] g_0 solves $[\omega\tau_z + \Delta_0\tau_\phi, g_0] = 0$.

$$g_1 = g_0 \frac{1}{\sqrt{\omega^2+\Delta_0^2}} \frac{1}{2} \left[g_0, \frac{\gamma_R g_R + \gamma_L g_L}{2} + \Delta_1 \tau_\phi \right]. \tag{4.43}$$

Likewise, the self-consistency equation gives

$$\Delta_1/\Delta_0 = -\gamma \left(\sum_\omega \frac{\omega \cosh\vartheta}{(\omega^2+\Delta_0^2)^{3/2}} \right) / \left(\sum_\omega \frac{\Delta_0^2}{(\omega^2+\Delta_0^2)^{3/2}} \right). \tag{4.44}$$

Since $\Delta_1 < 0$, superconductivity in the node is weakened. This contrasts with $S'/S/S'$ junctions where superconductivity is enhanced by the coupling to superconducting leads (see Appendix).

This reduction does not depend on $\varphi_{L/R}$ and should be assigned to the finite density of states at low energies in the triplet reservoirs ($\propto \cosh\vartheta$). It features an inverse proximity effect where quasiparticles, existing at zero energy in the leads, leak in the node and weaken the condensation mechanism. Such a leakage of singlet pairs in the leads may be viewed as a loss for the condensate. Again this is no surprise, by symmetry arguments, the phases $\varphi_{L/R}$ can only enter in the second order correction to Δ.

As a first consequence, the effective critical temperature T_c^* is decreased: $T_c^* < T_c$.

Then incorporating g_1 into Eq. (4.32), we find that the charge current at the L/R interface arises from the contribution of $\frac{1}{4\sqrt{\omega^2+\Delta_0^2}} \mathrm{Tr}[i\tau_z \left[\gamma_{R/L} g_{R/L} - g_0(\gamma_R g_R + \gamma_L g_L) g_0, \gamma_{L/R} g_{L/R}\right]$.

Thus, the charge current may be decomposed into a quasiparticle ($\propto a(T)$) and a condensate contribution ($\propto b(T)$), namely

$$I^{(2)}_{L/R} = \begin{pmatrix} \mp a(T) \frac{G_L G_R}{G_Q} \cos\chi \sin(\varphi_L - \varphi_R) \\ b(T) (\frac{G^2_{L/R}}{G_Q} \sin 2(\varphi_{L/R} - \phi) + \frac{G_L G_R}{G_Q} \cos\chi \sin(\varphi_L + \varphi_R - 2\phi)) \end{pmatrix} \tag{4.45}$$

where

$$a(T) = 2\pi T \sum_{\omega>0} \frac{\sinh^2\vartheta}{\sqrt{\omega^2+\Delta_0^2}} (2 - \frac{\Delta_0^2}{\omega^2+\Delta_0^2}) \tag{4.46}$$

$$b(T) = 2\pi T \sum_{\omega>0} \frac{\sinh^2\vartheta \Delta_0^2}{(\omega^2+\Delta_0^2)^{3/2}}. \tag{4.47}$$

Here, $b(T)$ is zero above the superconducting transition and is increasing as temperature is further decreased. By contrast, for $E_c \gg T_c$, $a(T)$ is non-monotonous, it reaches a maximum at finite temperature in the vicinity of the superconducting transition (around T_c in the weak coupling limit), see see Fig. 4.9.a. However, when $E_c \approx T_c$, both $a(T)$ and $b(T)$ are monotonous, see Fig. 4.9.b. Additionally, at any temperature $a(T) > b(T)$.

In the limit, where $E_c \gg T_c$, the anomalous function $(\sinh\vartheta)$ of the reservoirs may be taken as a constant and we find $a(T) \approx (\sinh^2\vartheta(0))\ln E_c/\max[\Delta_0(T), T]$ and $b(T) \approx (\sinh^2\vartheta(0))\Delta_0(T)^2/\max[\Delta_0^2(T), T^2]$, thus for $E_c \gg T_c$ we find $a(T) \gg b(T)$.

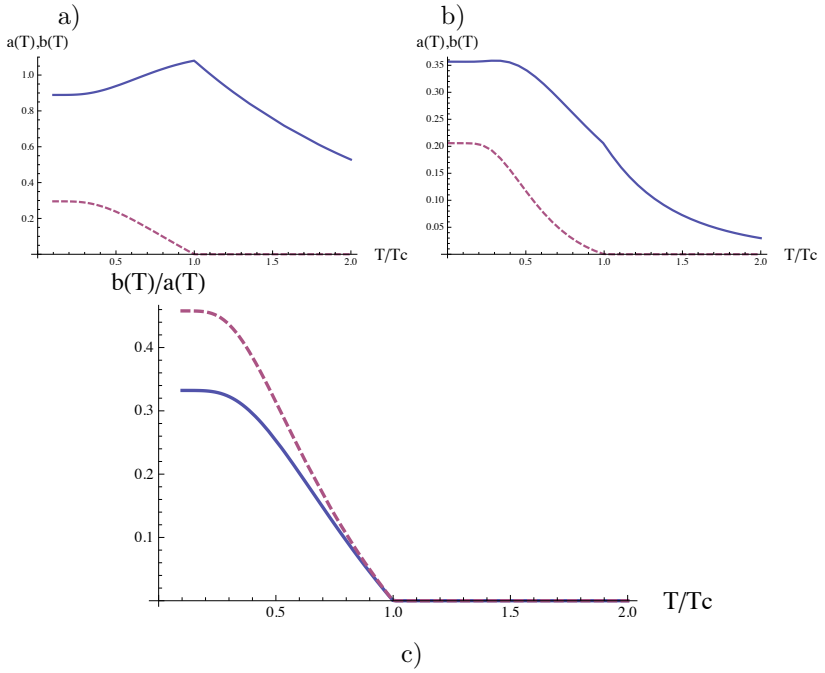

FIGURE 4.9: Temperature dependence of $a(T)$ and $b(T)$ as a function of T/T_c. a). $h' = 10T_c$, $a(T)$ is maximum at T_c. b). for $h' = 3T_c$, both $a(T)$ and $b(T)$ are monotonously increasing with decreasing temperature. Note that case b. may be realized only with very weak ferromagnets.c) Ratio $b(T)/a(T)$ for $h' = 10Tc$ (Thick line) and $h' = 3T_c$ (Dashed line)

Then, using Eqs. (4.34) and (4.33), the second order Josephson energy may be decomposed as $E_J^{(2)} = E_J^{\mathrm{Qp}} + E_J^{\mathrm{Cd}}$, where

$$E_J^{\mathrm{Qp}} = +a(T)\frac{G_L G_R}{G_Q^2} \times \cos\chi\cos(\varphi_L - \varphi_R) \tag{4.48}$$

$$E_J^{\mathrm{Cd}} = -b(T) \times \left(\frac{G_L^2}{2G_Q^2}\cos 2(\varphi_L - \phi) + \frac{G_R^2}{2G_Q^2}\cos 2(\varphi_R - \phi) + \frac{G_L G_R}{G_Q^2}\cos\chi\cos(\varphi_L + \varphi_R - 2\phi) \right). \tag{4.49}$$

See Fig. 4.10. E_J^{Qp} is the quasiparticle contribution, it correponds to the effective odd/odd-frequency coupling between the leads. The transport of one triplet pair is mediated by one triplet Andreev pair through the central node. Such triplet Andreev

pair consists of two quasiparticles of the same spin. This contribution exists when S is normal metallic and is reduced below the superconducting transition when $T < T_c$. Thus, the low energy cutoff is $\max[\Delta_0, T]$. Note that, as a function of χ, E_J^{Qp} changes sign and is suppressed when both reservoirs are incoherent, namely when $\chi = \pi/2$, . The case $\chi = 0$ and $\chi = \pi$ were obtained by Refs. []. In particular, we find that χ may serve as a parameter to control the quasiparticle contribution.

Then $E_J^{\mathrm{Cd}}(\propto \Delta_0^2)$ corresponds to the odd/even-frequency Josephson coupling between two triplet pairs from the leads and two singlet pairs from the central node. It exists only for $T < T_c$ and encloses three contributions. The terms $\propto \cos(2(\varphi_{L/R} - \phi))$ are the odd/even-frequency Josephson coupling at each L/R interfaces. Then, the term $\propto \cos(\varphi_L + \varphi_R - 2\phi)$ is a crossed coupling, where two triplet pairs, one from each lead, recombine in two singlet pairs of S.

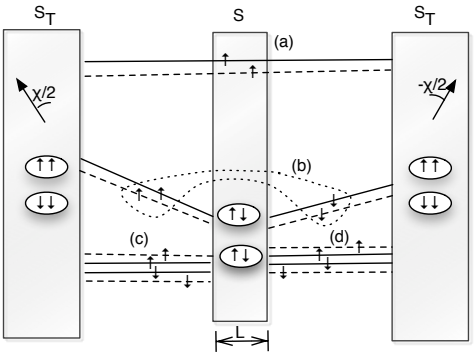

FIGURE 4.10: $S_T/S/S_T$ junction. Josephson energy of the $S_T/S/S_T$ Josephson junction. S_T are respectively the left and right reservoirs of triplet pairs with spin projection ± 1 along respectively $\chi/2$ and $-\chi/2$ axes, while S is the superconducting layer. The wavy line is a pictorial separation between the Cooper pairs of the condensate (even-frequency) and quasiparticles. Additionnaly, the spacer between S_T and S layers is fictive, it allows to represente the fictive Andreev reflections happening at interfaces. Then, (a) corresponds to the odd/odd Josephson coupling via quasiparticles in S. (b), (c) and (d) are the 3 possibles odd/even Josephson coupling carried by the condensate of Cooper pairs. Note that (b) is a crossed mechanism, 2 Cooper pairs from S recombine as two triplets, each of them belonging to a different triplet reservoir.

The phase ϕ may now be determined by minimizing the Josephson energy using Eqs. (4.35) and (4.36). In the following we consider $\varphi_{L/R} = \pm\frac{\varphi}{2}$ such that φ is the phase bias between reservoirs.

symmetric junction

In the case of a symmetric junction, ϕ satisfies

$$\sin 2\phi \cos\frac{\varphi+\chi}{2}\cos\frac{\varphi-\chi}{2} = 0, \tag{4.50}$$

$$\cos 2\phi \cos\frac{\varphi+\chi}{2}\cos\frac{\varphi-\chi}{2} > 0. \tag{4.51}$$

The minimization depends on 2ϕ as a consequence of the second order Josephson coupling between odd- and even-frequency superconductors[10]. As a result, the phases ϕ and $\phi+\pi$ are not distinguishable, and thus, ϕ is defined modulo π instead of 2π. For $\varphi, \chi \in [-\pi, \pi]$, the phase ϕ depends on the relative values of both φ and χ via,

$$\phi = \begin{cases} 0 & |\varphi| + |\chi| < \pi, \\ \pi/2 & |\varphi| + |\chi| > \pi. \end{cases} \tag{4.52}$$

Hence, as a function of both φ and χ, the phase ϕ is discontinuous and is either 0 or $\pi/2$ modulo π. However, we will show below that such discontinuity is an artifact of the symmetric case.

non-symmetric junction

In the case of a non-symmetric junction, for readability, we introduce $\gamma = \frac{\gamma_R+\gamma_L}{2}$ and $\bar{\gamma} = \frac{\gamma_R-\gamma_L}{2}$ (The symmetric junction corresponds $\bar{\gamma} = 0$). In equilibrium, the phase ϕ satisfies

$$\sin(2\phi)\left(\gamma^2\cos\frac{\varphi+\chi}{2}\cos\frac{\varphi-\chi}{2} + \bar{\gamma}^2\sin\frac{\varphi+\chi}{2}\sin\frac{\varphi-\chi}{2}\right) + \cos(2\phi)\gamma\bar{\gamma}\sin\varphi = 0 \tag{4.53}$$

$$\cos(2\phi)\left(\gamma^2\cos\frac{\varphi+\chi}{2}\cos\frac{\varphi-\chi}{2} + \bar{\gamma}^2\sin\frac{\varphi+\chi}{2}\sin\frac{\varphi-\chi}{2}\right) - \sin(2\phi)\gamma\bar{\gamma}\sin\varphi > 0 \tag{4.54}$$

Noticing the symmetries $\phi(\varphi,\chi) = \phi(\varphi,-\chi) = \pi - \phi(-\varphi,\chi)$, we solve Eqs. (4.53) and (4.54) on the reduced interval $\varphi, \chi \in [0, \pi]$. Fig. 4.11 shows that the discontinuity of the phase is smeared as the asymmetry is increased.

[10] An even number of pairs is necessary to build up a Josephson coupling.

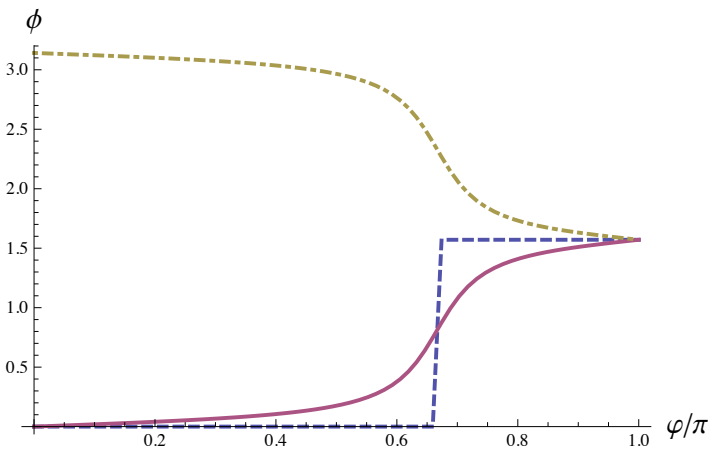

FIGURE 4.11: Realized superconducting phase in S as a function of $\varphi = \varphi_L - \varphi_R$ for $\chi = \pi/3$ (in the weak coupling limit) for different values of G_L/G_R: the dashed line (blue) is the symmetric case ($G_L = G_R$). The full and the dotted-dashed lines correspond to $G_L = 1.2G_R$ and $G_R = 1.2G_L$, respectively. For an asymmetric junction ($G_L \neq G_R$ the switching of the phase is smeared and presents a symmetry under the exchange $G_L \leftrightarrow G_R$ and $\varphi \leftrightarrow -\varphi$. Note that the ϕ is defined modulo π, the curves may be shifted by an multiple of π upward or downward.

In particular, for a slightly asymmetric junction ($\gamma \gg \bar{\gamma}$), the discontinuity broadens on the scale $\delta \simeq \frac{|\bar{\gamma}|}{\gamma} \tan\chi$. For $\bar{\gamma} > 0$, when $\varphi + \chi = \pi$, we find that $\phi = 3\pi/4[\pi]$, and when $-\varphi + \chi = \pi$ $\phi = \pi/4[\pi]$.

charge current

We are now in a position to plot the charge current flowing through the junction as a function of the phase bias (φ). Further using Eq. (4.45) and following the decomposition of the Josephson energy, the charge current may be decomposed into a quasiparticle ($I_{\rm Qp} = \frac{\partial E_J^{\rm QP}}{\partial \varphi_L}$) and a condensate contribution ($I_{\rm Cd} = \frac{\partial E_J^{\rm Cd}}{\partial \varphi_L}$), namely $I = I_{\rm Qp} + I_{\rm Cd}$[11]. The condensate contribution is ϕ- dependent and is carried by Cooper pairs in S. Then, the quasiparticle contribution depends only on the phase bias of the reservoir, it results from the proximity effect (Andreev pairs).

1. In the symmetric case, the current phase relation (CPR) takes the simple form

$$I(\varphi,\chi,T) = \frac{G^2}{G_Q}(a(T)\cos\chi - b(T)\mathrm{Sign}[\cos\varphi + \cos\chi])\sin\varphi, \quad (4.55)$$

$$I_{\rm QP} = \frac{G^2}{G_Q}a(T)\cos\chi\sin\varphi \quad (4.56)$$

$$I_{\rm Cond} = -\frac{G^2}{G_Q}b(T)\mathrm{Sign}[\cos\varphi + \cos\chi])\sin\varphi, \quad (4.57)$$

[11] the phase ϕ satisfies $I_L + I_R = 0$,such that the current conservation is obeyed and $I = I_L = -I_R$

where the $\phi-$ dependence is hidden in the Sign function. At the phase switching (when $|\varphi| + |\chi| = \pi$), the condensate is discontinuous, it reverses its sign. As a result, the full As a result, the condensate contribution is discontinuous and changes sign Thus, due to the ϕ dependence of the condensate contribu(stion, the full CPR is discontinuous as a function of φ. Additionally, the condensate and the quasiparticle contribution are either of the same or of opposite sign as a function of φ, see Fig. 4.12

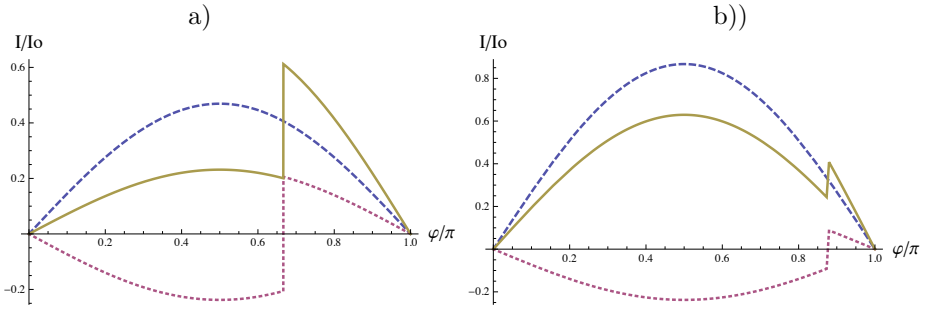

FIGURE 4.12: Current phase relation. I/I_0 (full line), condensate contribution I_{Cond}/I_0 (dotted line), quasiparticules contribution I_{QP}/I_0(dashed line) at $T = 0.5T_c$ for: a) $\chi = \pi/3$ and b) $\chi = \pi/8$. Both I/I_0 and I_{Cond}/I_0 are discontinuous at $\varphi = \pi - \chi$. The charge current is maximum for $\varphi = \pi - \chi$ on plot a) and for $\varphi = \pi/2$ in b) (see the arrow). Here $I_0 = G\gamma$, $h' = 10T_c$, $\kappa = 0.5$ and $\gamma_F = 10h'$.

2. In the non-symmetric case, the phase ϕ is a smooth function of φ set by Eqs. (4.53) and (4.54). Likewise, the charge current reads $I = I_{\text{Qp}} + I_{\text{Cd}}$, with

$$I_{\text{Qp}} = \frac{G_R G_L}{G_Q} a(T) \cos\chi \sin\varphi, \tag{4.58}$$

$$I_{\text{Cd}} = -G_L b(T) \left(\frac{G_L}{G_Q} \sin(\varphi - 2\phi) - \frac{G_R}{G_Q} \cos\chi \sin 2\phi \right). \tag{4.59}$$

Because the superconducting phase is changing smoothly as a function of φ, both, the condensate contribution and the CPR, are continuous and smooth see Fig. 4.13.

Critical current

When S is superconducting, we decomposed the current into a condensate contribution (odd/even Josephson coupling between the central island and the leads) and a quasiparticle contribution (effective odd/odd-frequency coupling between leads). As depicted in Fig. 4.12, both contribution may be either of the same or of opposite sign. Thus, to get more insight about the possible competition between quasiparticle and condensate

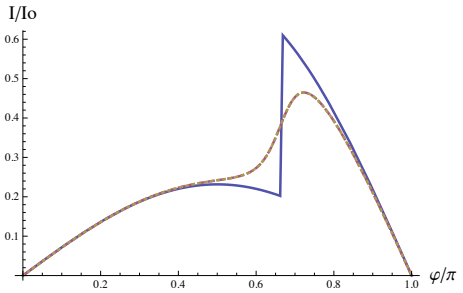

FIGURE 4.13: Current phase relation. Plot of I/I_0 as a function of the phase bias (φ) for $\chi = \pi/3$. The full line is the symmetric case while the dashed line corresponds to an asymmetric junction ($\frac{G_L - G_R}{G_L + G_R} = 0.1$). Here $I_0 = G\gamma$, $h' = 10T_c$, $\kappa = 0.5$ and $\gamma_F = 10h'$.

contributions, we now study the critical current of the junction I_c, where

$$I_c(T, \chi) = \max_{\varphi}[I(\varphi, T, \chi)]. \tag{4.60}$$

We will show that for a wide range of parameters, they are of opposite sign. The condensation mechanism (singlet pairs) tends to reduce the critical current of the junction.

Symmetric case

Let us start with the case of a symmetric junction, and separate the case $\chi > pi/2$ from the case $\chi < \pi/2$.

As shown in Fig. 4.12, as a function of φ, the maximum happens either at $\varphi = \pi/2$ or at $\varphi = \pi - |\chi|$.In particular,

- when $\chi < \pi/2$ the variation array reads

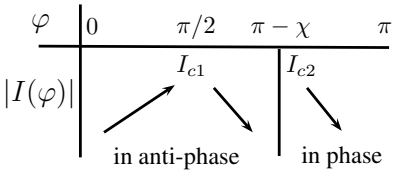

  Here "phase and anti-phase" means that the I_{QP} and I_{Cond} contributions are on this range respectively in phase or in anti-phase with

$$I_{c1} = |a(T)\cos\chi - b(T)| \tag{4.61}$$

$$I_{c2} = \sin\chi\,(a(T)\cos\chi + b(T)) \tag{4.62}$$

Therefore, the critical current simply reads: $I_c^<(\chi) = \mathrm{Max}[I_{c1}, I_{c2}]$, where "<"refers to the case $\chi < \pi/2$.

- when $\chi > \pi/2$ the variation array reads

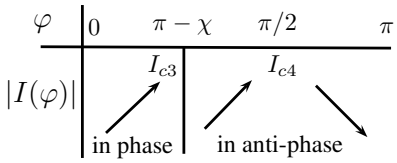

where

$$I_{c3} = \sin\chi(a(T)\cos(\pi-\chi) + b(T)) \tag{4.63}$$

$$I_{c4} = |a(T)\cos(\pi-\chi) - b(T)| \tag{4.64}$$

Hence, we find that $I_c^>(\chi) = \mathrm{Max}[I_{c3}, I_{c4}] = I_c^<(\pi-\chi)$.

Since $I_c(\chi) = I_c(\pi-\chi)$, we further restrict the study on $\chi \in [0, \pi/2]$ where the critical current reads

$$I_c(T) = \max[I_{c1}(T), I_{c2}(T)], \tag{4.65}$$

the I_{c1} and I_{c1} branches have been defined above. As a preliminary step, we study their χ and temperature dependences as a function of the triplet reservoirs parameters (h', κ, γ_F).

Study of the I_{c1} and the I_{c2} branches

The I_{c2} branch is monotonous and increases as temperature is decreased.

By contrast, the I_{c1} branch, as a function of temperature, presents one maximum at finite temperature $T_1 \neq 0$ with $T_1 \leq T_c$. Moreover, when there exists a temperature such that $I_{c1}(T) = 0$, a second maximum exists at zero temperature.

In particular, when E_c' is increased $T_1 \to T_c$ and the local maximum at zero temperature tends to disappear. In addition, we observe that $T_1 \approx T_c$ when approximately $\cos(\chi)T_c \lesssim \cos(\frac{\chi}{2})E_c'$, see Fig. 4.15.

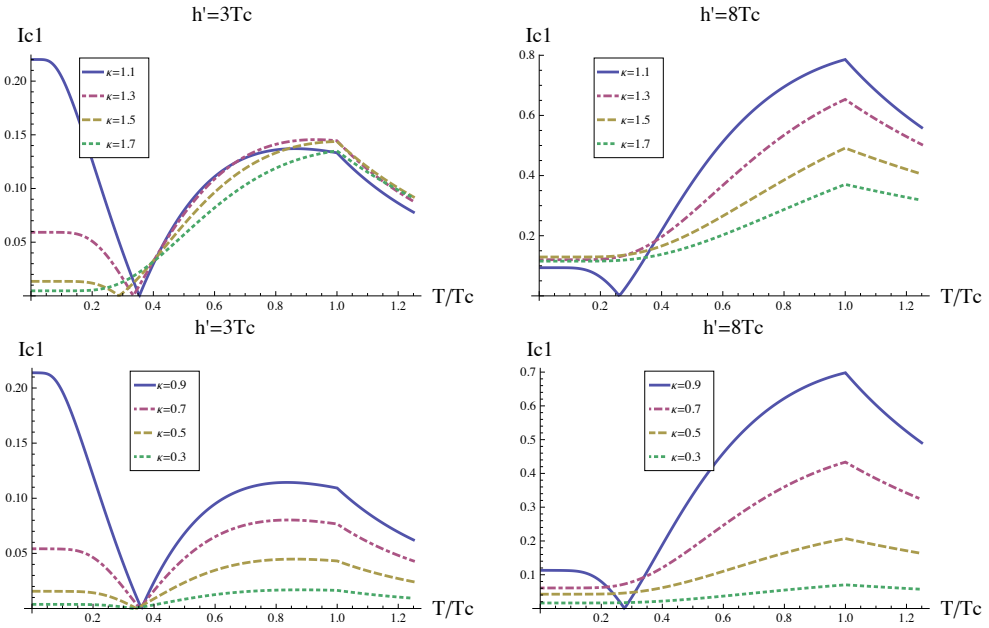

FIGURE 4.14: Temperature dependence of the I_{c1} branch for differents values of $\kappa = \gamma_S/h'$, with $\chi = \pi/3$ and $h' = 3T_c$ (left) and $h' = 8T_c$(right) ($\gamma_F = 10T_c$). I_{c1} has one or two maximum happening at $T_1, T_1' < T_c$. When $E = h'\sqrt{|1-\kappa^2|}$ is increased then the second maximum vanishes and $T_1 \to T_c$.

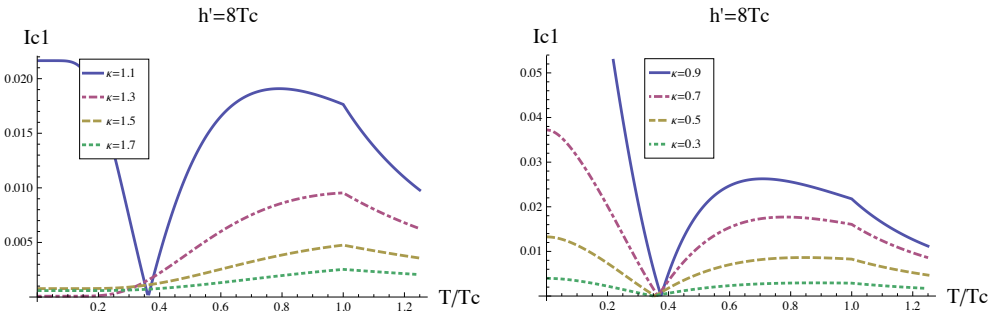

FIGURE 4.15: Temperature dependence of the I_{c1} branch for $\chi = \pi/3$, $h' = 8T_c$ at low $\gamma_F = T_c/100$). The second maximum at T_1' reappears as γ_F is lowered.

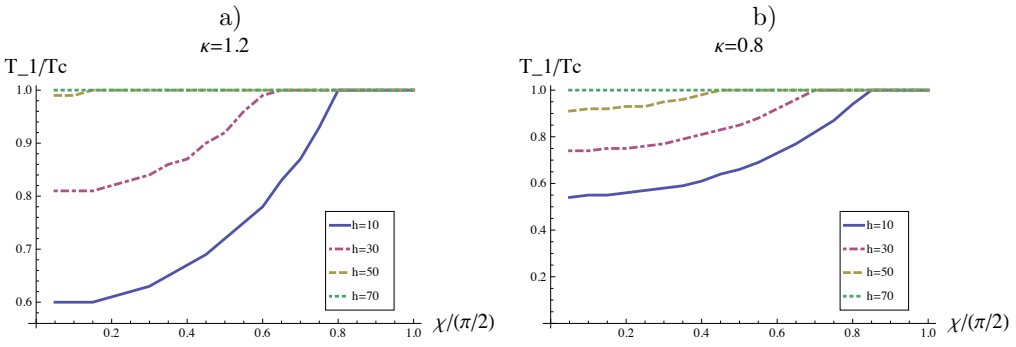

FIGURE 4.16: Temperature T_1 of the first maximum of I_{c1} as a function of χ for different value of h' and a)$\kappa = 1.2$, b)$\kappa = 0.8$. When $\chi \to \pi/2$ the maximum is at the superconducting transition $T_1 \to T_c$, while as h' is decrease T_1 departs from T_c.

The I_{c1} and I_{c2} branches, for a defined χ, may cross at $T = T_2$. The temperature T_2 is solution of $I_{c1}(T) = I_{c2}(T)$ which takes the form,

$$\frac{b(T_2)}{a(T_2)} = \frac{\cos\chi(1 \mp \sin\chi)}{1 - \sin^2\frac{\chi}{2}(1 \mp \sin\chi)}, \tag{4.66}$$

where the r.h.s is the function $f_{\pm}(\chi)$, see Fig. 4.17, and the l.h.s is monotonous and decreasing with increasing temperature: $b(T)/a(T) < 1$, and is maximum at $T = 0$. Since $B_0 = b(0)/a(0) < 1$ and $f_+(\chi) > 1$, Eq. (4.66) with the "+" sign has no solution. Defining the angle $\chi_2 = f_-^{-1}(B_0)$, we find that Eq. (4.66) has a unique solution if $\chi > \chi_2$, otherwise the branches never cross.

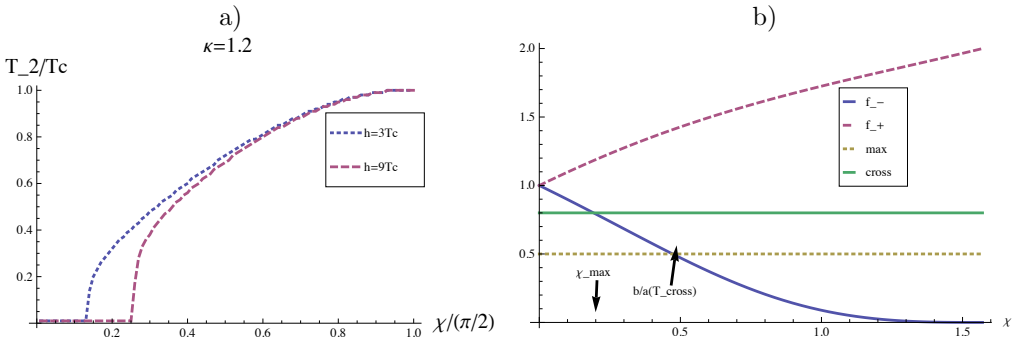

FIGURE 4.17: Crossing temperature of I_{c1} and I_{c2}. Plot (a) shows the dependence of T_2 on χ I_{c1}. Note that the temperature of crossing does not depend much on κ and h', when $T_2 = 0$, I_{c1} and I_{c2} don't cross.b) gives the criterion for the crossing. The crossing of $b(0)/a(0)$ with f_+ determines the threshold angle χ_2 below which no crossing occurs.

4.3.1.2 Critical current

As the critical current reads $I_c(T) = \max[I_{c1}(T), I_{c2}(T)]$, for a fixed χ and as a function of temperature, I_c lies either on the I_{c1} or on the I_{c2} branch (studied in the previous

section). When the magnetization direction between the leads is perpendicular ($\chi = \pi/2$), we obtain at any temperature $I_c = I_{c2}(T)$, the critical current is zero above T_c and monotonously increases as temperature is lowered.

When $\chi \neq \pi/2$, the temperature dependence of the critical current is richer.

At high temperature, when $T > T_c$, since the condensate contribution is absent, I_c lies on the I_{c1} branch: I_c is increasing as temperature is decreased. However, when $\chi \sim \pi/2$, the amplitude of I_{c1} is very small. Thus, by playing with the magnetic configuration, we can tune the amplitude of I_{c1}, it will be interesting when the condensate also contributes.

At $T < T_c$, the node S gets superconducting. Thus, the amplitude of I_{c2} develops and increases as temperature is further lowered. Remember, T_1 is the temperature of the first maximum (starting from T_c) and T_2 is the temperature of crossing between the branches, it uniquely exists if $\chi > \chi_2$. Thus, the critical current reads

$$I_c(T) = \begin{cases} I_{c2}(T) & 0 < T < T_2, \\ I_{c1}(T) & T > T_2. \end{cases} \tag{4.67}$$

Such a formula describes four generic variation scheme for the critical current, labelled by (a), (b1), (b2) and (c), (see Fig. 4.19):

- case (a): when $\chi < \chi_2$, $\forall T$, $I_c(T) = I_{c1}(T)$, then I_{c1} reaches its maximum at T_1. The critical current presents a global maximum at finite temperature $T = T_1$.
- cases (b1) and (b2) correspond to the situation where $T_1 > T_2$: the critical current goes on the I_{c2} branches at $T = T_2$ and reaches a maximum at $T = T_1$. Consequently T_2 is a local minima and
  - if $I_{c2}(0) > I_{c1}(T_1)$, T_1 is a global maximum (case (b1)),
  - otherwise $I_{c2}(0) < I_{c1}(T_1)$, namely T_1 is only a local maximum (case (b2)), the maximum critical current is achieved at zero temperature.

  We can introduce a second angle χ_2' to distinguish cases (b1) from (b2), where χ_2' solves

  $$\cos(\chi_2')\left(a(T_1) - \sin(\chi_2')a(0)\right) = \sin^2(\frac{\chi_2'}{2})b(0) - \cos^2(\frac{\chi_2'}{2})b(T_1). \tag{4.68}$$

  Then case (b1) corresponds to $\chi > \chi_2'$ whereas case (b2) correponds to $\chi < \chi_2'$.
- case (c) corresponds to the situation $T_1 < T_2$: as temperature is lowered the branch switching occurs before I_{c1} reaches its maximum. Hence, the critical current is stricly increasing as temperature is decreased, it does not present any extremum.

In the limit $E_c \gg T_c$, we find $\chi_2 = \pi/2 - \delta\chi$ and $\chi_2' = \pi/2 - \delta\chi'$ where $\delta\chi \sim 2(\ln \frac{E_c}{T_c})^{-1/3}$, and $\delta\chi' \sim 1/2(\ln(\Delta(0)/T_c))^{-1}$, as a result $T_1 \sim T_c$. Then, for $\chi < \chi_2'$, the critical current is visibly peaked at $T = T_1$, see Fig. 4.18.a. Furthermore, Fig 4.18.b shows that when the cutoff E_c is enhanced the critical current is enhanced, however the ratio $I_c(T_c)/I_c(0)$ is almost constant, see Fig 4.18.c.

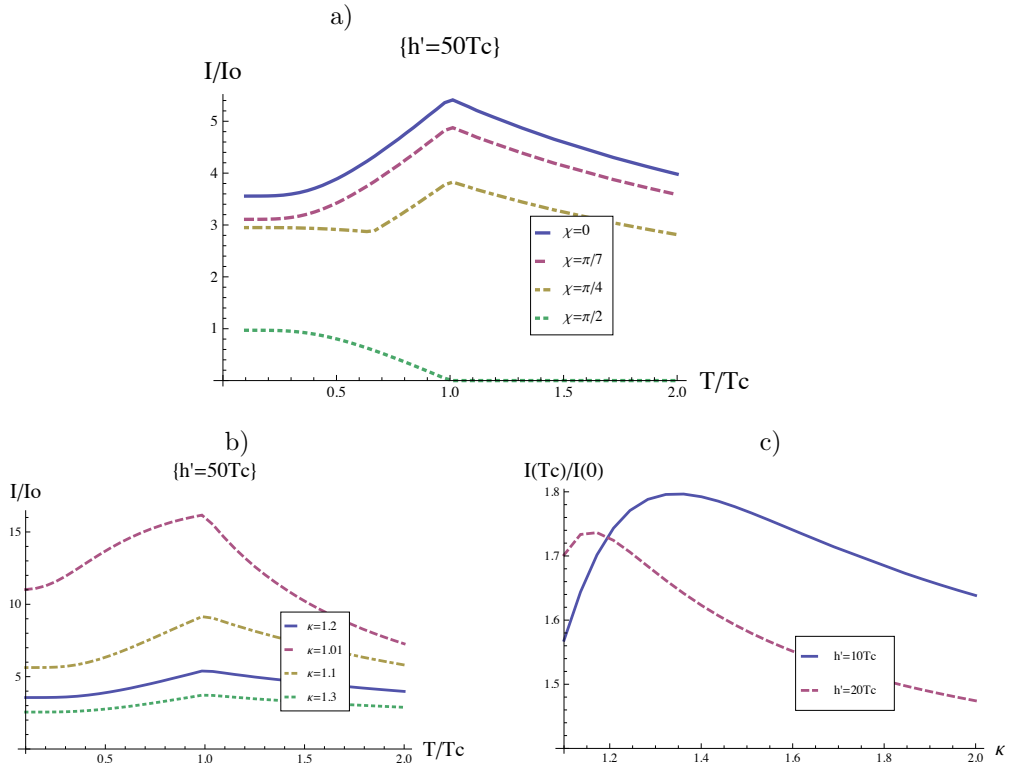

FIGURE 4.18: Critical current when $E_c \gg T_c$. a) Critical current as a function of temperature for different values of χ $(0, \pi/7, \pi/4, \pi/2)$ for $h' = 50T_c$ $(E > T_c)$, $\kappa = 1.2$, $\gamma_F = 10h'$. Case (a) (full line, dashed line), case (b1) (dotted line). b) Critical current as a function of temperature for $\chi = 0$, $h' = 10T_c$ and different values of κ. As $\kappa \to 1$, I_c is enhanced. c) Ratio $I_c(T_c)/I_c(0)$ for $\chi = 0$ and $\gamma_F = 10h'$ as a function of κ. The maximum does not happen when $\kappa \to 1$. Further the ratio is not negligeable $I_c(T_c)/I(0) > 1.5$ for $\chi = 0$.

As the cutoff of triplet reservoirs (E_c) is lowered the peak gets wider, see Fig. 4.19.a and 4.19.b. Essentially, when $T_c < E$, the peak is noticeable and evidences the efficiency of the odd/even coupling, see Fig. 4.19.a.

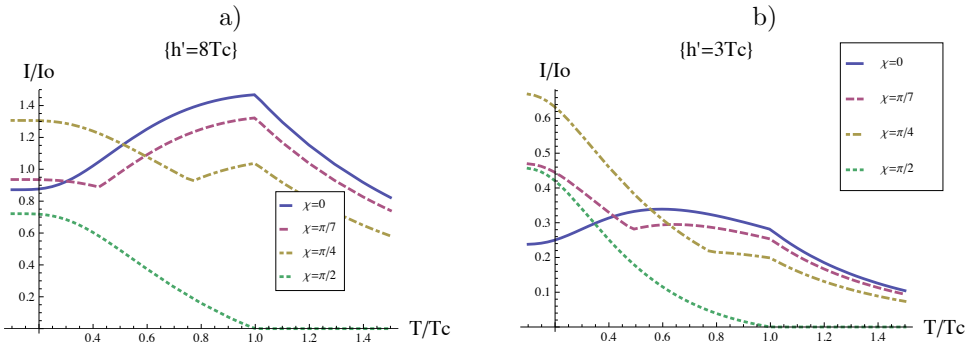

FIGURE 4.19: Critical current as a function of temperature for $\kappa = 1.2$ and for different values of χ $(0, \pi/7, \pi/4, \pi/2)$: a) for $h' = 8T_c$ and $\gamma_F = 10h'$, thus $E > T_c$, case(a) (full line), case(b1) (dashed line), case (b2) (dotted line). b) for $h' = 3T_c$ and $\gamma_F = 10h'$, thus $E < T_c$, case(a) (full line), case(b1) (dashed line), case (c) (dashed-dotted line). Note the blurring of the peak when $E < T_c$. The case $\chi = \pi/2$ is peculiar, as it lies between cases (c) and (b2). Here, $I_0 = G\gamma$.

non-symmetric junction

Let us now consider not-perfectly symmetric junctions, when $G_L \neq G_R$. As showed previously, as the asymmetry is increased and as a function of the phase bias φ, the switching of the superconducting phase between $\phi = 0$ and $\phi = \pi/2$ is smoother. The abrupt reversal of the condensate contribution is washed out. As a result, the CPR is continuous and critical current is lowered below the superconducting transition when $\chi \neq 0$. The temperature dependence of the critical current as a function of the asymmetry is depicted in Fig. 4.20.

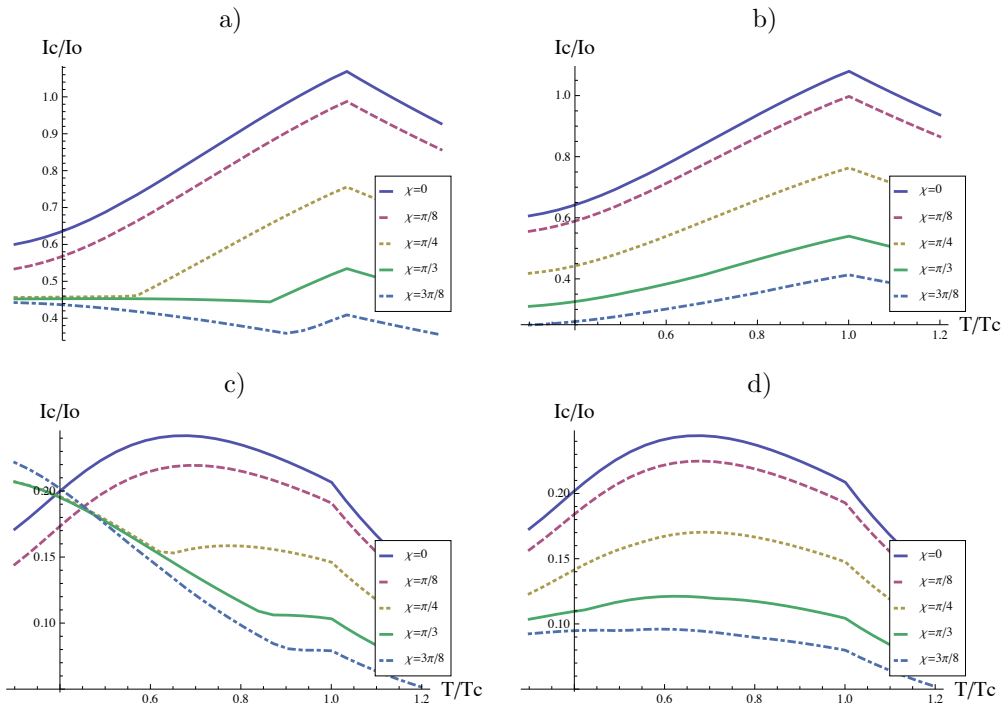

FIGURE 4.20: Critical current as a function of temperature for different values of χ $(0, \pi/8, \pi/4, 3\pi/8)$. Effect of the asymmetry of the conductances $G_L \neq G_R$ and of the relative value of h' and T_c. a) $G_L/G_R = 1.2$ $(h' = 10T_c)$, b) $G_L/G_R = 4$ $(h' = 10T_c)$ c) $G_L/G_R = 1.2$ $(h' = 3T_c)$, and d) $G_L/G_R = 4$ $(h' = 3T_c)$. Here, $I_0 = G_L\gamma_R$ and $\gamma_S = 0.5h$ and $\gamma_F = 10h$.

The asymmetry tends to preserve a global maximum in the vicinity of T_c of the critical current.

4.3.1.3 Conclusion

The study of the weak coupling limit, shows that the odd/even-frequency Josephson coupling is efficient. On average condensate and quasiparticle contributions are in competition for a wide range of parameters. The efficiency of the odd/even-frequency coupling is evidenced in the critical current temperature dependence: I_c presents a maximum at finite temperature, which disappears when magnetizations between triplet leads are almost perpendicular.

In the case of a symmetric junction $(G_L = G_R)$ the maximum is more pronounced when $\chi \to 0$ (collinear magnetization). However for non-symmetric junction, the maximum is preserve on a larger panel of magnetization angle χ.

Does this maximum survive at intermediate coupling? To answer the question we now compute the current for arbitrary couplings $\gamma_{L/R}$.

4.3.2 Full solution

4.3.2.1 Green function in the node

In the following, we consider only the symmetric case, namely, when $G_R = G_L = G$ and considering $\varphi_{L/R} = \pm\varphi/2$.

In particular, the equation governing the Green function in the superconducting node can be cast in the form

$$[A, g] = 0, \tag{4.69}$$

where $A = \omega\tau_z + \Delta\tau_\phi + \gamma(g_L + g_R)/2$ and $g^2 = 1$. In addition, the amplitude and phase of the superconducting order parameter (Δ, ϕ) satisfy Eq. (4.31).

How to solve Eq. (4.69)? Seemingly, $g = 1/\sqrt{A^2}.A$ solves both Eq. (4.69) and the normalization condition. Hence, Eq. (4.69) is simply a diagonalization problem.

While diagonalizing a matrix might be tricky, here the diagonalization of A^2 is fairly easy. Introducing for compactness the paramaters $C = \cos\frac{\varphi}{2}\cos\frac{\chi}{2}$ and $S = \sin\frac{\varphi}{2}\sin\frac{\chi}{2}$, A^2 can be written

$$\begin{aligned} A^2 = (\omega + \gamma\cosh\theta)^2 + \Delta^2 + (i\gamma\sinh\theta)^2(C^2 + S^2) \\ - 2(i\gamma\sinh\theta)^2 SC\sigma_z\tau_z + 2i\Delta\gamma\sinh\theta(\cos\phi C\sigma_x - \sin\phi S\sigma_y). \end{aligned} \tag{4.70}$$

Upon performing two rotations $R_1 = e^{-i\frac{\theta_1}{2}\sigma_z}$ and $R_2 = e^{-i\frac{\theta_2}{2}\sigma_y\tau_z}$ in the spin×Nambu space, we obtain

$$A^2 = R_2^\dagger R_1^\dagger\,(a - b\sigma_z\tau_z)\,R_1 R_2, \tag{4.71}$$

where the angles θ_1 and θ_2 satisfy

$$\cos\theta_1 = \cos\phi C/\sqrt{(\cos\phi C)^2 + (\sin\phi S)^2} \tag{4.72}$$

$$\sin\theta_1 = \sin\phi S/\sqrt{(\cos\phi C)^2 + (\sin\phi S)^2} \tag{4.73}$$

$$\cos\theta_2 = \beta_1/\sqrt{\beta_1^2+\beta_2^2} \tag{4.74}$$

$$\sin\theta_2 = \beta_2/\sqrt{\beta_1^2+\beta_2^2} \tag{4.75}$$

$$\beta_1 = iSC\gamma\sinh\vartheta \tag{4.76}$$

$$\beta_2 = \Delta\sqrt{(\cos\phi C)^2+(\sin\phi S)^2} \tag{4.77}$$

Furthermore,

$$a = (\omega+\gamma\cosh\theta)^2+\Delta^2+(i\gamma\sinh\theta)^2(C^2+S^2), \tag{4.78}$$

$$b = 2i\gamma\sinh\vartheta\sqrt{\beta_1^2+\beta_2^2}. \tag{4.79}$$

Finally, carrying out the inverse square root of the diagonalized form $\tilde{A}^2 = a - b\sigma_z\tau_z$ matrix, the Green function reads

$$g = R_2^\dagger R_1^\dagger \frac{1}{\sqrt{a-b\sigma_z\tau_z}} R_1 R_2 . A = R_2^\dagger R_1^\dagger \left(\tilde{a}-\tilde{b}\sigma_z\tau_z\right) R_1 R_2 . A. \tag{4.80}$$

At this stage, the superconducting order parameter is still to be determined via Eq. (4.31). The decomposition of Eq. (4.31) in its real and imaginary parts reads

$$\ln\frac{T_c}{T} = 2\pi T\sum_{\omega>0}\left(\frac{1}{\omega}-\frac{1}{8\Delta}\mathrm{Re}[e^{-i\phi}\mathrm{Tr}\left[(\tau_x-i\tau_y)(g+g^\dagger)\right]\right)], \tag{4.81}$$

$$0 = 2\pi T\sum_{\omega>0}\frac{1}{8\Delta}\mathrm{Im}[e^{-i\phi}\mathrm{Tr}\left[(\tau_x-i\tau_y)(g+g^\dagger)\right])]. \tag{4.82}$$

Before solving these equations, let us show that Eq. (4.82) gives the current conservation in the node. The current conservation principle in the node reads

$$\sum_{\omega>0}\mathrm{Im}\mathrm{Tr}\left(\tau_z[g,g_R+g_L]\right)=0. \tag{4.83}$$

Using Eq. (4.69), the terms in the sum can be transformed as

$$\mathrm{Im}\,\mathrm{Tr}\left[\tau_z[g,g_R+g_L]\right] = \frac{\Delta}{\gamma}\mathrm{Im}\mathrm{Tr}[\tau_z\tau_\phi g] = \frac{\Delta}{\gamma}\mathrm{Im}\mathrm{Tr}[(e^{i\phi}\tau_+ - e^{-i\phi}\tau_-)g] \tag{4.84}$$

$$= -\frac{\Delta}{\gamma}\mathrm{Im}\mathrm{Tr}[e^{-i\phi}\tau_-(g+g^\dagger)]. \tag{4.85}$$

As a result $0 = I_L + I_R = C\sum_{\omega>0}\mathrm{Im}\mathrm{Tr}[e^{-i\phi}\tau_-(g+g^\dagger)] = 0$, where C is a constant. Thus, we showed that the current conservation principle and the imaginary part of the self consistency equation (4.82) are equivalent.

Superconducting phase

In order to determine the phase ϕ taken in the node, we start with Eq. (4.82). In particular, the choice of a phase ϕ for which all the terms in the Matsubara sum in Eq. (4.82) solves as well Eq. (4.82)[12], namely

$$\begin{aligned}\mathrm{Im}[e^{-i\phi} \quad \mathrm{Tr} \quad & \Big[(\tau_x - i\tau_y)(\mathrm{Re}[\tilde{a}]\Delta\tau_\phi + \mathrm{Re}[i\gamma\sinh\vartheta\tilde{b}\sin\theta_2\cos\theta_1 C]\tau_x - \mathrm{Re}[i\gamma\sinh\vartheta\tilde{b}\sin\theta_2\sin\theta_1 S]\tau_y)\Big] \\ = \quad & 4\mathrm{Re}[i\gamma\sinh\vartheta\tilde{b}\sin\theta_2(-\sin\phi\cos\theta_1 C + \cos\phi\sin\theta_1 S] \\ = \quad & 4\mathrm{Re}[i\gamma\sinh\vartheta\tilde{b}\sin\theta_2]\sin(2\phi)\frac{(-C^2+S^2)}{\sqrt{(\cos\phi C)^2+(\sin\phi S)^2}} = 0. \end{aligned} \tag{4.86}$$

Interestingly, we end up with the same relation obtained in the weak coupling regime: $\sin 2\phi = 0$, therefore, $\phi = 0$ or $\phi = \pi/2$ modulo π[13]. To carry on, we consider the thermal equilibrium condition: the realized phase in the superconducting node minimizes the free energy. While the extremum condition is satisfied for both $\phi = 0$ and $\phi = \pi/2$, the condition of minimum reads $\frac{\partial(I_L+I_R)}{\partial\phi}(\phi) > 0$. Further using the derivative of Eq. (4.86) and neglecting the slow variation of $\tilde{b}$, the condition transforms as

$$\frac{\partial^2\mathcal{F}}{\partial^2\phi} \simeq K\frac{\mathrm{Re}[-i\gamma\sinh\vartheta\tilde{b}\sin\theta_2]}{\sqrt{(\cos\phi C)^2+(\sin\phi S)^2}} \times \cos(2\phi)\cos\frac{\varphi+\chi}{2}\cos\frac{\varphi-\chi}{2}, \tag{4.87}$$

where K is a positive constant. Thus, the chosen phase ϕ depends on the sign of $\cos\frac{\varphi+\chi}{2}\cos\frac{\varphi-\chi}{2}$.

As a result, we recover the condition derived in the weak coupling regime: the phase in the node is unchanged when the coupling γ is enhanced and is given by Eq. (4.52).

Fig. 4.21 shows the consistency of Eq. (4.52) where the variation of $\tilde{b}$ are neglected with the exact numerical minimization of the free energy.

[12] This argument has also been used in the weak coupling regime

[13] Here the phase is defined modulo π for the same reason that in the weak coupling limit, however now instead of considering only 2 pairs coherent process, all processes involving an even number of pairs enter

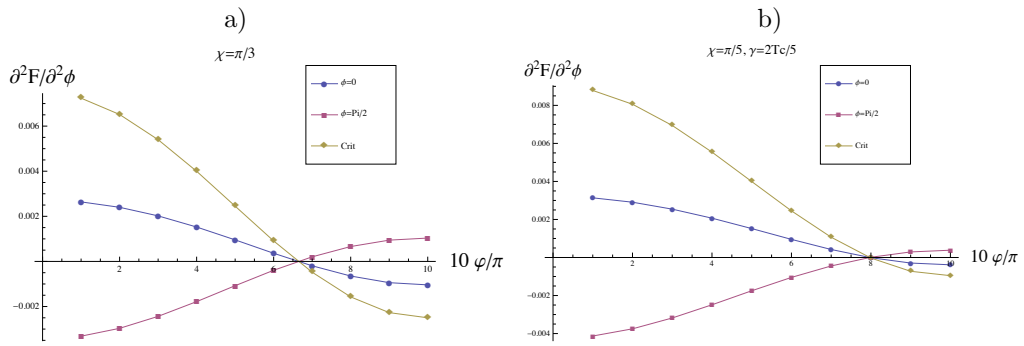

FIGURE 4.21: Mininization of the free energy: $(\partial^2\mathcal{F}/\partial^2\phi)_{\phi=0,\pi/2}$ as a function of φ for a)$\chi=\pi/3$ and b)$\chi=\pi/5$. The "crit" plot represents $\cos\frac{\varphi+\chi}{2}\cos\frac{\varphi-\chi}{2}$, note that when it is positive (resp. negative) $\phi=0$ (resp. $\phi=\pi/2$). The change of phase happens at the crossing and change of sign. Here, $\gamma=2T_c/5$, $h'=8T_c$, $\gamma_F=10T_c$, $\kappa=1.2$.

Amplitude of Δ

However, the amplitude $\Delta(T,\varphi,\phi)$ and consequently the temperature of superconducting transition strongly depends on γ. Eq. (4.81) can be rewritten as

$$\ln\frac{T_c}{T}=2\pi T\sum_{\omega>0}\left(\frac{1}{\omega}-\frac{f_\Delta(\omega,\phi,\varphi,\chi)}{\Delta}\right), \tag{4.88}$$

where

$$\begin{aligned} f_\Delta(\omega,\phi,\varphi,\chi)&=\mathrm{Re}[e^{-i\phi}\mathrm{Tr}\left[(\tau_x-i\tau_y)(g+g^\dagger)\right]\\ &=4\mathrm{Re}[\tilde{a}]\Delta+4\mathrm{Re}[i\gamma\sinh\vartheta\tilde{b}\sin\theta_2]\frac{(\cos^2\phi C^2-\sin^2\phi S^2)}{\sqrt{(\cos\phi C)^2+(\sin\phi S)^2}}. \end{aligned} \tag{4.89}$$

Due to the symmetry $f_\Delta(\omega,0,\varphi,\chi)=f_\Delta(\omega,\pi/2,\pi-\varphi,\pi-\chi)$, the superconducting amplitude satisfies: $\Delta_{\phi=0}(\varphi,\chi)=\Delta_{\phi=\pi/2}(\pi-\varphi,\pi-\chi)$.

Fig. 4.22 shows the temperature dependence of Δ for different couplings and phase bias. In particular, it shows that both φ and χ influence its amplitude. Remember that in the weak coupling regime, phase bias and χ-angle do not appear in the first order correction of Δ_0 for symmetry reason.

In particular, the superconducting transition in the node happens at $T_c^*<T_c$ and disappears when $\gamma\sim\Delta_0(0)$. At large coupling, the node inherits the odd-frequency nature of the leads: even and odd-frequency superconductivity compete.

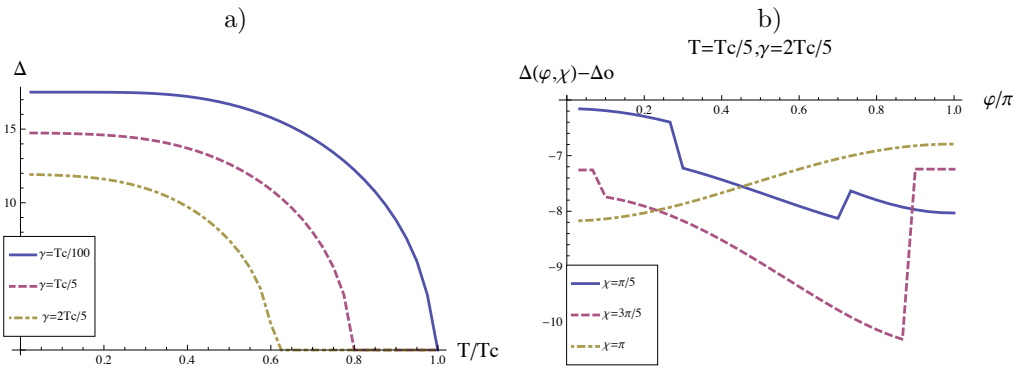

FIGURE 4.22: Superconducting order parameter a) Temperature dependence of Δ for different coupling, the case $\gamma = T_c/100$ refers to the weak coupling regime. The superconducting transition disappears when $\gamma \sim \Delta_0(0)$. b) Influence of the coupling to the leads $\Delta(T) - \Delta_0(T)$ as function of φ for different χ at $T = T_c/5$, with $\gamma = 2T_c/5$. Note that when $\phi = \pi/2$ superconductivity in the node is more weakened. Δ_0 is the amplitude of the order parameter for the bare node.

4.3.2.2 Charge current

We are now in position to compute the charge current flowing through S, using

$$I = G\pi T \sum_{\omega>0} \mathrm{Im}\mathrm{Tr}[\tau_z[g, g_R]]. \tag{4.90}$$

While in the weak coupling limit, we divided the current into a quasiparticle and a condensate contribution simply by considering the ϕ dependence. At intermediate coupling, such a separation is more subtle since higher order mechanism might be a mixture of "quasiparticle" and "Cooper pairs".

By inserting g in the current formula, we find $I = I_a + I_b$ where,

$$I_a = 2\pi T G\gamma \sum_{\omega} (i\sinh\vartheta)^2 \left(-\tilde{a}\sin\varphi\cos\chi + \tilde{b}\cos\theta_2\cos\varphi\sin\chi\right), \tag{4.91}$$

and,

$$I_b = 2\pi T G \sum_{\omega} \frac{\mathrm{Re}[\tilde{b}\sin\theta_2 i\sinh\vartheta]}{\sqrt{(C\cos\phi)^2 + (S\sin\phi)^2}} \Delta\sin\varphi \left(-((\cos\phi\cos\frac{\chi}{2})^2 + (\sin\phi\sin\frac{\chi}{2})^2\right). \tag{4.92}$$

Fig. 4.23 shows the critical current of the junction at intermediate coupling, ($\gamma < T_c$). Since the superconducting transition happens at lower temperature, the peak in the critical current happens at lower temperature, we recover cases (a), (b1), (b2) and (c) described in the weak coupling regime. However, as the even-frequency superconductivity in the node is weakened, the peak broadens.

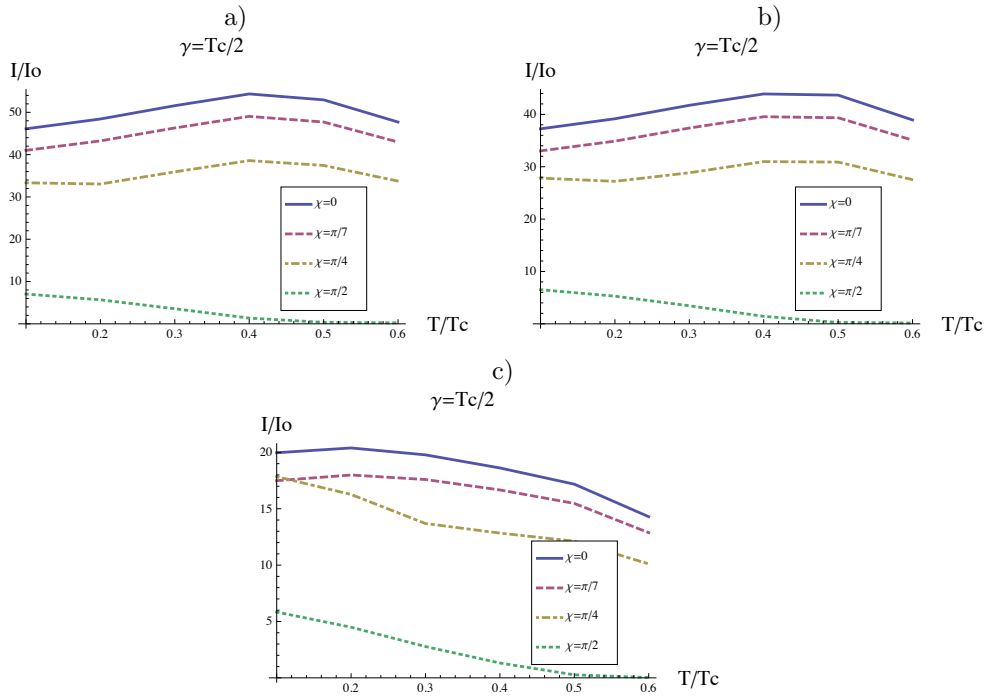

FIGURE 4.23: Critical current as a function of temperature ($10T/T_c$) at intermediate coupling $\gamma = T_c/2$ and $\gamma_F = 10h'$ for different values of χ.
a) $\kappa = 1.2$ and $h' = 8T_c$. b) $\kappa = 0.8$ and $h' = 8T_c$. c) $\kappa = 1.2$ and $h' = 3T_c$ ($E < T_c$).
Here $I_0 = \delta G_Q$.

4.4 Metallic junction

In the previous section, we computed the Josephson energy and the Josephson current of an $S_T/S/S_T$ junction within the framework of the circuit theory. We wish now to conjecture the result for a "true" junction by considering the effect of the finite thickness of each metallic layer [14]

Let us consider an $S'/F'F/S/FF'/S'$ multi-layer Josephson junction. Here, the $S'/F'/F$ structure realizes an effective spin-triplet odd-frequency superconducting reservoir. Using the result of the previous section, for a weak coupling of the S central layer with the $S/F'F$ structures [15]:

- odd/odd-frequency Josephson coupling mediated by Andreev pairs (Quasiparticle contribution) in the superconducting island. $\propto \cos\varphi \cos\chi \exp -l_S/\xi_N$.
- odd/even-frequency coupling: the current is carried by Cooper pairs through the S layer. While the direct second order Josephson coupling should not be affected

[14] Within the circuit theory metallic layers are assumed to be thin enough to be represented as a zero dimension island (node).
[15] or close to the critical temperature of the S' superconduting leads.

by the finite length of S, the crossed term requires a pair to extend over the full junctions such that $E_{J\text{cross}} \propto \cos\chi \cos(2\phi - \varphi_L + \varphi_R) \exp -(2l_S/\xi_S)$.

Note through the ferromagnetic layers F and F', the current is actually mediated by Andreev pairs induced via a proximity effect of S' leads. Thus, the quasiparticle and the condensate contribution would be of opposite (Resp. same)sign when $\chi < \pi/2$ (Resp. $\chi > \pi/2$). As a result, for a long central superconducting layer, by changing the relative angle between the magnetization of the leads, we might tune on and off the presence of a maximum at finite temperature.

4.5 Conclusion

To conclude we predict that at the superconducting transition of the node the odd/even Josephson coupling develops and is efficient. The condensate contribution strongly impacts the properties of the $S_T/S/S_T$ and is manifest in the critical current measurement. Especially we predict, that the critical current is maximum at finite temperature on a wide range of parameters. It contrasts with the properties of $S'/S/S'$ junction which exhibit a strong enhancement of the critical current at the superconducting transition, see Annexe. These observations hold as long as the relative magnetization direction between reservoir are not perpendicular. Indeed, when $\chi = \pi/2$ the quasiparticle contribution vanishes at all temperature while the condensate contributions starts below T_c^*. In the case of a weak coupling, $T_c^* \sim T_c$ but at high coupling T_c^* goes to zero, and the proximity effect suppresses the superconducting transition.

What about the measurability? The critical current of long tri-layer ferromagnetic junction has been measured [13, 14], we believe our $S_T/S/S_T$ is an extension of the tri-layer Josesphon experimental junction, where a superconducting layer is inserted in the middel of the tri-layer: $S'/F'/F/S/F/F'/S'$ junction, see Fig. 4.24. By manipulating the magnetization of the long F layers, the maximum at finite temperature should be tuned on and off.

Measuring such maximum in the critical current would provide a further evidence of the odd-frequency triplet nature of long-range correlations.

4.6 Appendix: $S_T/S/S_T$ junction versus $S'/S/S'$ junction

Let us compute the properties of an $S'/S/S'$[95] on the same footing than what we have done for the $S_T/S/S_T$ junction. The difference is that without the ferromagnetic layers,

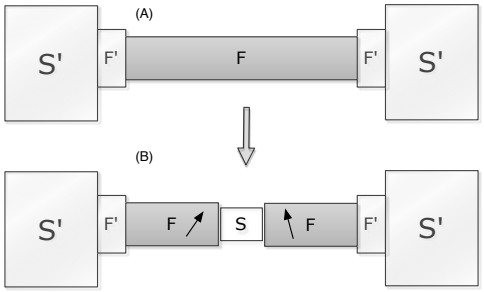

FIGURE 4.24: Experimental setup: a) model of the tri-layer ferromagnetic junctions ([13, 14]) b) Proposed junction

the leads are even-frequency superconductors (conventional). The Green functions in the leads, in the subgap regime, take on the simple form: $g_{R/L} = \tau_{\pm\varphi/2}$ and the Green function in the superconducting node obeys

$$[\omega\tau_z + \Delta\tau\phi + 1/2(\gamma_R g_R + \gamma_L g_L), g] = 0. \tag{4.93}$$

Introducing $\gamma = (\gamma_R + \gamma_L/)2$ and $\bar{\gamma} = (\gamma_R - \gamma_L/)2$, g can be written

$$g = \frac{\omega\tau_z + \Delta\tau_\phi + \gamma\cos(\varphi/2)\tau_x + \bar{\gamma}\sin(\varphi/2)\tau_y}{\sqrt{\omega^2 + (\Delta\cos\phi + \gamma\cos\varphi/2)^2 + (\Delta\sin\phi - \bar{\gamma}\sin\varphi/2)^2}}. \tag{4.94}$$

The superconducting order parameter obeys the self-consistency relation (4.31).

Superconducting phase

The thermal equilibrium condition allows to set the superconducting phase. The phase ϕ in the node minimizes the free energy $\mathcal{F}$ (Eqs. (**??**) and (**??**)).

Then using the relation: $\mathrm{Im\,Tr}\,[\tau_z[g, \gamma_R g_R + \gamma_L g_L]] = \Delta/C(\gamma\cos\phi\sin\varphi/2 + \bar{\gamma}\sin\phi\sin\varphi/2)$, the equilibrium conditions can be rewritten as

- $\frac{\partial\mathcal{F}}{\partial\phi}(\phi) = 0$ yields

$$\gamma\sin\phi\cos\varphi/2 + \bar{\gamma}\cos\phi\sin\varphi/2 = 0 \Rightarrow \tan\phi = -\frac{\bar{\gamma}}{\gamma}\tan\frac{\varphi}{2}, \tag{4.95}$$

- $\frac{\partial^2\mathcal{F}}{\partial^2\phi}(\phi) > 0$ yields

$$\gamma\cos\phi\cos\varphi/2 - \bar{\gamma}\sin\phi\sin\varphi/2 > 0. \tag{4.96}$$

In the limit of a perfectly symmetric junction, $\bar{\gamma} = 0$, and for $\varphi \in [-2\pi, 2\pi]$ we obtain

φ	-2π		$-\pi$		π		2π	..
ϕ	|	π	|	0	|	π	|

(4.97)

When $\varphi = (2n+1)\pi$ the phase abruptly switches (phase slip). When the junction is not symmetric, $\bar{\gamma} \neq 0$, the abrupt switching smears, see Fig. 4.25.

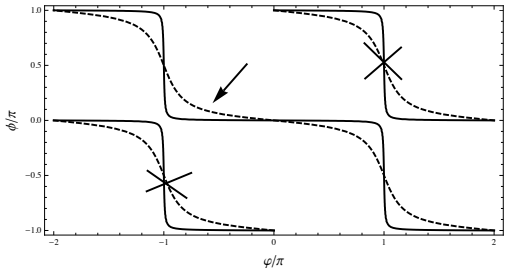

FIGURE 4.25: Superconducting phase ϕ as a function of φ for $\bar{\gamma}/\gamma = 0.5$ (dashed line) and $\bar{\gamma}/\gamma = 0.01$ (fulle line). The crossed plots correspond excited states, which do not minimizes the free energy. Note the smearing of the transition between $\phi = 0$ and $\phi = \pi$ as $\frac{\bar{\gamma}}{\gamma} = \frac{\gamma_L - \gamma_R}{\gamma_L + \gamma_R}$ is increased.

It is interesting to point out that the phase as a function of φ is 4π periodic, which seems strange, however the 2π periodicity can be obtained if we think of the coupling of the node with one node (phase $\varphi_i = \varphi/2$) then $\phi(\varphi_i)$ is $4\pi/2- = 2\pi-$periodic.

Amplitude of the order parameter

The amplitude of the superconducting order parameter is determined via

$$\ln \frac{T_c}{T} = 2\pi T \sum_{\omega>0} \left(\frac{1}{\omega} - \frac{1}{\Delta} \frac{\Delta + \gamma \cos\phi \cos\varphi/2 - \bar{\gamma} \sin\phi \sin\varphi/2}{\sqrt{\omega^2 + (\Delta\cos\phi + \gamma\cos\varphi/2)^2 + (\Delta\sin\phi - \bar{\gamma}\sin\varphi/2)^2}}\right). \quad (4.98)$$

Note that, $\Delta(\phi, \varphi) = \Delta(\pi + \phi, \varphi + 2\pi)$, see Fig. 4.26. The superconductivity is strongly enhanced by the coupling to the even-frequency leads, $T_c^* > T_c$.

Charge current

Let us now determine the charge current. At the right interface, we obtain

$$I = G\pi \sum \frac{\Delta \sin(\phi + \varphi/2) + \gamma_R/2 \sin\varphi}{\sqrt{\omega^2 + (\Delta\cos\phi + \gamma\cos\varphi/2)^2 + (\Delta\sin\phi - \bar{\gamma}\sin\varphi/2)^2}} \quad (4.99)$$

Similarly than in the $S_T/S/S_T$ junction, the current splits in a quasiparticle and a condensate contributions: $I = I_{\mathrm{QP}} + I_{\mathrm{Cond}}$.

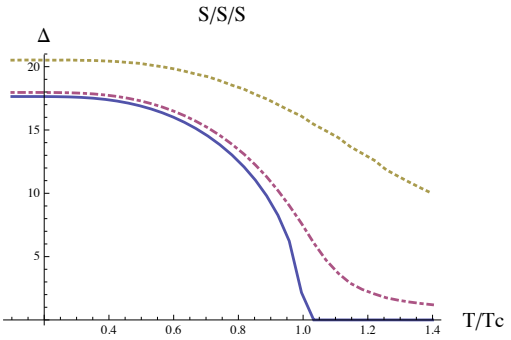

FIGURE 4.26: Amplitude of the order parameter Δ as a function of temperature for different coupling (with $\bar{\gamma} = 0$), $\gamma = 0$ (Full Line), $\gamma = 0.01T_c$ (dashed line), $\gamma = 0.1T_c$ (dotted line). The superconductivity in the node is strongly enhanced by the coupling to the superconducting lead (even-frequency). $\varphi = 0$

In particular, at lowest order in γ

$$I_{\mathrm{QP}} \propto \gamma_R \gamma_L \sin\varphi \tag{4.100}$$

$$I_{\mathrm{Cond}} \propto \gamma_R \Delta \sin(\phi - \varphi_R) \propto -\gamma_L \Delta \sin(\phi - \varphi_L) \tag{4.101}$$

For a symmetric junction, the phase slip at $\varphi = (2n+1)\pi$, generates a discontinuity in the condensate contribution and thus in the full current phase relation which disappears as soon as $\bar{\gamma} \neq 0$. The current through the junction is strongly enhanced when γ is increased, see Fig. 4.27.

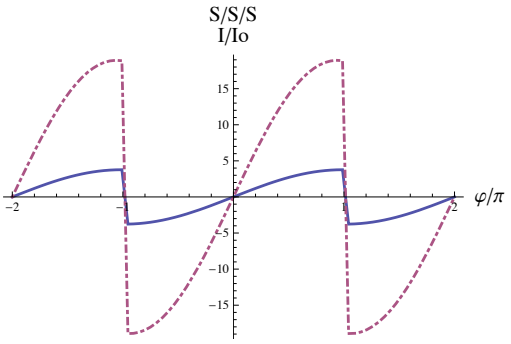

FIGURE 4.27: Current phase relation at $T = 0.3T_c$ for $\gamma = 0.1$ (full line) and $\gamma = 0.5$ (dashed line). Note the discontinuity, when $\bar{\gamma} \neq 0$ the discontinuity disappears.

Finally the critical current for a symmetrical junction reads,

$$I_c = G\pi T \sum \frac{\Delta}{\sqrt{\omega^2 + \Delta^2}}, \tag{4.102}$$

At $T = 0$ the critical current scales as, $I_c \sim \ln(\frac{\Delta_R}{\Delta})$, where$\Delta_R$ is the amplitude of the gap in the superconducting reservoirs.

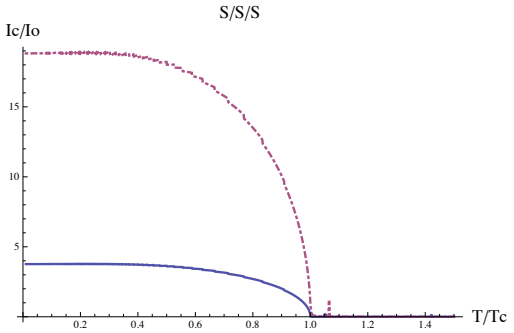

FIGURE 4.28: Critical current for $\gamma = 0.1$ (full line) and $\gamma = 0.5$ (dashed line).

Whereas in the $S_T/S/S_T$ junction, the maximum of the critical current happens at finite temperature, here it happens at $T = 0$, see Fig. 4.28.

Chapter 5

Andreev current induced by ferromagnetic resonance

While in the previous chapters, we studied the Josephson current at equilibrium in hybrid structures, we now address an out-of-equilibirum setup. In particular, we study charge transport through a metallic dot coupled to a superconducting and a ferromagnetic lead with a precessing magnetization due to ferromagnetic resonance. Using the quasiclassical theory, we find that the magnetization precession induces a dc current in the subgap regime even in the absence of a bias voltage. This effect is due to the rectification of the ac spin currents at the interface with the ferromagnet; it exists in the absence of a spin current in the superconductor. When the dot is strongly coupled to the superconductor, we find a strong enhancement in a wide range of parameters as compared to the induced current in the normal state.

5.1 Motivation

Let us start with the experiments performed by Moriyama *et al.* and Costache *et al.* [66, 67] presented in the chapter 1. In particular, the ferromagnetic resonance (FMR) acts as a spin pumping mechanism. Then, due interface effects, in non-symmetric junctions, the spin currents is partly rectified as a charge current. Experimentally, this is evidenced by measuring dc voltage peaks at excitation frequencies matching the FMR conditions.

While the experiments were performed at room temperature, one of the electrodes was made from aluminum. Thus we may ask the question what does change at low temperature when Al becomes superconducting?

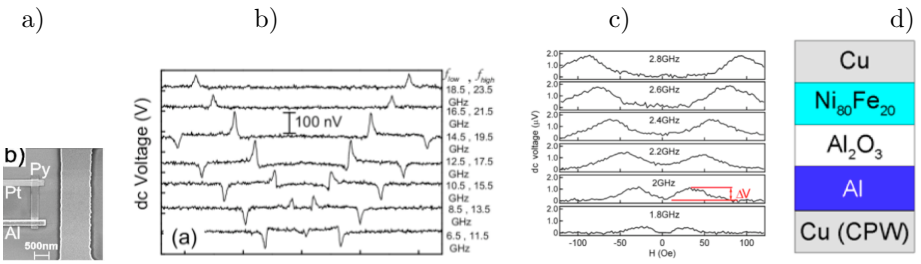

FIGURE 5.1: a),b) Junction and voltage peaks measured by Costache. c),d) Voltage peak and schematic junctions by Moriyama. Both experiments are similar and use Aluminum as the right electrode, it is natural to ask what happens at the superconducting transition of Al.

As pointed out above, the charge current originates from a spin current at the interface. Thus, in particular, we may wonder what happens in the subgap regime when the transport is mediated by Andreev reflections? As one electron of spin up pairs with one electrons of spin down to enter the superconctor, no spin current is possible, and the normal metal mechanism fails.

In a more general context, this problem tackles the interplay between the dynamics of the magnetization and superconductivity. This is a relatively new topic, up to now much of the effort has been devoted to the static case.

In a first part, we propose a model for the junction under FMR conditions. Then in a second part, the charge current is derived in the normal metallic case to confirm the validity of our model. In a third part, we further study the low temperature regime, where one electrode is superconducting.

5.2 Model

The junction used in the experiments consists of a ferromagnetic wire attached to a normal metallic lead on the left and a superconducting lead on the right, see the upper part in Fig. 5.2.

As mentioned, the main ingredients necessary to generate the effect in the normal state, are spin-dependent transmissions and a spin accumulation region. The simplest model meeting these requirement is depicted in Fig 5.2, where a metallic dot is connected to a ferromagnet (F) and a superconductor (S). The normal metallic dot represents the transition region between the ferromagnet and the superconducting lead, where the superconductivity is weakened due to the inverse proximity effect. The metallic dot inherits superconducting correlations from S. In particular, while the attraction and thus the order parameter exist only in S, due to the proximity effect in the normal metallic

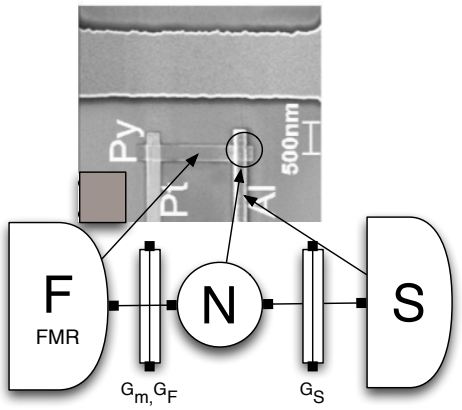

FIGURE 5.2: Node representation of the experimental junction of Costache *et al.* [66]. The metallic node materializes the transition region between the superconducting and the ferromagnetic region. It may accumulate charge. The interface with the ferromagnet is spin-dependent (G_m).

node N, superconducting correlations develop in N. Additionally, the superconducting lead, at thermal equilibrium, is superconducting below its critical temperature (T_c).

The magnetization precession is described by a time dependent exchange field, $\boldsymbol{J}(t) = J\boldsymbol{m}(t)$ with

$$\boldsymbol{m}(t) = (\sin\theta\cos\Omega t, \sin\theta\sin\Omega t, \cos\theta), \tag{5.1}$$

acting on the spin of the conduction electrons. Here the precession frequency Ω and the tilt angle θ, are both tunable with the external dc and rf fields under standard FMR conditions. We consider them as externally fixed parameters.

The precession of the magnetization drives the system out of equilibrium and, thus, may generate a current.

5.3 Formalism

Within the circuit theory [82], described in chapter 2, the metallic dot is a node (N) of mean level spacing δ, connected to a ferromagnetic lead (F) and a superconducting lead (S), see Fig. 5.3. The F/N connector is assumed spin dependent. Then $\hat{g}$, $\hat{g}_F$, and $\hat{g}_S$ are respectively the Green functions in the metallic node, the ferromagnet and the superconducting lead. They are 8×8 matrices in the Keldysh, Nambu and spin spaces, see Chapter 2.

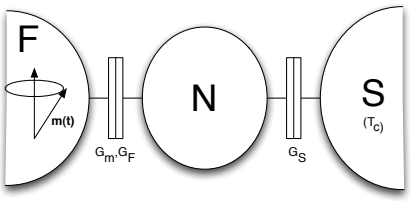

FIGURE 5.3: Model for the junction. The metallic node is connected to the precessing ferromagnet on the left and to the superconducting lead to the right. The left interface is spin-dependent $G_{\uparrow\downarrow} = G_F \pm G_m$.

Green function in the leads

- We assume the superconducting lead S to be at thermal equilibrium. Thus, we take

$$\hat{g}_S^{R/A}(E) = \frac{-iE\tau_z + \Delta\tau_x}{\sqrt{\Delta^2 - (E \pm i0^+)^2}}, \tag{5.2}$$

$$\hat{g}_S^K(E) = [\hat{g}_S^R(E) - \hat{g}_S^A(E)]f(E), \tag{5.3}$$

  where the order parameter Δ is chosen as real and $f(E) = \tanh(E/2T)$.

- Furthermore, the Green function in the ferromagnet F, $\hat{g}_F(t,t')$, is stationary in the rotational frame, following the precession of the magnetization. In particular, the Green function in the laboratory ($\hat{g}_F(t,t')$) and in the rotational frame are related via

$$\check{g}_F(t,t') = R(t)\hat{g}_F(t,t')R^\dagger(t'), \tag{5.4}$$

  where $R(t) = e^{i\frac{\Omega}{2}t\sigma_z}$.

  In the appendix A, we show that $\check{g}$ is stationary, namely $\check{g}_F(t,t') = \check{g}_F(t-t')$. In addition, its Fourier transform obeys

$$\left[(E + \frac{\Omega}{2}\sigma_z + J\boldsymbol{m}.\boldsymbol{\sigma})\tau_z - \check{\Sigma}, \check{g}_F\right] = 0, \tag{5.5}$$

  where $\check{g}_F(E) = \frac{1}{2\pi}\int dE\, \check{g}_F(t-t')\exp[iE(t-t')]$. The self-energy $\check{\Sigma} = -i\Gamma\hat{g}_N(E + (\Omega/2)\sigma_z)$ accounts for the spin relaxation. Here, $1/\Gamma$ is the inelastic scattering time and $\check{g}_N$ is the equilibrium Green function in a normal metal. Namely, $\hat{g}_N^{R/A} = \pm\tau_z$ and $\hat{g}_N^K = 2\tau_z f(E)$. For a large exchange field, $J \gg \Omega, \Gamma$, the solution of Eq. (5.5) takes the form

$$\check{g}_F^{R/A} = \pm\tau_z, \tag{5.6}$$

$$\check{g}_F^K = 2\tau_z(f_+ + f_- \cos\theta\, \boldsymbol{m}\cdot\boldsymbol{\sigma}), \tag{5.7}$$

where $f_{\pm}(E) = (f(E+\Omega/2) \pm f(E-\Omega/2))/2$.

Green function in the normal metallic node

Then, the Green function in the metallic node $\hat{g}$ obeys[1]

$$-i\frac{2\pi G_Q}{\delta}\left[-i\partial_t\tau_z, \hat{g}(t,t')\right] + \hat{I}_F + \hat{I}_S = 0. \tag{5.8}$$

The boundary conditions at the F/N and N/S interfaces are accounted by the matrix currents $\hat{I}_{S/F}$. Namely,

- The tunneling through the F/N interface is assumed to be spin-dependent [81], and the leakage current takes the form

$$\hat{I}_F(t,t') = \frac{G_F}{2}[\hat{g}_F(t,t'), \hat{g}(t,t')] + \frac{G_m}{4}[\{\boldsymbol{m}(t)\cdot\boldsymbol{\sigma}\tau_z, \hat{g}_F(t,t')\}, \hat{g}(t,t')], \tag{5.9}$$

  where G_F is the normal conductance of the interface whereas G_m is the spin-dependent part. The magnetization of the barrier follows the precession in F with the same tilt angle[2] . As a result, the conductance for spin up/down electron, with respect to the $\boldsymbol{m}(t)$ magnetization axes, is $G_{\uparrow/\downarrow} = G_F \pm G_m$. Within the quasi-classical approximation, we assume $|G_m| \ll G_l$. Thus, G_m may be treated perturbatively in the following.

- At the N/S interface the matrix current reads

$$\hat{I}_S(t,t') = \frac{G_S}{2}[\hat{g}_S(t,t'), \hat{g}(t,t')], \tag{5.10}$$

  where G_S is the conductance of the interface.

Rotational frame

In the rotational frame, the problem is stationary. Using Eq. (5.4) , the equation for $\hat{g}$ (5.8) transforms as

[1] Here σ_i, τ_j are the Pauli matrices in spin and Nambu spaces, $G_Q = e^2/\hbar$ is the conductance quantum, and δ is the mean level spacing in the normal node. δ is assumed to be the smallest energy scale in the system.

[2] We neglect the term $\propto -i\frac{G_\phi}{2}[\boldsymbol{m}.\boldsymbol{\sigma}\tau_z, \check{g}]$ responsible for a spin-dependent phase shift acquired across the interface. Acting like an extra exchange field along $\boldsymbol{m}$ it is a source of spin-relaxation which may inhibit the spin accumulation. Note that while in general this term is small, for tunnel barriers in may be large as compared with the normal conductance and may inhibit the spin-pumping.

$$-i\frac{2\pi G_Q}{\delta}\left[(E\tau_z+\frac{\Omega}{2}\sigma_z)\tau_z,\check{g}\right]+\check{I}_F+\check{I}_S=0. \tag{5.11}$$

The spin dependent energy shift $\pm\Omega/2$ is a spin-resolved chemical potential induced by the transformation from the laboratory to the rotational frame. Accordingly, the leakage currents take the form

$$\check{I}_F = \frac{G_F}{2}[\check{g}_F,\check{g}]+\frac{G_m}{4}[\{\boldsymbol{m}\cdot\boldsymbol{\sigma}\tau_z,\check{g}_F\},\check{g}], \tag{5.12}$$

$$\check{I}_S = \frac{G_S}{2}[\check{g}_S,\check{g}], \tag{5.13}$$

where $\check{g}_S(E)=\hat{g}_S(E+\frac{\Omega}{2}\sigma_z)$.

Spin and Charge currents

The charge currents at both interfaces are given by

$$I_{F/S}=\frac{1}{16e}\int dE\ \mathrm{Tr}[\tau_z\hat{I}^K_{F/S}]=\frac{1}{16e}\int dE\ \mathrm{Tr}[\tau_z\check{I}^K_{F/S}]. \tag{5.14}$$

They are the same in both frames. The current conservation is automatically satisfied by Eq. (5.11) and ensures that $I=I_F=-I_S$.

The spin currents in the rotational frame are given by

$$\boldsymbol{I}_{F/S}=-\frac{1}{32e^2}\int dE\ \mathrm{Tr}[\boldsymbol{\sigma}\check{I}^K_{F/S}]. \tag{5.15}$$

In the laboratory frame, they decompose into a dc contribution along the precession axis, $I_{\alpha,z}$, and an ac component in the perpendicular plane,

$$I_{\alpha,x/y}(t)=I_{\alpha,x/y}\cos\Omega t\mp I_{\alpha,y/x}\sin\Omega t, \tag{5.16}$$

where $\alpha=F,S$. Contrarily to the charge current, the spin currents do not need to be conserved. Eq. (5.11) yields

$$\boldsymbol{I}_F+\boldsymbol{I}_S-\frac{\Omega}{16\delta}\int dE\ \mathrm{Tr}[(\hat{\mathbf{e}}_z\times\boldsymbol{\sigma})\tau_z\hat{g}^K]=0. \tag{5.17}$$

Thus, only the dc spin current along the z-axes is conserved.

For better readibility, we normalize the conductance by: $G_\Sigma = G_F + G_S$ and energies by the Thouless energy $E_g = G_\Sigma \delta/(4\pi G_Q)$. In particular, we introduce the dimensionless conductances $\gamma_\alpha = G_\alpha/G_\Sigma$, $(\alpha = S, F, m)$ as well as the dimensionless energies $\epsilon = E/E_g$ and $\omega = \Omega/(2E_g)$. Note that $\gamma_S + \gamma_F = 1$.

Therefore, combining Eqs. (5.11),(5.12) and (5.13), $\check{g}$ obeys

$$[-i(\epsilon + \omega\sigma_z)\tau_z + \gamma_S \check{g}_S + \gamma_F \check{g}_F + \gamma_m[\frac{1}{2}\{\boldsymbol{m}.\boldsymbol{\sigma}\tau_z, \check{g}_F\}, \check{g}] = 0. \tag{5.18}$$

While our main interest is the FMR-induced current in the subgap regime of S, we start with the simpler normal metallic case ($\Delta = 0$) to validate our model.

5.4 The normal metallic state

Green function and charge current

At temperature higher than the critical temperature ($T > T_c$), the right lead is in its normal state, $\Delta = 0$.

In the absence of superconductivity, the advanced and retarded Green function in the metallic node are trivial $\hat{g}^{R/A} = \check{g}^{R/A} = \pm\tau_z$. Using Eq. (2.81), the Keldysh component may be written as[3].

$$\hat{g}^K = \{\tau_z, \check{\varphi}\} = 2\check{\varphi}\tau_z, \tag{5.19}$$

where $\check{\varphi}$ plays the role of a distribution function.

Using Eq. (5.18), the distribution function $\check{\varphi}$ obeys

$$2\check{\varphi} - i\omega[\sigma_z, \check{\varphi}] + \gamma_m\{\boldsymbol{m}.\boldsymbol{\sigma}, \check{\varphi}\}\tau_z = 2(\gamma_S f_S + \gamma_F f_F) + \gamma_m\{\boldsymbol{m}.\boldsymbol{\sigma}, f_F\}\tau_z. \tag{5.20}$$

where $f_S = f_+ + f_-$ and $f_F = f_+ + f_- \cos\theta\, \boldsymbol{m}.\boldsymbol{\sigma}$. Furthermore, the charge currents at each interfaces can be expressed in terms of $\check{\varphi}$ via

$$I_S = \frac{G_\Sigma}{4e}\int dE\ \gamma_S \mathrm{Tr}[\tau_z(\check{\varphi} - f_S)], \tag{5.21}$$

$$I_F = \frac{G_\Sigma}{4e}\int dE\ \mathrm{Tr}[\gamma_F\tau_z(\check{\varphi} - f_F) + \gamma_m(\check{\varphi} - \frac{\{f_F, \boldsymbol{m}.\boldsymbol{\sigma}\}}{2})], \tag{5.22}$$

with $I_S = -I_F$.

[3] In absence of superconductivity, the second equality is trivial.

The exact solution for $\check{\varphi}$ can be derived from Eq. (5.20) for arbitrary γ_m. However, since our final goal is the study of the superconducting case, where we treat the case $\gamma_m \ll 1$ and expand $\check{\varphi}$ as $\check{\varphi} = \check{\varphi}_0 + \gamma_m \check{\varphi}_1 + \dots$.

Consequently, the charge and spin currents can be rewritten respectively as $I_{S/F} = I^{(0)}_{S/F} + I^{(1)}_{S/F} + \dots$, and $\boldsymbol{I}_{S/F} = \boldsymbol{I}^{(0)}_{S/F} + \boldsymbol{I}^{(1)}_{S/F} + \dots$, where $I^{(1)}_{S/F}, \boldsymbol{I}^{(1)}_{S/F} \propto \gamma_m$.

There is a remarkable relation in the normal state between the zeroth order spin current and the first order charge current. In particular, the zeroth order spin current at the left interface reads

$$\boldsymbol{I}^{(0)}_F = -\frac{G_F}{8e^2}\int dE\ \mathrm{Tr}\,[\boldsymbol{\sigma}(\check{\varphi}_0 - f_F)]. \tag{5.23}$$

Then, the first order charge currents at the left and right interfaces

$$I^{(1)}_S = \frac{G_S}{4e}\int dE\ \mathrm{Tr}\,[\tau_z \check{\varphi}_1], \tag{5.24}$$

$$I^{(1)}_F = \frac{G_F}{4e}\int dE\ \mathrm{Tr}\,[\tau_z \check{\varphi}_1 + \frac{G_m}{4e}\int dE\ \mathrm{Tr}\,[\boldsymbol{m}.\boldsymbol{\sigma}(\check{\varphi}_0 - f_F)]. \tag{5.25}$$

Then using the charge conservation relation $I^{(1)} = I^{(1)}_F = -I^{(1)}_S$ and recognizing the expression of the zeroth order spin current in $I^{(1)}_F$, we obtain

$$I^{(1)} = 2e\frac{\gamma_S \gamma_m}{\gamma_F}\boldsymbol{I}^{(0)}_F.\boldsymbol{m} \tag{5.26}$$

Therefore, to derive both the zeroth order spin current and the first order charge current, only $\check{\varphi}^{(0)}$ is needed.

At lowest order ($\gamma_m = 0$), Eq. (5.20) is solved by

$$\check{\varphi}_0 = f_+ + f_-\left((\gamma_F \cos^2\theta + \gamma_S)\sigma_z + \gamma_F \frac{\sin\theta\cos\theta}{1+\omega^2}(\sigma_x - \omega\sigma_y)\right). \tag{5.27}$$

As a result, the zeroth order charge current is null: $I^{(0)}_{S/F} \propto \mathrm{Tr}[\tau_z(\check{\varphi}_0 - f_{S/F})] = 0$. However, the zeroth order spin current is non-zero and at the left interface we find

$$I^{(0)}_{F,x} = \frac{G_F E_g}{2e^2}\frac{\omega(\gamma_S + \omega^2)}{1+\omega^2}\sin\theta\cos\theta, \tag{5.28}$$

$$I^{(0)}_{F,y} = \frac{G_F E_g}{2e^2}\frac{\omega(\gamma_F \omega)}{1+\omega^2}\sin\theta\cos\theta, \tag{5.29}$$

$$I^{(0)}_{F,z} = -\frac{G_F E_g}{2e^2}\omega\gamma_S \sin^2\theta. \tag{5.30}$$

Note that in the limit, $\gamma_S \ll 1$, the dc spin current along the z-axes is neglible. By contrast, in the limit $\gamma_F \ll \gamma_S$, i.e. $\gamma_S \sim 1$, the ac and dc components are of the same magnitude. The first order charge current reads

$$I^{(1)} = 2e\frac{\gamma_S\gamma_m}{\gamma_F}(\cos\theta I^{(0)}_{F,z} + \sin\theta I^{(0)}_{F,x}) = I_0\frac{\gamma_F\gamma_S}{1+\omega^2}\omega^3, \tag{5.31}$$

where $I_0 = (G_m E_g/e)\sin^2\theta\cos\theta$. Note that in the limit $\gamma_S \sim 1$, we obtain $\sin\theta I^{(0)}_{F,x} \simeq -\cos\theta I^{(0)}_{F,x}$. Namely the ac and dc spin currents partially cancel each. As a result, at low ω while $I^{(0)}_{F,x} \propto I^{(0)}_{F,x} \propto \omega$, the charge current is vanishingly small ($I^{(1)} \propto \omega^3$).

At large precession frequency, $\omega \gg 1$, the current scales linearly with frequency, $I \simeq (G_F G_S G_m/2eG_\Sigma^2)\Omega\sin^2\theta\cos\theta$. In particular, in an open-circuit geometry, this would correspond to an FMR-induced dc voltage $eV = (G_m/2G_\Sigma)\Omega\sin^2\theta\cos\theta$ in accordance with both previous theoretical predictions [62, 65] and experiments [66, 67], see Fig. 5.4.

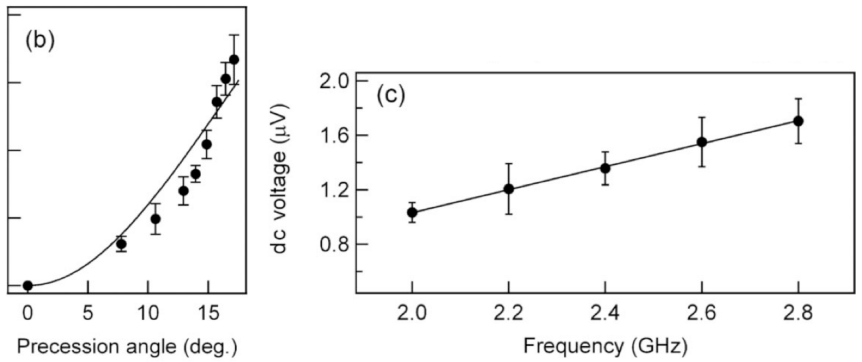

FIGURE 5.4: Amplitude of the dc voltage peaks across a Al /AlO/NiFe/Cu junction measured at the FMR of NiFe [67]. b) dc-voltage amplitude as a function of the tilt angle θ. For small θ, $V \propto \theta^2$. c) Frequency dependence of the voltage peaks. Note the linear dependence $V \propto \Omega$. The results fit the circuit representation prediction in the regime $\Omega \gg E_g$ and $\theta \ll 1$.

At $\omega \ll 1$, spin-relaxation mechanisms induced by the tunnel coupling of the dot to the leads tend to suppress the effect.

5.5 The superconducting state

Having verified that the theory reproduce the experimental results in the normal state, we now turn to the superconducting case. In the subgap regime the transport is mediated via Andreev reflection. Since one electron with spin up necessary pairs with a spin-down electron to enter the superconductor S, no spin current is possible at the N/S interface.

Thus $\boldsymbol{I}_S = 0$. Then, due to the conservation of the spin current along the z-axis, $I_{F,z} = 0$ as well. However, an ac spin current may be present at the interface with the ferromagnet. Then, the Andreev charge current would originate entirely from the rectification of this ac spin current.

Restricting ourselves to energy scales Ω and E_g much smaller than Δ, the Green function in the superconducting lead takes the simple form $\check{g}_S^{R(A)} = \tau_x$ and $\hat{g}_S^K = 0$. Consequently, the charge current at the N/S interface takes the simple form

$$I_S = \frac{G_m E_g \gamma_S}{16e} \int d\epsilon \, \mathrm{Tr}[i\tau_y \check{g}^K]. \tag{5.32}$$

5.5.1 Perturbative expansion

Taking γ_m as a small parameter, we search for a perturbative solution of Eq. (5.18) in the form $\check{g} = \check{g}_0 + \gamma_m \check{g}_1 + \ldots$

5.5.1.1 Zeroth order Green function

At lowest order in γ_m, the equation reads

$$\left[\begin{pmatrix} A_0^R & A_0^K \\ 0 & A_0^A \end{pmatrix}, \check{g}_0 \right] = 0, \tag{5.33}$$

where

$$A_0^{R/A} = -i(\epsilon + \omega\sigma_z)\tau_z \pm \gamma_F \tau_z + \gamma_S \tau_x, \tag{5.34}$$

$$A_0^K = 2\gamma_F f_F \tau_z. \tag{5.35}$$

Due to the proximity effect, now the retarded and advanced Green functions of the dot are modified as well. In particular, to zeroth order in γ_m, the equations for $\check{g}_0^{R/A}$ read

$$\left[[-i(\epsilon + \omega\sigma_z) \pm \gamma_F]\tau_z + \gamma_S \tau_x, \check{g}_0^{R/A} \right] = 0. \tag{5.36}$$

An explicit solution is given by

$$\check{g}_0^{R/A} = \frac{\gamma_S \tau_x + [-i(\epsilon + \omega\sigma_z) \pm \gamma_F]\tau_z}{\sqrt{\gamma_S^2 - (\epsilon + \omega\sigma_z \pm i\gamma_F)^2}}. \tag{5.37}$$

Here, γ_S plays the role of an effective minigap due to the coupling with the S lead [96], ω acts as an effective exchange field, and γ_F yields a broadening of the energy levels due to

the coupling with the F lead. Note that the effective field ω, splits the superconducting singularities.

Following the same steps as for the normal state, we cast the zeroth order Keldysh function in the form $\check{g}_0^K = \check{g}_0^R\check{\varphi}_0 - \check{\varphi}_0\check{g}_0^A$. It obeys

$$\check{g}_0^R(A_0^R\check{\varphi}_0 - \check{\varphi}_0 A_0^R) - (A_0^R\check{\varphi}_0 - \check{\varphi}_0 A_0^R)\check{g}_0^A = \check{g}_0^R A_0^K - A_0^K\check{g}_0^A, \tag{5.38}$$

where we used the relations $[A_0^{R/A}, g_0^{R/A}] = 0$. Eq. (5.38) is solved by

$$\check{\varphi}_0 = f_+ + f_-\cos\theta\left[\frac{\gamma_F\sin\theta}{\omega^2+\gamma_F^2}(\gamma_F\sigma_x - \omega\sigma_y) + \cos\theta\sigma_z\right]. \tag{5.39}$$

Note that γ_S does not enter the result. In the subgap regime of the superconducting lead S, electrons can only thermalize with the ferromagnetic node.

Without surprise, it yields $I^{(0)} = 0$, since no charge are accumulated in the normal metallic node, (no τ_z component in $\check{\varphi}_0$).

Since in the superconducting state, no relation exists between the first order charge and zeroth order spin current, we need to compute the first order Green function, $\check{g}_1$.

5.5.1.2 First order Green function

The normalization condition $\check{g}^2 = 1$ yields at first order $\{\check{g}_0, \check{g}_1\} = 0$. Therefore, the first order Green function can be cast in the form $\check{g}_1 = \check{g}_0\check{X} - \check{X}\check{g}_0$, which automatically account for the normalization. Note that $\check{X}$ is not unique: $\check{X}$ and $\check{X}+\check{x}$,where $[\check{g}_0, \check{x}] = 0$, generate the same $\check{g}_1$. The equation for $\check{X}$ reads

$$\left[[A_0, \check{X}], \check{g}_0\right] = [A_1, \check{g}_0], \tag{5.40}$$

where $A_1 = \begin{pmatrix} \boldsymbol{m}.\boldsymbol{\sigma} & 2f_F\boldsymbol{m}.\boldsymbol{\sigma} \\ 0 & -\boldsymbol{m}.\boldsymbol{\sigma} \end{pmatrix}$. It is convenient to transform Eq. (5.40) into

$$\left[[A_0, \check{X}], \check{g}_0\right] = \left[A_1', \check{g}_0\right], \tag{5.41}$$

where $A_1' = \begin{pmatrix} \sin\theta\sigma_x & (2f_F\boldsymbol{m}.\boldsymbol{\sigma} - \{\cos\theta\sigma_z, \check{\varphi}_0\}) \\ 0 & -\sin\theta\sigma_x \end{pmatrix}$. A trivial calculation shows that $[A_1 - A_1', \check{g}_0] = 0$ and thus validates the transformation.

Then, because $\check{X}$ is defined modulo a function commuting with g_0, we can reduce Eq. (5.41) to

$$[A_0, \check{X}] = A_1'. \tag{5.42}$$

For the advanced and retarded components we find

$$\check{X}^{R/A} = \mp\frac{\sin\theta}{2\omega}\left(i\frac{\gamma_S}{\epsilon \pm i\gamma_F}\tau_x + \tau_z\right)\sigma_y. \tag{5.43}$$

Note that $\check{X}^A(\epsilon) = \sigma_x\tau_z\check{X}^R(-\epsilon)\sigma_x\tau_z$.

The equation for the Keldysh component is more complex and reads

$$A_0^R\check{X}^K - \check{X}^K A_0^A = 2f_F\boldsymbol{m}.\boldsymbol{\sigma} - \{\cos\theta\sigma_z, \check{\varphi}_0\} + \check{X}^R A_0^K - A_0^K\check{X}^A. \tag{5.44}$$

Incorporating the expressions for $\check{X}^{R/A}$ in the last expression, we find that the Keldysh component can be decomposed as $\check{X}^K = X_z^K\tau_z + X_x^K\tau_x$, where X_z^K and X_x^K solve the coupled equations

$$\begin{aligned} 2\gamma_F X_z^K - i\omega[\sigma_z, X_z^K] &= 2\sin\theta[\sin\theta\cos\theta f_- + f_+(\sigma_x - \frac{\gamma_F}{\omega}\sigma_y)], \\ 2\epsilon X_x^K - 2i\gamma_S X_z^K + \omega\{\sigma_z, X_x^K\} &= 2i\frac{\gamma_F\gamma_S\sin\theta}{\omega(\gamma_F^2+\epsilon^2)}[\gamma_F f_+\sigma_y - \epsilon f_-\cos\theta(\cos\theta\sigma_x - \sin\theta\sigma_z)]. \end{aligned}$$

5.5.1.3 Charge current

We are now in a position to evaluate the current at the right interface, using Eq. (5.32). Inserting the solution for $\check{g}_1^K$ and using the property $\check{g}_0^R(-\epsilon) = -\sigma_x\tau_z\check{g}_0^A(\epsilon)\sigma_x\tau_z$, we obtain the current

$$I = \frac{1}{2}I_0\frac{\gamma_S^2\omega}{\gamma_F^2+\omega^2}\int d\epsilon\,\frac{\epsilon f_-}{(\gamma_F^2+\epsilon^2)(\epsilon+\omega)}\sum_{\pm}\frac{-\gamma_F(\epsilon+\omega)\pm i(\gamma_F^2-\epsilon\omega)}{\sqrt{\gamma_S^2-(\epsilon+\omega\pm i\gamma_F)^2}}. \tag{5.45}$$

The current as a function of frequency for different values of $\gamma_F = 1-\gamma_S$ is shown in Fig. 5.5.

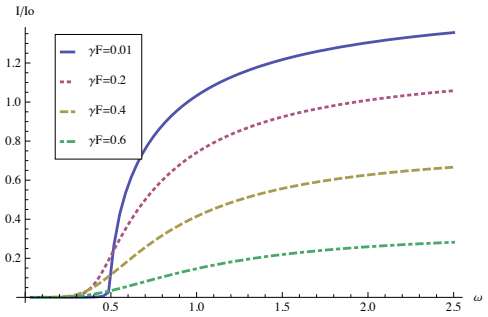

FIGURE 5.5: Andreev current induced by ferromagnetic resonance as a function of $\omega = \Omega/2E_g$ for different values of $\gamma_F = G_F/(G_F+G_S)$. Here $I_0 = (G_m E_g/e)\sin^2\theta\cos\theta$.

Simple analytic expressions can be found in different asymptotic regimes. We derive the result at temperature $T = 0$ and introduce $\gamma = \sqrt{\gamma_F^2 + \gamma_S^2}$. Then,

- At low frequencies, $\omega \ll \gamma$, the FMR induced current is given by

$$I \simeq \frac{10}{3} I_0 \frac{\gamma_F \gamma_S^2}{\gamma^7} \omega^5 \tag{5.46}$$

  The large power ω^5 indicates that the presence of the minigap strongly inhibits the spin accumulation in the dot.

- At large frequencies, $\omega \gg \gamma$, the current saturates. The frequency-independent value is given by

$$I \simeq \frac{\pi}{2} I_0 \operatorname{sign}(\omega) \times \begin{cases} \gamma_S^2 & \gamma_S \ll \gamma_F, \\ 1 & \gamma_S \gg \gamma_F. \end{cases} \tag{5.47}$$

  This saturation can be understood as the inefficiency of Andreev processes at energies larger than the minigap.

- The crossover between these asymptotic regimes is different depending on whether the dot is more strongly coupled to the superconductor or to the ferromagnet.

  – If the dot is weakly coupled to the superconductor, $\gamma_S \ll \gamma_F$, a smooth crossover happens at $\omega \sim 1 \gg \gamma_S$ with a typical current $I/I_0 \sim \gamma_S^2$.

  – By contrast if the dot is weakly coupled to the ferromagnet $\gamma_F \ll \gamma_S$, the crossover in the region $\omega \sim 1/2$ is described by

$$I = I_0 \times \begin{cases} \gamma_F/(2\sqrt{-\delta\omega}) & -1 \ll \delta\omega \ll -\gamma_F, \\ 2\sqrt{\delta\omega} & \gamma_F \ll \delta\omega \ll 1, \end{cases} \tag{5.48}$$

  where $\delta\omega = \omega - 1/2$, with a typical current $I/I_0 \sim \sqrt{\gamma_S}$ at $\omega = 1/2$.

While in the regime of very large or very small frequencies, the Andreev current is suppressed as compared with the normal state, there is in fact a wide intermediate regime, where it may be strongly enhanced. Comparing Eqs. (5.31) and (5.47), we notice that, if the metallic node is strongly coupled to the superconductor, in the regime $1/2 < \omega < 1/\gamma_F$, the induced current in the superconducting state, I_S, exceeds the one in the normal state, I_N, see Fig. 5.6. The enhancement is of the order of $I_S/I_N \sim 1/\gamma_F$. In the normal state, the rectified ac-spin current contribution competes with the dc contribution, as they have the same amplitude but opposite signs. By contrast in the superconducting state the dc-spin current is absent. Therefore, the rectification of the ac-spin current is efficient and generates a large charge current. The ratio between the

current in the superconducting state and the current in the normal state reflects the ratio between Andreev and normal state conductances in an $N'/N/S$ junction, see Fig. 5.6.

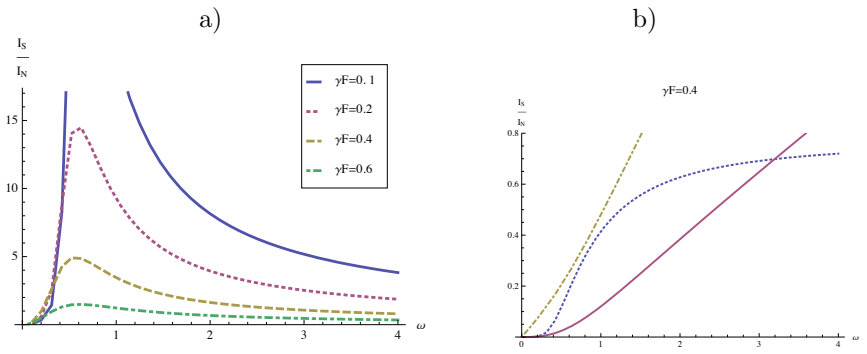

FIGURE 5.6: a) Ratio of the current in the superconducting (I_S) and the normal state (I_N) for different values of γ_F. b) Induced current in the superconducting state (dotted line) and in the normal state for $\gamma_F = 0.4$. The thin line shows the contribution to the normal state current due to the rectification only.

Refinements

So far we assumed that the magnetization in the ferromagnet is uniform. However, boundary effects may lead to a suppression of the magnetization in the vicinity of the F/N interface. This would result in a different resonance frequency at the barrier than in the ferromagnetic reservoir and, consequently, in a tilt angle $\theta_B \neq \theta$ at FMR. The effect can be accounted for by replacing $\boldsymbol{m}$ with $\boldsymbol{m}_B = (\sin\theta_B, 0, \cos\theta_B)$ in Eq. (5.12). In particular, at $\theta_B = 0$, the spin dependent conductance G_m refers to the constant axis $\hat{\mathbf{z}}$. In the normal case, the relation between spin and charge currents, Eq. (5.26), now reads $I = (2e\gamma_m\gamma_S/\gamma_F)\boldsymbol{m}_B.\boldsymbol{I}_F$. While at $\theta_B = \theta$ the rectification of the in-plane ac spin currents always dominates over the conversion of the dc spin current along the z-axes into a charge current, this effect is completely suppressed at $\theta_B = 0$. As a consequence, at $\theta_B = 0$, the charge current, $I = -(G_m E_g/e)\omega\gamma_S^2 \sin^2\theta$, has the opposite sign compared to Eq. (5.31). In general, both effects are important. The sign reversal occurs at $\tan\theta_B = [1 - \gamma_F\omega^2/(\gamma_S + \omega^2)]\tan\theta$.

In the superconducting case, the charge current is entirely due to the dynamic rectification of the ac-spin current since the dc-spin current along the z-axes is always zero. As a result we find that the charge current vanishes at $\theta_B = 0$. This general result can be obtained by replacing I_0 by $I_0^B = (G_m E_g/e)\sin\theta_B \sin\theta\cos\theta$.

5.6 Conclusion

In summary, we demonstrate that a subgap charge current in an F/S junction may be induced by ferromagnetic resonance. The effect is due to the rectification of ac spin currents generated by the precessing magnetization in the ferromagnet. In the normal case, a competing effect of conversion of a dc spin current into a charge current exists. This effect is absent in an F/S junction as the superconductor cannot carry a subgap spin current. As a consequence, the induced current in the superconducting state may be strongly enhanced as compared to the normal state. Interesting non-equilibrium phenomena should be expected in ferromagnetic Josephson junctions under ferromagnetic resonance conditions due to the interplay of the effect studied here with the possible dynamical generation of long-range triplet correlations.

5.7 Appendix A: spin relaxation model in the ferromagnetic lead

In this appendix, we derive the expression for the Green function in the ferromagnetic wire under FMR conditions. To this end, we concentrate on the full junction shown in Fig. 5.7 and use the circuit theory. The ferromagnet F is now a intermediate node of mean level spacing δ_F. In addition to the connection with the node N, it is further connected to a normal metallic lead N' considered at equilibrium. We will show below that N' ensures the spin relaxation of the ferromagnet under FMR conditions.

The ferromagnetic node is asumed to be large compared to the metallic node N and acts as a bath for it. Consequently by assuming that $\hat{g}_F$ is unaffected by the proximity of the metallic node N[4], its Green function $\hat{g}_F$ obeys

$$\left[(-i\partial t + \boldsymbol{J}(t).\boldsymbol{\sigma})\tau_z + i\Gamma\hat{g}_N, \hat{g}_F(t,t')\right] = 0, \tag{5.49}$$

where $\hat{g}_N$ is the Green function in the left metallic lead. It is assumed to be in equilibrium with $\hat{g}_N^{R/A} = \pm\tau_z$ and $\hat{g}_N^K = 2f(E)\tau_z$. Γ gives the escape rate and is expressed in terms of the conductance of the N'/F interface, via $\Gamma = \delta_F \frac{G_N}{2\pi G_Q}$. It thus ensures the spin relaxation.

Then, it is convenient to turn to the rotating frame, where the problem is stationary. Namely, using Eq. (5.4) $\check{g}(t,t')$ obeys

[4] We thus neglect the leakage current in the metallic node.

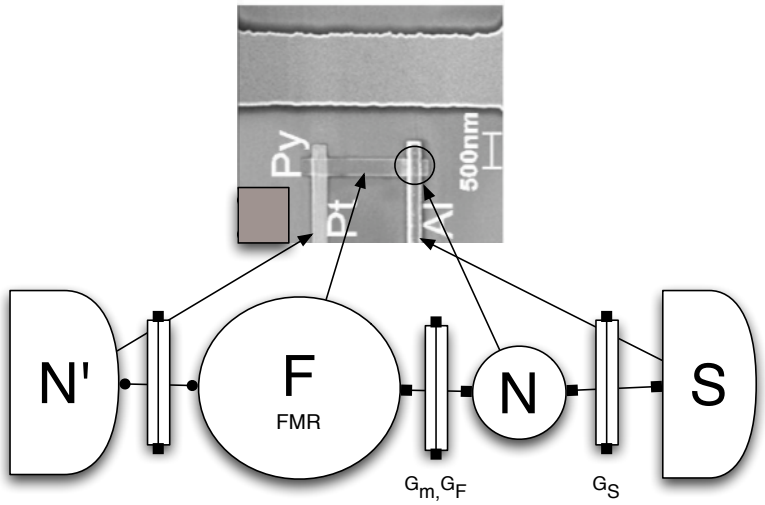

FIGURE 5.7: Full representation of the experimental junction of Costache *et al.* [66]. The metallic node materializes the transition region between the superconducting and the ferromagnetic region. It may accumulate both spin and charge. The interface with the ferromagnet is spin-dependent (G_m). Additionally, the ferromagnetic node F is further connected to the normal metallic lead N'.

$$\left[(-i\partial_t + J\boldsymbol{m}.\boldsymbol{\sigma} + \frac{\Omega}{2}\sigma_z)\tau_z + i\Gamma\check{g}_N(t,t'), \check{g}_F(t,t')\right] = 0. \tag{5.50}$$

As the problem is now stationary depending on $t - t'$, Eq. (5.50) can be further Fourrier transformed, namely

$$\left[(E + J\boldsymbol{m}.\boldsymbol{\sigma} + \frac{\Omega}{2}\sigma_z)\tau_z + i\Gamma\check{g}_N(E), \check{g}_F(E)\right] = 0. \tag{5.51}$$

For a large exchange field, $J \gg \Omega, \Gamma$, the solution of Eq. (5.51) takes the form

$$\check{g}_F^{R(A)} = \pm\tau_z, \tag{5.52}$$

$$\check{g}_F^K = 2\tau_z(f_+ + f_- \cos\theta\, \boldsymbol{m}\cdot\boldsymbol{\sigma}), \tag{5.53}$$

where $f_\pm(E) = 1/2(f(E + \Omega/2) \pm f(E - \Omega/2))$.

5.8 Appendix B: derivation of the first order charge current

Derivation of the coupled equations on X^K

Here, we show the derivation of the needed components of X^K. Starting from Eq. (5.44), the equation for $\check{X}^K$ may be rewritten as

$$A_0^R\check{X}^K - \check{X}^K A_0^A = (2f_F\boldsymbol{m}.\boldsymbol{\sigma} - \{\cos\theta\sigma_z, \check{\varphi}_0\}) + \check{X}^R A_0^K - A_0^K\check{X}^A. \tag{5.54}$$

For simplicity, we omit the check on $\check{X}$ and $\check{g}$. Then, the l.h.s of Eq. (5.54) can be rewritten as

$$\begin{aligned} A_0^R X^K - X^K A_0^A &= [-i(\epsilon+\omega\sigma_z)\tau_z + \gamma_S\tau_x, X^K] + \gamma_F\{\tau_z, X^K\} \\ &= \left[-i\omega[\sigma_z, X_z^K] + 2\gamma_F X_z^K\right] \\ &\quad + \left[-2i\epsilon X_x^K - i\omega\{\sigma_z, X_x^K\} - 2\gamma_S X_z^K)\right]\tau_z\tau_x \end{aligned} \tag{5.55}$$

The r.h.s is a sum of two contributions, namely

$$X^R A_0^K - A_0^K X^A = 2\gamma_F\frac{\sin\theta}{\omega}\left(\left[-\frac{\gamma_S\epsilon}{\epsilon^2+\gamma_F^2}f_-\cos\theta(\boldsymbol{y}\wedge\boldsymbol{m}) + \frac{\gamma_S\gamma_F}{\epsilon^2+\gamma_F^2}f_+\sigma_y\right]\tau_z\tau_x + f_+\sigma_y\right) \tag{5.56}$$

and,

$$2f_F\,\boldsymbol{m}.\boldsymbol{\sigma} - \{\cos\theta\sigma_z, \check{\varphi}\} = 2\cos\theta\sin^2\theta f_- + 2f_+\sin\theta\sigma_x \tag{5.57}$$

As the r.h.s is a sum of τ_0 and $\tau_z\tau_x$, we may decompose X^K as $X^K = X_x^K\tau_x + X_z^K\tau_z$. It yields Eq. (5.45).

The derivation of the current will show that only the $\sigma_\pm$-component of X_x^K and X_z^K are needed (where $\sigma_\pm = 1/2(\sigma_0 \pm \sigma_z)$.

To determine $X_{x,\pm}^K$ and $X_{z,\pm}^K$, we project Eq. (5.45) onto the $\sigma_\pm$-matrices. We obtain

$$X^K_{z,\pm} = \sin^2\theta\cos\theta f_- \frac{1}{\gamma_F}, \tag{5.58}$$

$$X^K_{x,\pm} = i\gamma_S \sin^2\theta\cos\theta f_- \left(\frac{1}{\gamma_F}\frac{1}{\epsilon\pm\omega} \pm \frac{\gamma_F\epsilon}{\omega(\gamma_F^2+\epsilon^2)(\epsilon\pm\omega)}\right). \tag{5.59}$$

Note that $X^K_{x,\pm}(-\epsilon) = -X^K_{x,\mp}(\epsilon)$.

First order current

We now derive the charge current formula (5.45).

For readability, in the following we omit indices, e.g. $g^{R/A} = \check{g}_0^{R/A}$. In addition, $g_{i,j}$ denotes the $\tau_i\,\sigma_j$ component of g, i.e. the index i denotes the Nambu component ($i = x, y, z$) while j accounts for the spin projection ($j = \pm, x, y$).

Using Eq. (5.13), we now derive the charge current at the N/S interface, to first order in γ_m. It is a sum of two contributions, namely

$$I_S^{(1)} = \frac{G_m E_g}{16e}\gamma_S \int d\epsilon \overbrace{\mathrm{Tr}[i\tau_y(g^R X^K - X^K g^A)]}^{1} + \overbrace{\mathrm{Tr}[i\tau_y(g^R\varphi - \varphi g^A)X^A - X^R(g^R\varphi - \varphi g^A))]}^{2}, \tag{5.60}$$

- The first contribution (1) gives

$$(1) = \mathrm{Tr}[\tau_z\tau_x(g^R + g^A)X^K] = 2\sum_{\pm}\left[(g^R+g^A)_{x,\pm}X^K_{z,\pm} - (g^R+g^A)_{z,\pm}X^K_{x,\pm}\right]. \tag{5.61}$$

  Using the relations $g^R_{x/z} = \pm(g^A_{x/z})^*$ and $g^R_\pm(\epsilon) = (g^R_\mp(-\epsilon))^*$, the integration of (1) can be simplified to

$$\int d\epsilon\,(1) = 4\int d\epsilon\,\frac{1}{\gamma_F}(g^R_{x+} + g^{R*}_{x+})\sin^2\theta\cos\theta f_- - (g^R_{z+} - g^{R*}_{z+})X^K_{x,+}. \tag{5.62}$$

  Introducing the short-hand notation $D_\pm = \sqrt{\gamma_S^2 - (\epsilon+\omega\pm i\gamma_F)^2}$, we may further reduce Eq. (5.62) to

$$\int d\epsilon\,(1) = 4\gamma_S \sin^2\theta\cos\theta \int d\epsilon\, f_- \frac{1}{\omega(\epsilon^2+\gamma_F^2)} \sum_{\pm} \frac{1}{D_\pm}\left[\frac{\mp i(\omega(\gamma_F^2+\epsilon^2)+\gamma_F^2\epsilon)}{(\epsilon+\omega)} - \gamma_F\epsilon\right]. \tag{5.63}$$

- The second contribution (2) gives

$$(2) = \mathrm{Tr}[-i\tau_y\varphi((X^R+X^A)g^R + g^A(X^R+X^A))], \tag{5.64}$$

where $X^R + X^A = -\frac{\sin\theta\gamma_F\gamma_S}{\omega(\epsilon^2+\gamma_F^2)}\tau_x\sigma_y = -\Theta\tau_x\sigma_y$.

Then, using the relation $g^A(\epsilon) = -\sigma_x\tau_z g^R(-\epsilon)\sigma_x\tau_z$, (2) can also be simplified to

$$\begin{aligned}
\mathrm{Tr}[-i\tau_y\varphi(X^R+X^A)g^R] &= 2\sum_{\pm}(\varphi_y \pm i\varphi_x)\Theta g^R_{z,\pm}, &(5.65)\\
\mathrm{Tr}[-i\tau_y\varphi g^A(X^R+X^A)] &= \mathrm{Tr}[\tau_z\sigma_y\varphi(g^A)(-\Theta)] = -2\Theta\mathrm{Tr}[\sigma_y\sigma_x\varphi\sigma_x(g_z^R)_{(-\epsilon)}]\\
&= 2\Theta\sum_{\pm}(\varphi_y \pm i\varphi_z)g^R_{z\pm}(-\epsilon). &(5.66)
\end{aligned}$$

As a result, the integration of (2) gives

$$\begin{aligned}
\int d\epsilon\,(2) &= 4\int d\epsilon\,\Theta\sum_{\pm}(\varphi_y \pm i\varphi_x)(g^R_{z\pm}(\epsilon))\\
&= 4\int d\epsilon\,\gamma_S \sin\theta^2\cos\theta f_- \frac{\gamma_F^2}{\omega(\epsilon^2+\gamma_F^2)(\omega^2+\gamma_F^2)}\sum_{\pm}\frac{(-\omega \pm i\gamma_F)(\mp i(\epsilon+\omega)+\gamma_F)}{D_\pm}\\
&= 4\int d\epsilon\,\gamma_S \sin\theta^2\cos\theta f_- \frac{\gamma_F^2}{\omega(\epsilon^2+\gamma_F^2)}\sum_{\pm}\frac{\pm i + \epsilon(\gamma_F \pm i\omega)/(\gamma_F^2+\omega^2)}{D_\pm}. &(5.67)
\end{aligned}$$

We can now gather (1) and (2),

$$\int d\epsilon[(1)+(2)] = 4\gamma_S\sin^2\theta\cos\theta\int d\epsilon f_- \frac{\epsilon\omega}{(\omega^2+\gamma_F^2)(\epsilon+\omega)(\epsilon^2+\gamma_F^2)}\sum_{\pm}\frac{\pm i(\gamma_F^2-\epsilon\omega)+\gamma_F(\epsilon+\omega)}{\sqrt{\gamma_S^2-(\epsilon+\omega\pm i\gamma_F)^2}}. \tag{5.68}$$

Finally, the first order charge current reads

$$I^{(1)} = I_0\frac{1}{4}\frac{\gamma_S^2\omega}{\gamma_F^2+\omega^2}\int d\epsilon\, f_- \frac{\epsilon}{(\epsilon^2+\gamma_F^2)(\epsilon+\omega)}\sum_{\pm}\frac{\pm i(\gamma_F^2-\epsilon\omega)+\gamma_F(\epsilon+\omega)}{\sqrt{\gamma_S^2-(\epsilon+\omega\pm i\gamma_F)^2}}, \tag{5.69}$$

where $I_0 = \sin^2\theta\cos\theta(G_m E_g)/e$.

Conclusion

In diffusive metals, only s-wave superconducting correlations are robust with respect to disorder. As a result, taking into account the spin and frequency dependencies of superconducting correlations, two classes of symmetry for superconductivity may exist. Namely, the wavefunction is either spin-singlet even-frequency or spin-triplet odd-frequency. While the spin-singlet even-frequency symmetry is realized in conventional superconductors, the natural question arises whether the spin-triplet odd-frequency symmetry is realized in nature. The proximity effect in a ferromagnet offers a unique opportunity to study such a question, and was the guideline of the thesis. In particular, an homogeneous magnetization induces both singlet and triplet correlations with zero spin projection along the magnetization axes. Due to the dephasing of electrons with opposite spin by the exchange field, the proximity effect is short-range. The first experimental evidences of short-range triplet correlations are, e.g., the observed oscillations of the critical current in hybrid S/F junctions [37] and the oscillation of the density of states in a homogeneous ferromagnet attached to a superconductor [52].

By contrast, an inhomogeneous magnetization may induce singlet and triplet correlations with all spin-projections. Among them, the triplet correlations between electrons of the same spin are insensitive to the presence of the exchange field and can propagate on a long range. Recently, a long-range proximity effect has been observed in trilayer ferromagnetic junctions [13, 14]. It is predicted to originate from the transport of triplet pairs with parallel spins with respect to the magnetization axes of the long central ferromagnetic layer. However, the experiments do not give further evidence about the triplet symmetry of the correlations.

In chapter 3, we showed that a bilayer geometry is enough to measure a long-range Josephson current. In contrast to the trilayer, here the Josephson current transports pairs of triplet pairs through the long ferromagnetic layer. Indeed, single Cooper pair processes are forbidden by symmetry. As a result, the current phase relation is superharmonic. Thus, the measurement of this peculiar superharmonicity would provide further evidence of the triplet nature of the current [97].

In chapter 4, we further studied the consequences of symmetries. We proposed to artificially build a triplet reservoir using the proximity effect in a bilayer ferromagnet. By connecting two of them through a singlet superconductor, we may study the competition between triplet and singlet superconducting correlations. Such a competition would be observed in the critical current of the junction. In particular, the critical current may present a maximum at a temperature close to the transition of the central superconducting layer.

In the second part of the thesis (chapter 5), we focused on out-of-equilibrium hybrid junctions where the magnetization is homogeneous in space but precesses in time. More precisely, the ferromagnetic resonance (FMR) realizes an alternative way to generate spin and charge currents, and has been observed at room temperature in $N'/F/N$ junctions. In particular, in the normal state the FMR induces a spin current. Then due to spin-dependent interfaces, it is transformed into a measurable charge current [62, 66, 67]. The question we addressed was whether such a current survives below the superconducting transition. In the subgap regime, while spin conservation at the F/S interface prohibits dc-spin currents, we showed that an ac-spin current in the ferromagnet is dynamically rectified at the spin-dependent interface as an Andreev charge current [98].

Perspectives

- While in $S/F/S$ junction, an inhomogeneous magnetization (in space) generates long-range triplet correlations, theoretically, it has been predicted that an inhomogeneity in time, e.g., a dynamical precession of the magnetization, may also generate such triplets [99]. Experimentally, it would be manifest, in homogeneous $S/F/S$ junctions, via an enhancement of the critical current when the ferromagnet is under FMR conditions. However, this work considers only transparent interfaces. Thus, it disregards the possible spin and charge accumulation at the interface predicted in chapter 5.

  As a perspective, we propose to include the interface effects in the study of the $S/F/S$ Josephson junction under FMR conditions. In particular, it might induce an interesting combination of a dc and an ac triplet Josephson effects. The ac-effect would stem from a charge accumulation at interfaces.

- Then, as aforesaid, the generation of spin-polarized triplet supercurrents is very promising for spintronics. However, in chapter 3 and 4, the current-carrying triplet pairs consist of an equal superposition of spin-up and spin-down electrons. As a result the current is not spin-polarized.

The idea would be to go beyond the quasiclassical theory which neglects the band splitting between majority and minority spin species. In particular, taking into account different densities of states for both spin species ($\nu_\uparrow \neq \nu_\downarrow$) might change the picture. It might induce spin-unbalanced triplets and generate the desired spin-polarized supercurrents.

Conclusion (Francais)

Au sein des métaux diffusifs, seules les corrélations s-waves survivent au désordre. Au regard des symétries relatives au spin et à la fréquence, deux classes de symétrie sont admises : la fonction d'onde d'une paire supraconductrice doit être soit singulet et paire en fréquence, soit triplet et impaire en fréquence. Alors que la symétrie singulet est celle de la supraconductivité conventionelle, la symétrie triplet impaire en fréquence existe-t-elle dans la nature ? L'effet de proximité dans des métaux ferromagnétique offre ici une opportunité unique d'étudier cette question, et est le fil directeur de la thèse. Au sein d'une aimantation uniforme une superposition de correlations singulets et triplets sont induites ; elles ont une projection totale, par rapport à l'axe de l'aimantation, nulle. A cause du déphasage entre les électrons de spin opposés induit par le champ Zeeman, l'effet de proximité est à courte portée. Les premières évidences expérimentales de la présence de corrélations triplets furent par exemple l'oscillation du courant critique dans les jonctions π ou l'oscillation de la densité d'état.

Une aimantation non-uniforme du métal ferromagnetique peut induire des corrélations singulets et triplets selon toutes les projections de spin. Parmi ces dernières, les correlations entre électrons ayant le même spin par rapport à l'aimantation d'un domaine sont insensibles à la présence du champ Zeeman associé. Ainsi, elles peuvent pénetrer le métal ferromagnetique sur une longue portée. Un tel effet de proximité longue portée a récemment été observé dans des jonctions Josephson ferromagnétiques tri-couches non-collinéaires. Le courant au sein de la couche centrale (longue) serait porté par des paires triplets avec des spins parallèles selon l'axe d'aimantation. Cependant, les observables ne portent pas de signatures inéquivoques de la symétrie triplet des corrélations.

Dans le chapitre 3, nous avons prédit que, en fait, une jonction ferromagnétique bi-couche est suffisante pour générer un effet Josephson longue portée. Par rapport à la prédiction de la tri-couche, le courant Josephson est, cette fois, porté par des paires de paires triplets au sein de la couche épaisse. En effet, par un argument de symétrie, les processus à une seule paire ne peuvent être que courte portée. La relation courant phase devient donc super-harmonique pour une bicouche longue. La mesure expérimentale de

cette superharmonicté confirmerait la prédiction du caractère triplet du courant longue portée. Dans le chapitre 4, nous avons poursuivi l'étude des symétries supraconductrices induites et leurs signatures. On a proposé la rélisation d'un réservoir supraconducteur triplet artificiel utilisant l'effet de proximité dans la bicouche ferromagnétique. Mettre en contact deux de ces réservoirs effectifs via un ilôt supraconduteur conventionnel permet l'étude de l'intéraction entre supraconductivité triplet impaire en fréquence et singulet paire en fréquence. On a prédit que la compétition entre symétrie triplet et singulet est directement observable par la mesure du courant critique en fonction de la température. Le courant critique présente pour un large panel de paramètres un maximum au voisinage de la transition supraconductrice de l'ilôt central.

Dans la deuxième partie de cette thèse, (chapitre 5), nous nous sommes intéressé aux propriétés hors équilibre des jonctions hybrides S/F. Au lieu d'étudier une variation spatiale de l'aimantation, nous avons considéré une inhomogeinité dans le temps. En particulier, la résonnance ferromagnétique (RFM), précession de l'aimantation agit comme une pompe à spin. La RFM est une alternative au voltage pour induire des courants de spins et de charges. La confirmation expérimentale du mécanisme a été faite, aprés sa prédiction, dans des jonctions N'/F/N à température ambiante. La RFM induit un courant de spin qui est rectifié en courant de charges par des effets d'interfaces sensibles aux spins. La question était donc : lorsque l'échantillon est refroidit, que se passe-t-il sous la transition supraconductrice de l'électrode N . Dans le regime sous le gap, aucun courant de spin n'est possible à l'interface avec le supraconducteur. Cependant, nous avons montré la présence d'un courant de spin alternatif présent dans le métal ferromagnétique qui est rectifié, dynamiquement à l'interface sensible au spin, en un courant Andreev continu de charges.

Bibliography

[1] P. W. Anderson and H. Suhl. Spin alignment in the superconducting state. *Phys. Rev.*, 116:898–900, Nov 1959. doi: 10.1103/PhysRev.116.898. URL http://link.aps.org/doi/10.1103/PhysRev.116.898.

[2] Bernd T Matthias, E Corenzwit, JM Vandenberg, and HE Barz. High superconducting transition temperatures of new rare earth ternary borides. *Proceedings of the National Academy of Sciences*, 74(4):1334–1335, 1977.

[3] M Ishikawa and Fischer. Magnetic ordering in the superconducting state of rare earth molybdenum sulphides. *Solid State Communications*, 24(11):747–751, 1977.

[4] A. I. Larkin and Y.N. Ovchinnikov. Inhomogeneous state of superconductors. *Zh. Eksp. Teor. Fiz*, 47(1136), 1964.

[5] Peter Fulde and Richard A Ferrell. Superconductivity in a strong spin-exchange field. *Physical Review*, 135(3A):A550, 1964.

[6] Dai Aoki, Andrew Huxley, Eric Ressouche, Daniel Braithwaite, Jacques Flouquet, Jean-Pascal Brison, Elsa Lhotel, and Carley Paulsen. Coexistence of superconductivity and ferromagnetism in urhge. *Nature*, 413(6856):613–616, 2001.

[7] SS Saxena, P Agarwal, K Ahilan, FM Grosche, RKW Haselwimmer, MJ Steiner, E Pugh, IR Walker, SR Julian, P Monthoux, et al. Superconductivity on the border of itinerant-electron ferromagnetism in uge2. *Nature*, 406(6796):587–592, 2000.

[8] A. I. Buzdin. Proximity effects in superconductor-ferromagnet heterostructures. *Rev. Mod. Phys.*, 77:935–976, Sep 2005. doi: 10.1103/RevModPhys.77.935. URL http://link.aps.org/doi/10.1103/RevModPhys.77.935.

[9] V.L. Berezinskii. *Pis'ma Zh. Eksp. Teor. Fiz.*, 20(628), 1974.

[10] AF Volkov, FS Bergeret, and Konstantin B Efetov. Odd triplet superconductivity in superconductor-ferromagnet multilayered structures. *Physical review letters*, 90 (11):117006, 2003.

[11] F. S. Bergeret, A. F. Volkov, and K. B. Efetov. Odd triplet superconductivity and related phenomena in superconductor-ferromagnet structures. *Rev. Mod. Phys.*, 77:1321–1373, Nov 2005. doi: 10.1103/RevModPhys.77.1321. URL http://link.aps.org/doi/10.1103/RevModPhys.77.1321.

[12] Mathias Duckheim and Piet W Brouwer. Andreev reflection from noncentrosymmetric superconductors and majorana bound-state generation in half-metallic ferromagnets. *Physical Review B*, 83(5):054513, 2011.

[13] JWA Robinson, JDS Witt, and MG Blamire. Controlled injection of spin-triplet supercurrents into a strong ferromagnet. *Science*, 329(5987):59–61, 2010.

[14] Trupti S. Khaire, Mazin A. Khasawneh, W. P. Pratt, and Norman O. Birge. Observation of spin-triplet superconductivity in co-based josephson junctions. *Phys. Rev. Lett.*, 104:137002, Mar 2010. doi: 10.1103/PhysRevLett.104.137002. URL http://link.aps.org/doi/10.1103/PhysRevLett.104.137002.

[15] Matthias Eschrig. Spin-polarized supercurrents for spintronics. *Physics Today*, 64: 43, 2011.

[16] Alexandre M Zagoskin. *Quantum theory of many-body systems: techniques and applications*, volume 1. Springer New York, 1998.

[17] A. F. Andreev. The thermal conductivity in the intermediate state in superconductors. *Sov. Phys. JETP*, 19(1228), 1964.

[18] P. G. De Gennes and D. S. James. *Physics Letters*, 4(151), 1963.

[19] P de Gennes. *Superconductivity of metals and alloys*. Addison-Wesley New York, 1989.

[20] M. J. M. de Jong and C. W. J. Beenakker. Andreev reflection in ferromagnet-superconductor junctions. *Phys. Rev. Lett.*, 74:1657–1660, Feb 1995. doi: 10.1103/PhysRevLett.74.1657. URL http://link.aps.org/doi/10.1103/PhysRevLett.74.1657.

[21] C. W. J. Beenakker. Quantum transport in semiconductor-superconductor microjunctions. *Phys. Rev. B*, 49(19), 1992.

[22] Carlo WJ Beenakker. Random-matrix theory of quantum transport. *Reviews of modern physics*, 69(3):731, 1997.

[23] I. O. Kulik. *Sov. Phys. JETP*, 30(944), 1970.

[24] I. O. Kulik and A. N. Omelyanchuk. Properties of superconducting microbridges in the pure limit. *Sov. J . Low Temp. Phus.*, 3(7), 1977.

[25] B. D. Josephson. Possible new effects in superconductive tunneling. *Phys. Lett.*, 1 (251), 1962.

[26] M. L. Della Rocca, M. Chauvin, B. Huard, H. Pothier, D. Esteve, and C. Urbina. Measurement of the current-phase relation of superconducting atomic contacts. *Phys. Rev. Lett.*, 99:127005, Sep 2007. doi: 10.1103/PhysRevLett.99.127005. URL http://link.aps.org/doi/10.1103/PhysRevLett.99.127005.

[27] AA Golubov, M Yu Kupriyanov, and E Il'Ichev. The current-phase relation in josephson junctions. *Reviews of modern physics*, 76(2):411, 2004.

[28] Chikara Ishii. Josephson currents through junctions with normal metal barriers. *Progress of theoretical Physics*, 44(6):1525–1547, 1970.

[29] John Bardeen and Jared L Johnson. Josephson current flow in pure superconducting-normal-superconducting junctions. *Physical Review B*, 5(1):72, 1972.

[30] F Zhou, Ph Charlat, B Spivak, and B Pannetier. Density of states in superconductor-normal metal-superconductor junctions. *Journal of low temperature physics*, 110(3-4):841–850, 1998.

[31] LN Bulaevskii, VV Kuzii, and AA Sobyanin. Superconducting system with weak coupling with a current in the ground state. *Zh. Eksp. Teor. Fiz*, 25(314), 1977.

[32] A. I. Buzdin, L. N. Bulaevskii, and S. V. Panyukov. Critical current oscillation as a function of the exchange field and the thickness fo the ferromagnetic metal (f) in a s-f-s josephson junction. *Pis'ma Zh. Eksp. Teor. Fiz.*, 35(147), 1982.

[33] T Kontos, M Aprili, J Lesueur, F Genet, B Stephanidis, and R Boursier. Feromagnetic π-junctions. *Phys. Rev. Lett*, 89(137007), 2002.

[34] V. V. Ryazanov, V. A. Oboznov, A. Yu. Rusanov, A. V. Veretennikov, A. A. Golubov, and J. Aarts. Coupling of two superconductors through a ferromagnet: Evidence for a π junction. *Phys. Rev. Lett.*, 86:2427–2430, Mar 2001. doi: 10.1103/PhysRevLett.86.2427. URL http://link.aps.org/doi/10.1103/PhysRevLett.86.2427.

[35] Andreas Bauer, Johannes Bentner, M Aprili, ML Della Rocca, Matthias Reinwald, Werner Wegscheider, and Christoph Strunk. Spontaneous supercurrent induced by ferromagnetic π junctions. *Physical review letters*, 92(21):217001, 2004.

[36] Hermann Sellier, Claire Baraduc, Fran çois Lefloch, and Roberto Calemczuk. Half-integer shapiro steps at the 0-π crossover of a ferromagnetic josephson junction.

Phys. Rev. Lett., 92:257005, Jun 2004. doi: 10.1103/PhysRevLett.92.257005. URL http://link.aps.org/doi/10.1103/PhysRevLett.92.257005.

[37] VA Oboznov, VV Bol'ginov, AK Feofanov, VV Ryazanov, and Alexandre I Buzdin. Thickness dependence of the josephson ground states of superconductor-ferromagnet-superconductor junctions. *Physical review letters*, 96(19):197003, 2006.

[38] EA Demler, GB Arnold, and MR Beasley. Superconducting proximity effects in magnetic metals. *Physical Review B*, 55(22):15174, 1997.

[39] A Kadigrobov, RI Shekhter, and M Jonson. Quantum spin fluctuations as a source of long-range proximity effects in diffusive ferromagnet-super conductor structures. *EPL (Europhysics Letters)*, 54(3):394, 2001.

[40] FS Bergeret, AF Volkov, and KB Efetov. Long-range proximity effects in superconductor-ferromagnet structures. *Physical review letters*, 86(18):4096, 2001.

[41] Carolin Klose, Trupti S. Khaire, Yixing Wang, W. P. Pratt, Norman O. Birge, B. J. McMorran, T. P. Ginley, J. A. Borchers, B. J. Kirby, B. B. Maranville, and J. Unguris. Optimization of spin-triplet supercurrent in ferromagnetic josephson junctions. *Phys. Rev. Lett.*, 108:127002, Mar 2012. doi: 10.1103/PhysRevLett.108.127002. URL http://link.aps.org/doi/10.1103/PhysRevLett.108.127002.

[42] PG De Gennes. Coupling between ferromagnets through a superconducting layer. *Physics Letters*, 23(1):10–11, 1966.

[43] AI Buzdin, AV Vedyayev, and NV Ryzhanova. Spin-orientation–dependent superconductivity in f/s/f structures. *EPL (Europhysics Letters)*, 48(6):686, 1999.

[44] LR Tagirov. Proximity effect and superconducting transition temperature in superconductor/ferromagnet sandwiches. *Physica C: Superconductivity*, 307(1):145–163, 1998.

[45] R Mélin and D Feinberg. What is the value of the superconducting gap of a f/s/f trilayer? *EPL (Europhysics Letters)*, 65(1):96, 2004.

[46] J. J. Hauser. Coupling between ferrimagnetic insulators through a superconducting layer. *Phys. Rev. Lett.*, 23:374–377, Aug 1969. doi: 10.1103/PhysRevLett.23.374. URL http://link.aps.org/doi/10.1103/PhysRevLett.23.374.

[47] G. Deutscher and F. Meunier. Coupling between ferromagnetic layers through a superconductor. *Phys. Rev. Lett.*, 22:395–396, Mar 1969. doi: 10.1103/PhysRevLett.22.395. URL http://link.aps.org/doi/10.1103/PhysRevLett.22.395.

[48] JY Gu, C-Y You, JS Jiang, J Pearson, Ya B Bazaliy, and SD Bader. Magnetization-orientation dependence of the superconducting transition temperature in the ferromagnet-superconductor-ferromagnet system: Cuni/nb/cuni. *Physical review letters*, 89(26):267001, 2002.

[49] AA Golubov, Y Tanaka, Y Asano, and Y Tanuma. Odd-frequency pairing in superconducting heterostructures. *Journal of Physics: Condensed Matter*, 21(16): 164208, 2009.

[50] R. Meservey and P.M. Tedrow. Spin-polarized electron tunneling. *Physics reports*, 238:173–243, 1994.

[51] Shiro Kawabata, Yasuhiro Asano, Yukio Tanaka, and Alexander A Golubov. Robustness of spin-triplet paring and the singlet-triplet paring-crossover in superconductor/ferromagnet hybrids. *arXiv preprint arXiv:1302.6281*, 2013.

[52] T. Kontos, M. Aprili, J. Lesueur, F. Genêt, B. Stephanidis, and R. Boursier. Josephson junction through a thin ferromagnetic layer: Negative coupling. *Phys. Rev. Lett.*, 89:137007, Sep 2002. doi: 10.1103/PhysRevLett.89.137007. URL http://link.aps.org/doi/10.1103/PhysRevLett.89.137007.

[53] Y Tanaka, Y Tanuma, and AA Golubov. Odd-frequency pairing in normal-metal/superconductor junctions. *Physical Review B*, 76(5):054522, 2007.

[54] Audrey Cottet. Inducing odd-frequency triplet correlations in a normal metal. *Phys. Rev. Lett.*, 107(17):177001, 2011.

[55] RJ Soulen Jr, JM Byers, MS Osofsky, B Nadgorny, T Ambrose, SF Cheng, Pr R Broussard, CT Tanaka, J Nowak, JS Moodera, et al. Measuring the spin polarization of a metal with a superconducting point contact. *Science*, 282(5386):85–88, 1998.

[56] Shashi K Upadhyay, Akilan Palanisami, Richard N Louie, and RA Buhrman. Probing ferromagnets with andreev reflection. *Physical review letters*, 81(15):3247, 1998.

[57] Mark Johnson and R. H. Silsbee. Interfacial charge-spin coupling: Injection and detection of spin magnetization in metals. *Phys. Rev. Lett.*, 55:1790–1793, Oct 1985. doi: 10.1103/PhysRevLett.55.1790. URL http://link.aps.org/doi/10.1103/PhysRevLett.55.1790.

[58] M. N. Baibich, J. M. Broto, A. Fert, F. Nguyen Van Dau, F. Petroff, P. Etienne, G. Creuzet, A. Friederich, and J. Chazelas. Giant magnetoresistance of (001)fe/(001)cr magnetic superlattices. *Phys. Rev. Lett.*, 61:2472–2475, Nov 1988.

doi: 10.1103/PhysRevLett.61.2472. URL http://link.aps.org/doi/10.1103/PhysRevLett.61.2472.

[59] G. Binasch, P. Grünberg, F. Saurenbach, and W. Zinn. Enhanced magnetoresistance in layered magnetic structures with antiferromagnetic interlayer exchange. *Phys. Rev. B*, 39:4828–4830, Mar 1989. doi: 10.1103/PhysRevB.39.4828. URL http://link.aps.org/doi/10.1103/PhysRevB.39.4828.

[60] John C Slonczewski. Current-driven excitation of magnetic multilayers. *Journal of Magnetism and Magnetic Materials*, 159(1):L1–L7, 1996.

[61] L Berger. Emission of spin waves by a magnetic multilayer traversed by a current. *Physical Review B*, 54(13):9353, 1996.

[62] Yaroslav Tserkovnyak, Arne Brataas, and Gerrit EW Bauer. Enhanced gilbert damping in thin ferromagnetic films. *Physical Review Letters*, 88(11):117601, 2002.

[63] Charles Kittel. On the theory of ferromagnetic resonance absorption. *Phys. Rev.*, 73:155–161, Jan 1948. doi: 10.1103/PhysRev.73.155. URL http://link.aps.org/doi/10.1103/PhysRev.73.155.

[64] Charles Kittel and RW Hellwarth. *Introduction to solid state physics*, volume 10. 1957.

[65] Xuhui Wang, Gerrit EW Bauer, Bart J van Wees, Arne Brataas, and Yaroslav Tserkovnyak. Voltage generation by ferromagnetic resonance at a nonmagnet to ferromagnet contact. *Physical review letters*, 97(21):216602, 2006.

[66] MV Costache, M Sladkov, SM Watts, CH Van der Wal, and BJ Van Wees. Electrical detection of spin pumping due to the precessing magnetization of a single ferromagnet. *Physical review letters*, 97(21):216603, 2006.

[67] Takahiro Moriyama, R Cao, X Fan, G Xuan, BK Nikolić, Y Tserkovnyak, J Kolodzey, and John Q Xiao. Tunnel barrier enhanced voltage signal generated by magnetization precession of a single ferromagnetic layer. *Physical review letters*, 100(6):067602, 2008.

[68] Daniel Huertas-Hernando, Yu. V. Nazarov, and W. Belzig. Absolute spin-valve effect with superconducting proximity structures. *Phys. Rev. Lett.*, 88:047003, Jan 2002. doi: 10.1103/PhysRevLett.88.047003. URL http://link.aps.org/doi/10.1103/PhysRevLett.88.047003.

[69] Xavier Waintal and Piet W. Brouwer. Magnetic exchange interaction induced by a josephson current. *Phys. Rev. B*, 65:054407, Jan 2002. doi: 10.1103/PhysRevB.65.054407. URL http://link.aps.org/doi/10.1103/PhysRevB.65.054407.

[70] NG Pugach and Alexandre I Buzdin. Magnetic moment manipulation by triplet josephson current. *Applied Physics Letters*, 101(24):242602–242602, 2012.

[71] Jørgen Rammer and HA Smith. Quantum field-theoretical methods in transport theory of metals. *Reviews of modern physics*, 58(2):323–359, 1986.

[72] S Fujita. Thermodynamic evolution equation for a quantum statistical gas. *Journal of Mathematical Physics*, 6:1877, 1965.

[73] IUA Kukharenko and SG Tikhodeev. A diagram technique in the theory of relaxation processes. *Zhurnal Eksperimental'noi i Teoreticheskoi Fiziki*, 83:1444–1456, 1982.

[74] Robert Mills, Harry L Morrison, M Moshinsky, Marcos Moshinsky, FJ Wuilleumier, Dionys Baeriswyl, I Lindgren, Yu V Novozhilov, Philippe Nozieres, Raymond F Bishop, et al. Propagators for many particle systems an elementary treatment.

[75] Julian Schwinger. On the green's functions of quantized fields. i. *Proceedings of the National Academy of Sciences*, 37(7):452–455, 1951.

[76] L.P. Kadanoff, G. Baym, and D. Pines. *Quantum statistical mechanics*. Benjamin, New York, 1962.

[77] Gert Eilenberger. Transformation of gorkov's equation for type ii superconductors into transport-like equations. *Zeitschrift für Physik*, 214(2):195–213, 1968.

[78] Klaus D. Usadel. Generalized diffusion equation for superconducting alloys. *Phys. Rev. Lett.*, 25:507–509, Aug 1970. doi: 10.1103/PhysRevLett.25.507. URL http://link.aps.org/doi/10.1103/PhysRevLett.25.507.

[79] AV Zaitsev. Quasiclassical equations of the theory of superconductivity for contiguous metals and the properties of constricted microcontacts. *Zh. Eksp. Teor. Fiz*, 86:1742–1758, 1984.

[80] M Yu Kupriyanov and VF Lukichev. Influence of boundary transparency on the critical current of" dirty" ss's structures. *Zh. Eksp. Teor. Fiz*, 94:139, 1988.

[81] Audrey Cottet, Daniel Huertas-Hernando, Wolfgang Belzig, and Yuli V Nazarov. Spin-dependent boundary conditions for isotropic superconducting green's functions. *Physical Review B*, 80(18):184511, 2009.

[82] Yuli V Nazarov and Yaroslav M Blanter. *Quantum transport: introduction to nanoscience*. Cambridge University Press, 2009.

[83] M. Eschrig, J. Kopu, J. C. Cuevas, and Gerd Schön. Theory of half-metal/superconductor heterostructures. *Phys. Rev. Lett.*, 90:137003, Apr 2003. doi: 10.1103/PhysRevLett.90.137003. URL http://link.aps.org/doi/10.1103/PhysRevLett.90.137003.

[84] V. Braude and Yu. V. Nazarov. Fully developed triplet proximity effect. *Phys. Rev. Lett.*, 98:077003, Feb 2007. doi: 10.1103/PhysRevLett.98.077003. URL http://link.aps.org/doi/10.1103/PhysRevLett.98.077003.

[85] Luka Trifunovic. Long-range superharmonic josephson current. *Phys. Rev. Lett.*, 107:047001, Jul 2011. doi: 10.1103/PhysRevLett.107.047001. URL http://link.aps.org/doi/10.1103/PhysRevLett.107.047001.

[86] A. S. Mel'nikov, A. V. Samokhvalov, S. M. Kuznetsova, and A. I. Buzdin. Interference phenomena and long-range proximity effect in clean superconductor-ferromagnet systems. *Phys. Rev. Lett.*, 109:237006, Dec 2012. doi: 10.1103/PhysRevLett.109.237006. URL http://link.aps.org/doi/10.1103/PhysRevLett.109.237006.

[87] A. Buzdin and MV Kuprianov. Transition temperature of a superconductor-ferromagnet superlattice. *Pis'ma Zh. Eksp. Teor. Fiz.*, 52(1089), 1990.

[88] M. Fauré, A. I. Buzdin, A. A. Golubov, and M. Yu. Kupriyanov. Properties of superconductor/ferromagnet structures with spin-dependent scattering. *Phys. Rev. B*, 73:064505, Feb 2006. doi: 10.1103/PhysRevB.73.064505. URL http://link.aps.org/doi/10.1103/PhysRevB.73.064505.

[89] Ya. M. Blanter and F. W. J. Hekking. Supercurrent in long sffs junctions with antiparallel domain configuration. *Phys. Rev. B*, 69:024525, Jan 2004. doi: 10.1103/PhysRevB.69.024525. URL http://link.aps.org/doi/10.1103/PhysRevB.69.024525.

[90] B. Crouzy, S. Tollis, and D. A. Ivanov. Josephson current in a superconductor-ferromagnet junction with two noncollinear magnetic domains. *Phys. Rev. B*, 75:054503, Feb 2007. doi: 10.1103/PhysRevB.75.054503. URL http://link.aps.org/doi/10.1103/PhysRevB.75.054503.

[91] A.I. Buzdin. Peculiar properties of the josephson junction at the transition from 0 to π state. *Phys. Rev. B*, 72(100501(R)), 2005.

[92] M. Houzet, V. Vinokur, and F. Pistolesi. Superharmonic josephson relation at 0π-junction transition. *Phys. Rev. B*, 72:220506, Dec 2005. doi: 10.1103/PhysRevB.72.220506. URL http://link.aps.org/doi/10.1103/PhysRevB.72.220506.

[93] S. M. Frolov, D. J. Van Harlingen, V. A. Oboznov, V. V. Bolginov, and V. V. Ryazanov. Measurement of the current-phase relation of superconductor/ferromagnet/superconductor π josephson junctions. *Phys. Rev. B*, 70:144505, Oct 2004. doi: 10.1103/PhysRevB.70.144505. URL http://link.aps.org/doi/10.1103/PhysRevB.70.144505.

[94] Jacob Linder, Takehido Yokohama, and Asle Subdo. Role of interface transparency and spin-dependent scattering in diffusive ferromagnet/superconductor heterostructures. *Phys. Rev. B*, 77(174514), 2008.

[95] M Yu Kupriyanov, A Brinkman, AA Golubov, M Siegel, and H Rogalla. Double barrier josephson structures as the novel elements for superconducting large scale integrated circuits. *Physica C: Superconductivity*, 326(16):45, 1999.

[96] CWJ Beenakker. Andreev billiards. In *Quantum Dots: a Doorway to Nanoscale Physics*, pages 131–174. Springer, 2005.

[97] Caroline Richard, Manuel Houzet, and Julia S Meyer. Superharmonic long-range triplet current in a diffusive josephson junction. *Physical Review Letters*, 110(21): 217004, 2013.

[98] J.S. Meyer C. Richard, M. Houzet. Andreev current induced by ferromagnetic resonance. *Phys. Rev. Lett*, 109(057002), 2012.

[99] Manuel Houzet. Ferromagnetic josephson junction with precessing magnetization. *Phys. Rev. Lett.*, 101:057009, Aug 2008. doi: 10.1103/PhysRevLett.101.057009. URL http://link.aps.org/doi/10.1103/PhysRevLett.101.057009.

Summary

Interplay of ferromagnetism and superconductivity

While ferromagnetism and conventional superconductivity appear as antagonist phases of nature, the proximity effect in hybrid superconductor (S) / ferromagnet (F) structures offers a unique opportunity to study their interplay. In particular, spin-triplet odd-frequency superconducting correlations may be induced in a diffusive ferromagnet. In a first part, we study the equilibrium current that may flow in hybrid S/F Josephson junctions. In particular, we predict the existence of a long range triplet current through a non-collinear bilayer ferromagnet with a peculiar superharmonic current phase relation. This can be viewed as the Josephson effect between a conventional superconductor and an effective triplet superconductor generated at the end of the bilayer ferromagnet. The competition between singlet and triplet superconductivity may also be observed in the critical current of more complicated junctions. Namely, the critical current flowing between two effective triplet reservoirs through a conventional superconducting layer may display a maximum at finite temperature. In a second part, we explore the combination of superconductivity and ferromagnetism to generate spin currents for applications in spintronics. Ferromagnetic resonance (FMR) is a spin-pumping mechanism which may be used to generate spin currents without applying a voltage. Due to interface effects, signatures of an FMR induced spin current have been measured at room temperature in a normal metal adjacent to a ferromagnet under FMR. We predict the effect to survive at low temperatures when the adjacent metal becomes superconducting.

Résumé (Francais)

Interaction entre supraconductivité et ferromagnétisme

Le ferromagétisme et la supraconductivité conventionnelle sont deux phases antagonistes dont la compétition peut être étudiée dans les structures hybrides supraconducteur (S) / métal ferromagnétique (F). En particulier, une supraconductivité triplet impaire en fréquence peut être induite dans une couche ferromagnétique en régime diffusif. Dans une premire partie, on étudie les courants qui circulent à l'équilibre dans de telles jonctions hybrides S/F. On prédit l'existence d'un courant triplet à longue portée dans une bicouche ferromagnétique d'aimantation non uniforme. La relation courant phase a la particularité d'être superharmonique. Ceci peut être interprété comme un effet Josephson entre un supraconducteur conventionel et un supraconducteur triplet artificiellement induit à l'extrémité de la bicouche ferromagnétique. La compétition entre supraconductivité singulet et triplet peut aussi être observée dans le courant critique de certaines jonctions hybrides : le courant circulant entre deux reservoirs triplets au travers d'une couche supraconductrice conventionnelle peut présenter un maximum à température finie. Dans une seconde partie, on explore la combinaison de la supraconductivité et du ferromagnétisme avec en perspective la génération de courants de spin pour la spintronique. La resonance ferromagnetique (RFM) est un mécanisme de pompage de spin qui permet de générer des courants de spin sans appliquer de tension. Grâce à des effets d'interface, les signatures d'un courant de spin induit par RFM ont déjà été mesurées à température ambiante au bord d'un métal normal attaché à une couche ferromagnétique sous RFM. On prédit que l'effet survit à basse température quand le métal normal devient supraconducteur.

Interplay of ferromagnetism and superconductivity

Ferromagnetism and conventional superconductivity appear as antagonist phases of nature. The proximity effect in hybrid superconductor (S)/ ferromagnet (F) structures offers a unique opportunity to study their interplay. While the correlations in a conventional dirty superconductor are s-wave spin-singlet even-frequency, s-wave spin-triplet odd-frequency correlations may be induced in a ferromagnet attached to a superconductor. We first study the equilibrium currents and the symmetry of superconducting correlations in hybrid multi-layered Josephson junctions. We look for signatures of spin-triplet equilibrium currents in either the full current phase relation or the critical current. Then, more on a spintronics side, we study the combination of a ferromagnetic resonance with superconductivity towards alternative ways to voltage to induce spin or charge currents.

Keywords: hybrid structures, superconductivity, ferromagnetism, triplet, odd-frequency

Interaction entre supraconductivité et ferromagnétisme

Le ferromagnétisme et la supraconductivité conventionelle sont deux phases antagonistes de la nature dont l'interaction peut être étudiée grâce à l'effet de proximité dans les structures hybrides supraconductrices (S) / ferromagnétiques. Alors que la supraconductivité conventionelle, dans la limite sale, a la symétrie s-wave singulet de spin et paire en fréquence, une supraconductivité s-wave triplet de spin et impaire en fréquence peut être induite dans un métal ferromagnétique attaché à un supraconducteur. On étudie d'abord les courants à l'équilibre ainsi que la symétrie des corrélations dans les jonctions Josephson hybrides multi-couches. En particulier, on cherche des signatures du caractère triplet des courants d'équilibres dans la relation courant phase ou dans le courant critique. Puis, d'un point de vue plus spintronique, on montre que la combinaison de la résonance ferromagnétique avec la supraconductivité permet d'induire des courants de spin et de charge sans appliquer de tension.

Mots clés : structure hybrides, supraconductivité, ferromagnétisme, triplet, impair en fréquence